

Special Issue: *Australopithecus sediba*

The Vertebrae, Ribs, and Sternum of *Australopithecus sediba*

SCOTT A. WILLIAMS

Center for the Study of Human Origins, Department of Anthropology, New York University, 25 Waverly Place, New York, NY 10003, USA; New York Consortium in Evolutionary Primatology, New York NY 10024, USA; and, Evolutionary Studies Institute, University of the Witwatersrand, Private Bag 3, Wits 2050, Johannesburg, SOUTH AFRICA; sawilliams@nyu.edu

MARC R. MEYER

Department of Anthropology, Chaffey College, Rancho Cucamonga, CA 91737, USA; marc.meyer@chaffey.edu

SHAHED NALLA

Department of Human Anatomy and Physiology, Faculty of Health Science, University of Johannesburg, PO Box 524, Auckland Park 2006, Johannesburg; and, Evolutionary Studies Institute, University of the Witwatersrand, Private Bag 3, Wits 2050, Johannesburg, SOUTH AFRICA; shahedn@uj.ac.za

DANIEL GARCÍA-MARTÍNEZ

Paleoanthropology Group, Museo Nacional de Ciencias Naturales (MNCN-CSIC), J.G. Abascal 6, 28006 Madrid; Faculty of Sciences, Biology Department, Universidad Autónoma de Madrid, 28049 Madrid, SPAIN; and, Evolutionary Studies Institute, University of the Witwatersrand, Private Bag 3, Wits 2050, Johannesburg, SOUTH AFRICA; dan.garcia@mncn.csic.es

THIERRA K. NALLEY

Western University of Health Sciences, College of Osteopathic Medicine of the Pacific, Department of Medical Anatomical Sciences, Pomona, CA 91766, USA; tnalley@westernu.edu

JENNIFER EYRE

Center for the Study of Human Origins, Department of Anthropology, New York University, 25 Waverly Place, New York, NY 10003 and New York Consortium in Evolutionary Primatology, New York, NY 10024, USA; je988@nyu.edu

THOMAS C. PRANG

Center for the Study of Human Origins, Department of Anthropology, New York University, 25 Waverly Place, New York, NY 10003, and New York Consortium in Evolutionary Primatology, New York, NY 10024, USA; cody.prang@nyu.edu

MARKUS BASTIR

Paleoanthropology Group, Museo Nacional de Ciencias Naturales (MNCN-CSIC), J.G. Abascal 6, 28006 Madrid, SPAIN; and, Evolutionary Studies Institute, University of the Witwatersrand, Private Bag 3, Wits 2050, Johannesburg, SOUTH AFRICA; mbastir@mncn.csic.es

PETER SCHMID

Anthropological Institute and Museum, University of Zurich, Winterthurerstr. 190, CH-8057 Zurich, SWITZERLAND; and, Evolutionary Studies Institute, University of the Witwatersrand, Private Bag 3, Wits 2050, Johannesburg, SOUTH AFRICA; smidi@aim.uzh.ch

STEVEN E. CHURCHILL

Department of Evolutionary Anthropology, Box 90383, Duke University, Durham, NC 27708, USA; and, Evolutionary Studies Institute, University of the Witwatersrand, Private Bag 3, Wits 2050, Johannesburg, SOUTH AFRICA; churchy@duke.edu

LEE R. BERGER

Evolutionary Studies Institute, University of the Witwatersrand, Private Bag 3, Wits 2050, Johannesburg, SOUTH AFRICA; profleeberger@yahoo.com

submitted: 29 September 2017; accepted 24 August 2018

ABSTRACT

Australopithecus sediba is known from two partial skeletons, Malapa Hominins 1 and 2 (MH1 and MH2), a juvenile male and an adult female, respectively. Forty-eight elements of the axial skeleton, including vertebrae, ribs, a sternum, and a sacrum, are known from MH1 and MH2. Here, we describe these ~2.0 Ma fossils and provide raw data and plots of standardized measurements. We revisit the serial positions of the previously described vertebrae and ribs proposed in their initial announcements and provide revised identifications. Additionally, we include in our descriptions and analyses new axial material. Finally, we also test the hypothesis that multiple species are represented in the MH1 and MH2 material and specifically that MH1's lumbar vertebrae belong to a member of the genus *Homo*, whereas those of MH2 belong to *Australopithecus*. We do not find support for this hypothesis, and instead attribute differences between MH1 and MH2 to their age difference and incomplete growth of the vertebral body in juvenile MH1.

This special issue is guest-edited by Scott A. Williams (Department of Anthropology, New York University) and Jeremy M. DeSilva (Department of Anthropology, Dartmouth College). This is article #3 of 9.

INTRODUCTION

Australopithecus sediba, thus far recovered only from the site of Malapa in the Cradle of Humankind, South Africa, dated to ca. 2.0 Ma (Dirks et al. 2010; Pickering et al. 2011), is largely known from two relatively complete partial skeletons, Malapa Hominin 1 (MH1, a subadult, presumed male) and Malapa Hominin 2 (MH2, an adult, presumed female) (Berger et al. 2010; Carlson et al. 2011; Churchill et al. 2013, 2018 a, b; de Ruiter et al. 2013, 2018; DeSilva et al. 2013, 2018; Irish et al. 2013; Kibii et al. 2011; Kivell et al. 2011, 2018; Schmid et al. 2013; Williams et al. 2013, 2018; Zipfel et al. 2011). Elements of the postcranial axial skeleton (hereafter, axial skeleton: vertebral column, ribs, and sternum) are not well-represented in the hominin fossil record, particularly in association as partial skeletons. *Australopithecus sediba* preserves 48 fossils from the axial skeleton (Berger et al. 2010; Meyer et al. 2017; Schmid et al. 2013; Williams et al. 2013). The MH1 axial skeleton is represented by 18 fossils, including nine vertebrae (Table 1) and nine ribs (Table 2). The MH2 axial skeleton is known from 30 fossils, including 12 vertebrae (Table 3), a sacrum composed of five fused elements (described in Churchill et al. 2018a), 16 ribs (Table 4), and a manubrium sterni.

The axial skeleton of *Au. sediba* is therefore well-represented among Pliocene and early Pleistocene hominins in terms of number of preserved fossil elements, each comparable in preservation to known australopiths (*Au. africanus*: Sts 14 and StW 431; *Au. afarensis*: A.L. 288-1) and *Homo erectus* (KNM-WT 15000) partial skeletons. The *Au. sediba* material increases the number of Pliocene/early Pleistocene partial skeletons by approximately 30% and the number of axial remains by approximately 40%. Although the vertebral and costal material has been discussed in the literature previously (Arlegi et al. 2017; Bastir et al. 2016; Been et al. 2014; Berger et al. 2010; Meyer and Haeusler 2015; Meyer et al. 2015, 2017, 2018; Randolph-Quinney et al. 2016; Russo and Williams 2015; Schmid et al. 2013; Tardieu et al. 2013; Thompson and Almécija 2017; Williams 2011a,b, 2012a,b; Williams and Russo 2015, 2016; Williams et al. 2013, 2016), here we provide the first full descriptions of the fossils,

along with basic analyses comparing *Au. sediba* to recent modern human and chimpanzee material, and to other available Plio-Pleistocene fossil hominins.

Additionally, we briefly address the hypothesis that the Malapa hominins represent two intermingled species rather than a single taxon (Been and Rak 2014; Rak and Been 2014). Been and Rak (2014) proposed that MH1 lumbar vertebrae belong to *Homo*, whereas MH2 lumbar vertebrae belong to *Australopithecus*; in contrast, Rak and Been (2014) proposed that the MH1 mandible is more similar to *Australopithecus*, whereas that of MH2 resembles *Homo* in shape. Here, we compare the MH1 and MH2 lumbar vertebrae to other available fossil hominin lumbar vertebrae to test the hypothesis that they group with subadult *Homo* and adult *Australopithecus*, respectively. We find no support for this hypothesis.

MATERIALS AND METHODS

Individual fossil specimens are described qualitatively and quantitatively (to the extent possible given the state of preservation of the element). They are compared to a sample of 28 chimpanzees (*P. troglodytes*; n=11 adult females, 13 adult males, 4 subadults, defined as individuals with unfused ring apophyses), 92 modern humans (*H. sapiens*) from the Hamann-Todd collection at the Cleveland Museum of Natural History (n=49, 23, 22; subadult humans sampled ranged in known age from 5–16 years), and available fossil hominins.

We studied original fossils of the following taxa: *Au. afarensis* (A.L. 288-1, A.L. 333, 333x, 333w, and 444 specimens, KSD-VP-1/1), *Au. africanus* (Sts 14, Sts 73, StW 431, StW 8/41, StW 458, StW 572), *Au. robustus* (SKW 4776, SKX 41692, SK 3981a and b, SK 853), *H. erectus* (KNM-WT 15000, Dmanisi Skull 3 individual), and *H. naledi* (U.W. 101 and U.W. 102). For serial identification of vertebral and costal elements used in comparative analyses, we follow published accounts (Berger et al. 2015; Cook et al. 1983; Haeusler et al. 2002, 2012; Hawks et al. 2017; Johanson et al. 1982; Latimer et al. 2016; Lovejoy et al. 1982; Meyer 2005, 2016; Meyer et al. 2015, 2017; Robinson 1972; Sanders 1995, 1998; Ward et

TABLE 1. INVENTORY OF THE MH1 VERTEBRAE (juvenile male *Australopithecus sediba*).

Specimen	Anatomical Position ¹	Body ²	Neural Arch ²	Transverse Processes ²	Spinous Processes ²
U.W. 88-71	n.-h.				
U.W. 88-73	n.-h.				
U.W. 88-72	C3	p	p	p	p
U.W. 88-9	C7	c	c	c	c
U.W. 88-11	upper T	c	c	c	c
U.W. 88-37	middle T	c	c	c	c
U.W. 88-69	lower T	p	p	c	p
U.W. 88-70	lower T	p	p	c	p
U.W. 88-90	lower T	p	p	c	-
U.W. 88-92	middle L	c	c	c	c
U.W. 88-152	middle L	c	c	p	p

¹n.-h.=determined to be a non-hominin vertebral fragment; C=cervical; T=thoracic; L=lumbar.

²c=complete or largely preserved; p=partial; -=not preserved.

al. 2012; Williams et al. 2017). Our seriation of the *Au. sediba* ribs and vertebrae (Figure 1) are mostly consistent with that found in Schmid et al. (2013) and Williams et al. (2013), with some minor revisions reflecting new findings.

The measurements reported in quantitative analyses are based on the Martin measurements defined in Bräuer (1988) and supplemented with additional measurements, following the published literature (e.g., Bonmatí et al. 2010; Franciscus and Churchill 2002; Gómez-Olivencia et al. 2013; Jellema et al. 1993; Latimer and Ward 1993; Meyer 2005; Robinson 1972; Sanders 1995; White et al. 2011; Williams et al. 2017). All linear measurements are presented in mm; angles are presented in degrees (°). Directional anatomical abbreviations used in this manuscript include the following:

DV, dorsoventral(ly); SI, superior-inferior(ly); IE, internal-external(ly); ML, mediolateral(ly); PD, proximodistal(ly).

They are as follows (Martin measurements [defined in Bräuer 1988] are shown as M#):

1. Vertebral body superior transverse width (MαW7): defined in Bräuer (1988) as the superior vertebral body transverse diameter at the most laterally projecting points.
2. Vertebral body superior dorsoventral length (Mα4): defined in Bräuer (1988) as the superior vertebral body DV diameter measured at the sagittal midline.
3. Vertebral body inferior transverse width (Mα8): defined in Bräuer (1988) as the inferior vertebral body transverse diameter at the most laterally projecting

TABLE 2. INVENTORY OF THE MH1 RIBS (juvenile male *Australopithecus sediba*).

Specimen	Anatomical Position ¹	Side ¹	Preserved Anatomical Portions ¹					
			Head	Neck	Tubercle	Posterior Angle	Shaft	Sternal End
U.W. 88-148	1	r	p	c	c	-	c	c
U.W. 88-86/41	6 (or 7)	r	-	p	c	c	p	c
U.W. 88-15/131	6 (or 7)	l	-	p	c	c	p	-
U.W. 88-155	7 (or 8)	l	-	-	-	p	p	-
U.W. 88-165	7-9	r	-	-	-	-	p	-
U.W. 88-74	7-9	l	-	-	-	-	-	c
U.W. 88-17	11-12	l	-	-	-	-	p	-
U.W. 88-13	?	r	-	-	-	-	p	c
U.W. 88-141	?	r	-	-	-	-	p	-

¹?=indeterminate; r=right; l=left; c=complete or largely preserved; p=partial; -=not preserved.

TABLE 3. INVENTORY OF THE MH2 VERTEBRAE (adult female *Australopithecus sediba*).

Specimen	Anatomical Position ¹	Body ²	Neural Arch ²	Transverse Processes ²	Spinous Processes ²
U.W. 88-93	C3	c	c	c	c
U.W. 88-83	C6	c	p	c	p
U.W. 88-188 ³	upper T	c	p	c	-
U.W. 88-189 ³	middle T	c/o	p/o	c	p
U.W. 88-190 ³	mid-low T	p/o	p/o	c/o	p
U.W. 88-191 ³	mid-low T	p/o	p/o	p/o	p
U.W. 88-96	mid-low T	-	p	p	p
U.W. 88-114 ³	antepenult. T	c/o	p/o	c/o	c/o
U.W. 88-43 ³	penult. T	c/o	c/o	c/o	c/o
U.W. 88-44 ³	last T	c/o	c/o	c/o	p/o
U.W. 88-127/153	penult. L	c	p	-	p
U.W. 88-126/138	last L	c	p	p	c
U.W. 88-137/125	S1-5	p	p	p	p

¹C=cervical, T=thoracic, L=lumbar, S=sacral.

²c=complete or largely preserved; p=partial; o=obscured by matrix/other fossils; -=not preserved. "/o" indicates that one part or one side of the specimen is obscured.

³Specimen remains partially encased in matrix and was virtually rendered.

- points.
4. Vertebral body inferior dorsoventral length (MαW5): defined in Bräuer (1988) as the inferior vertebral body DV diameter measured at the sagittal midline.
 5. Vertebral body superior-inferior ventral height (MαW1): defined in Bräuer (1988) as the ventral SI height of the vertebral body at the sagittal midline.
 6. Vertebral body superior-inferior dorsal height (MαW2): defined in Bräuer (1988) as the dorsal SI height of the vertebral body at the sagittal midline.
 7. Vertebral body wedging angle: calculation provided in DiGiovanni et al. (1989) as [arctangent (((SI dorsal height-superior DV length)/2)/SI ventral height)*2)].
 8. Spinal canal dorsoventral length (MαW10): defined in Bräuer (1988) as DV spinal canal diameter measured at the sagittal midline.

TABLE 4. INVENTORY OF MH2 RIBS (adult female *Australopithecus sediba*).

Specimen	Anatomical Position ¹	Side ¹	Preserved Anatomical Portions ¹					
			Head	Neck	Tubercle	Posterior Angle	Shaft	Sternal End
U.W. 88-198 ²	1	r	c	c	c	c	c	c
U.W. 88-187	1	l	c	c	p	-	-	-
U.W. 88-58	2	r	-	p	c	c	p	-
U.W. 88-178	2	l	c	c	c	-	-	-
U.W. 88-166	3	r	c	c	p	c	p	-
U.W. 88-61	4	r	-	p	c	c	c	c
U.W. 88-167/154	5	r	-	p	c	c	p	c
U.W. 88-145	?	r	-	-	-	-	p	-
U.W. 88-147	?	r	-	-	-	p	p	-
U.W. 88-192	?	l	-	-	-	-	p	-
U.W. 88-193	?	l	-	-	-	-	p	-
U.W. 88-59	?	?	-	-	-	-	p	-
U.W. 88-60	9 (or 10)	r	-	-	-	-	p	-
U.W. 88-143	?	?	-	-	-	-	p	-
U.W. 88-144	?	?	-	-	-	-	p	-
U.W. 88-199	?	?	-	-	-	-	p	-

¹?=indeterminate; r=right; l=left; c=complete or largely preserved; p=partial; -=not preserved.

²Specimen remains partially encased in matrix and was virtually rendered.

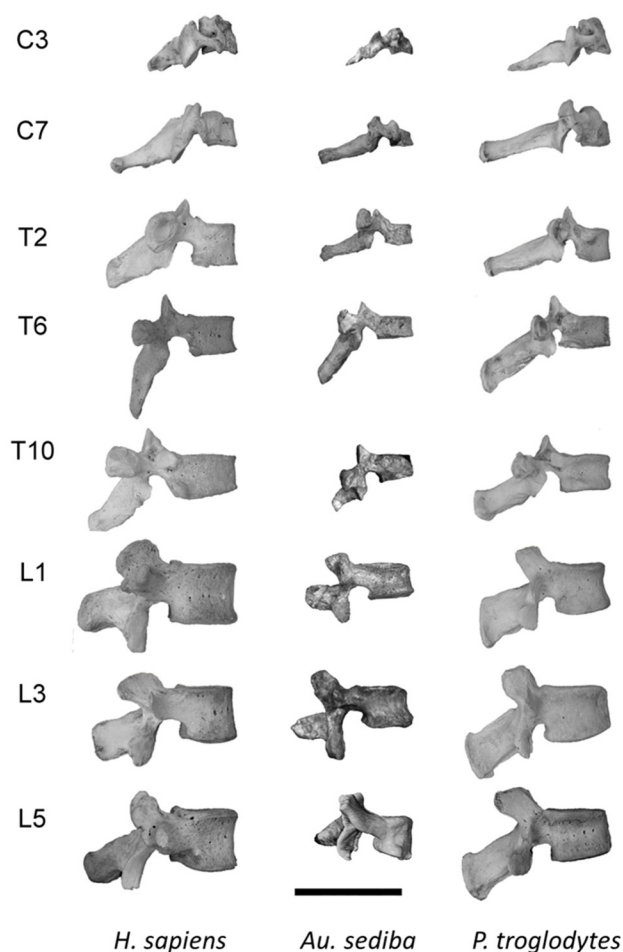


Figure 1. The most complete vertebrae free of breccia belonging to MH1 and MH2. *Au. sediba* (middle) is flanked by corresponding adult human (left) and chimpanzee (right) vertebrae. Many of the MH2 vertebrae are still embedded in matrix. Just two (C3, L5) are shown here; the remainder (those of MH1) have not completed vertebral body growth (scale is 50mm).

9. Spinal canal transverse width (MαW11): defined in Bräuer (1988) as transverse spinal canal diameter measured at the roots of the vertebral arch.
10. Superior-inferior inter-articular facet height: SI inter-articular facet distance, measured from the most superior aspect of the superior articular facet (SAF) to the most inferior aspect of the inferior articular facet (IAF) on the same side. The right side is measured unless it is broken or pathological, in which case the left side is measured. If the two sides are asymmetrical and one is not pathological, the mean is recorded.
11. Maximum inter-SAF transverse width: maximum (max.) inter-SAF distance, measured from the lateral aspect of one superior articular facet to the lateral aspect of the other.
12. Minimum inter-SAF transverse width: minimum (min.) inter-SAF distance, measured from the medial aspect of one superior articular facet to the medial aspect of the other.

13. Maximum inter-IAF transverse width: maximum (max.) inter- IAF distance, measured from the lateral aspect of one inferior articular facet to the lateral aspect of the other.
14. Minimum inter-IAF width: minimum (min.) inter-IAF distance, measured from the medial aspect of one inferior articular facet to the medial aspect of the other.
15. SAF superior-inferior height: SAF SI diameter, measured at the sagittal midline. The right side is measured unless it is broken or pathological, in which case the left side is measured. If the two sides are asymmetrical and one is not pathological, the mean is recorded.
16. SAF transverse width: SAF transverse diameter, measured from the most medial to the most lateral border of the articular surface. The right side is measured unless it is broken or pathological, in which case the left side is measured. If the two sides are asymmetrical and one is not pathological, the mean is recorded.
17. IAF superior-inferior height: IAF SI diameter, measured at the sagittal midline. The right side is measured unless it is broken or pathological, in which case the left side is measured. If the two sides are asymmetrical and one is not pathological, the mean is recorded.
18. IAF transverse width: IAF transverse diameter, measured from the most medial aspect to the most lateral border of the articular surface. The right side is measured unless it is broken or pathological, in which case the left side is measured. If the two sides are asymmetrical and one is not pathological, the mean is recorded.
19. Spinous process angle (MαW12): defined in Bräuer (1988) as the angle that is formed from the superior surface of the vertebral body and the upper edge of the spinous process. We modify this measurement slightly by measuring the angle along its long axis, which allows for the inclusion of fossils with a damaged or missing superior edge of the spinous process. An angle of 180° is equivalent to a spinous process with a long axis parallel to the superior surface of the vertebral body (i.e., horizontal or neutral in orientation).
20. Spinous process length (MαW13): defined in Bräuer (1988) as the distance from the top edge of the vertebral arch to the most dorsal tip of the spinous process. Measured with calipers.
21. Transverse process dorsoventral angle: the dorsoventral angle that is formed from the sagittal midplane of the vertebra to the long axis of the transverse process, along the middle from its base to its tip. This contrasts with Ward et al. (2012), where the transverse process angle is measured along the costal facet. We justify the use of the long axis because lower thoracic vertebrae and lumbar vertebrae lack costal facets. The right side is measured unless it is broken or pathological, in which case the left side is measured. If the two sides are asymmetrical and one is not pathological, the

- mean is recorded.
22. Transverse process length: the distance from the internal edge of the spinal canal at its closest point to the base of the transverse process to the tip of the transverse process. The right side is measured unless it is broken or pathological, in which case the left side is measured. If the two sides are asymmetrical and one is not pathological, the mean is recorded.
 23. SAF orientation: the angle formed between the sagittal midplane of the vertebra to the medial and lateral edges of the SAF. The right side is measured unless it is broken or pathological, in which case the left side is measured. If the two sides are asymmetrical and one is not pathological, the mean is recorded.
 24. Pedicle superior-inferior height: SI diameter of the pedicle, measured at its midpoint. The right side is measured unless it is broken or pathological, in which case the left side is measured. If the two sides are asymmetrical and one is not pathological, the mean is recorded.
 25. Pedicle transverse width: transverse breadth of the pedicle, measured at its midpoint. The right side is measured unless it is broken or pathological, in which case the left side is measured. If the two sides are asymmetrical and one is not pathological, the mean is recorded.
 26. Pedicle dorsoventral length: DV diameter of the pedicle, measured anterior from its junction with the superior articular process to its junction with the dorsal edge of the vertebral body. The right side is measured unless it is broken or pathological, in which case the left side is measured. If the two sides are asymmetrical and one is not pathological, the mean is recorded.
 27. Lamina superior-inferior height: SI dimension of the lamina, measured on one side between the spinous process and the SAF and the IAF. The right side is measured unless it is broken or pathological, in which case the left side is measured. If the two sides are asymmetrical and one is not pathological, the mean is recorded.
 28. Lamina transverse width: transverse dimension of the lamina, measured at its minimum breadth across the pars interarticularis.
 29. Rib shaft superior-inferior height (M β R1): maximum SI height of the rib shaft.
 30. Rib shaft internal-external thickness (M β R2): maximum IE thickness of the rib shaft.
 31. Rib articular tubercle superior-inferior height: maximum height of the costo-transverse articular tubercle. From Franciscus and Churchill (2002).
 32. Rib articular tubercle mediolateral width: maximum ML width of the cost-transverse articular tubercle. From Franciscus and Churchill (2002).
 33. Rib neck superior-inferior diameter: minimum SI height of the rib neck (between the articular tubercle and the distal articular margin of the head). From Franciscus and Churchill (2002).
 34. Rib neck internal-external width: minimum IE width of the neck of the rib.
 35. Manubrium sterni superior-inferior length (M β S2): SI length of the manubrium at midline.
 36. Manubrium sterni maximum mediolateral breadth (M β S4): Maximum ML breadth of the manubrium.
 37. Manubrium sterni mediolateral breadth at rib 1: ML breadth of the manubrium measured from the center of the 1st rib articulation. Illustrated in White et al. (2011).

Raw data on *Au. sediba* fossils are published in Tables A1-A4. Measurements were taken with Mitutoyo digital calipers and a clear plastic 180° medical goniometer on the original fossils and reported at the tenth decimal place. Linear measurements are log₁₀ transformed for the creation of biplots (with 95% confidence ellipses for extant taxa). Angles and ratios created from raw linear measurements are shown in boxplots for visualization purposes. Three-dimensional models of the material presented in this manuscript that could be feasibly laser scanned or segmented from microCT scans are available for download by registered users at <https://www.morphosource.org/>.

RESULTS

CERVICAL VERTEBRAE OF MH1

U.W. 88-72: Upper Cervical Vertebra

U.W. 88-72 is a partial cervical vertebra preserving the inferior aspect of the right side of the vertebral body and most of the neural arch (Figure A1). The inferior surface of the body lacks a ring apophysis. The right pedicle, IAF, and partial transverse foramen are preserved. The lamina is nearly complete, with the left side sheared off at the pars interarticularis. The base of the spinous process is present, but the process is broken distally. The left side of the vertebral body is sheared ventrolaterally such that the superior aspect of the body is missing, along with the left side of the inferior body. The left SAF, both IAFs, and transverse process are missing. The neural arch is broken on both sides at the lamina and has been refit. Much of what is preserved of this element is abraded, obscuring potentially informative morphology.

The inferior vertebral body measures 11.1mm DV at the midline. When the preserved right portion of the vertebral body is measured to the sagittal midline and doubled, the inferior vertebral body is estimated to be 13.5mm in the widest transverse dimension. The spinal canal measures approximately 16mm transversely by 14mm DV. The preserved right IAF measures 9.2mm DI and 8.9mm in transverse diameter. The facet can be measured to the sagittal midline of the vertebra and doubled, resulting in maximum and minimum inter-IAF transverse widths of approximately 36.6mm and 19mm, respectively. The preserved spinous process is very short (7.8mm DV) and is probably broken distally.

Because the superior aspects of the vertebral body and the SAFs are missing, most of the diagnostic morphol-

ogy used to differentiate the axis (C2) from subaxial cervical vertebrae is not present and therefore cannot be used to assess the identity of this vertebra. The ventral end of the inferior vertebral body projects inferiorly as in both C2 and C3 vertebrae, but not in other cervical vertebrae. The exposed region lateral to the superiorly sheared vertebral body is wide dorsoventrally, obscuring the transverse foramen in superior view. In this morphology, U.W. 88-72 is somewhat similar to C2 vertebrae; however, the IAF is positioned lateral to the lamina rather than directly on it as in C2 vertebrae. Therefore, we consider this specimen to be a C3 vertebra.

Compared to extant taxa and other fossil hominin taxa, both adult and subadult *Au. sediba* specimens fall out with chimpanzees in having small body dimensions. In contrast, large male *Au. afarensis* (KSD-VP-1/1i) and juvenile *H. erectus* from Dmanisi (D2674) fall within the 95% confidence intervals of human adults and subadults. The maximum and minimum transverse distances between IAFs largely separate humans from chimpanzees (Figure A3). U.W. 88-72, U.W. 88-93, and KSD-VP-1/1i fall out with chimpanzees. In contrast, D2674 falls just outside the chimpanzee 95% ellipse and within those of adult and subadult humans. The relative lengths of the spinous processes of both *Au. sediba* specimens fall within the ellipses of human subadults, while that of D2674 falls within the overlapping 95% ellipses of human subadults and adults (see Figure A3). The KSD-VP-1/1i spinous process is long and well within the range of chimpanzees.

U.W. 88-9: Last Cervical Vertebra

U.W. 88-9 is a complete last cervical (C7) vertebra missing only the inferior one-third of the left IAF (Figure 2). The vertebral body lacks ring apophyses, consistent with the juvenile status of MH1. The ventral aspect of the body is cracked superiorly and abraded somewhat inferiorly.

The vertebral body is wide transversely (maximum measurement of 17.1mm) relative to the DV measurement (10.4mm at the sagittal midline), with tall uncinat processes (5.3mm in SI height on average, measured from the lateral aspects of the superior vertebral body). The vertebral body measures 7.1mm in superoinferior ventral height at the midline and 7.7mm in dorsal height. The spinal canal is triangular in shape, measuring 10.8mm in DV length and 17.5mm in transverse width.

The transverse processes bear asymmetrical transverse foramina and the left one is significantly larger than the right. The SAFs, which measure 10.7mm in transverse width and 8.6mm in SI height on average, lead into shelf-like non-articular fossae on the laminae. The IAFs measure 12.4mm wide and 8.9mm tall on average. The maximum and minimum inter-SAF transverse distances are 37.6mm and 17.2mm, respectively; maximum and minimum inter-IAF distances are 37.3mm and 15.9mm. The SI inter-articular facet height is 17.9mm.

The spinous process is 26.3mm in DV length and oriented at 165° relative to the coronal plane. It terminates in a blunt, flat, rounded terminus that lacks an epiphysis. The

lamina measures 9.4mm in SI height and 36.3mm in transverse width at the *pars interarticularis*.

Compared to extant samples and other fossil hominin last cervical vertebrae, the U.W. 88-9 vertebral body is small, especially in superior transverse width, where it falls far from the human distribution and within the 95% confidence ellipse of chimpanzees (Figure A4). In contrast, KNM-WT 15000 R (*H. erectus*) falls well within the human 95% ellipse (although there is extensive overlap with chimpanzees as well). The inferior body dimensions are both larger, with U.W. 88-9 falling within the subadult human 95% confidence ellipse (see Figure A4). The vertebral body is short in SI height relative to the SI inter-articular facet height as in subadult humans, chimpanzees, and juvenile *H. erectus* KNM-WT 15000 R (Figure A5), consistent with incomplete SI vertebral body growth. Spinal canal dimensions place U.W. 88-9 in the middle of the chimpanzee distribution, well below both transverse and DV dimensions in humans (Figure A6). KNM-WT 15000 R also falls outside the human 95% ellipses and within those of chimpanzees, whereas *Au. afarensis* (KSD-VP-1/1a) falls out well within the human distribution. Figure A6 shows that both the vertebral body and spinal canal transverse dimensions are small in U.W. 88-9, in contrast with KNM-WT 15000 R. The spinous process length of U.W. 88-9 is well within the distributions of humans and chimpanzees, but its angle is only slightly caudally-oriented, outside the range of human variation and well within the chimpanzee distribution (Figure A7). KNM-WT 15000 R produces an even higher angle, outside the range of adult chimpanzees (Figure A7).

THORACIC VERTEBRAE OF MH1

U.W. 88-11: Upper Thoracic Vertebra

U.W. 88-11 is a mostly complete upper thoracic vertebra (Figure 3). The left inferior aspect of the spinous process is chipped away, and the lateral edge of the left articular facet, pedicle, body, and IAF are sheared off, along with the entire left transverse process. The right SAF is abraded a small amount superiorly. Ring apophyses are not present on the vertebral body.

U.W. 88-11 does not articulate with U.W. 88-9, yet is clearly an upper thoracic vertebra. The SAFs are widely spaced, the vertebral body and spinal canal are wide relative to their DV dimensions, and the spinous process orientation is not drastically distinct from that of U.W. 88-9, suggesting U.W. 88-11 is the second thoracic vertebra (T2). The vertebral body measures 20.4mm at its maximum transverse dimension (measured from the right side to midline and doubled) and 12mm at the sagittal midline. Midline ventral and dorsal SI body heights are 8.7mm and 9.1mm, respectively.

The spinal canal is ovoid in shape (DV length of 9.5mm in sagittal diameter; 13.3mm in transverse diameter). The pedicles measure 8.2mm in SI height and 6.5mm in transverse width. Shelf-like fossae sit just inferior to the SAFs on the laminae. The SAFs are both damaged slightly, the right one superiorly and the left one laterally, but trans-



Figure 2. U.W. 88-9 (MH1) in dorsal (top left), ventral (top right), superior (middle left), inferior (middle right), left lateral (bottom left), and right lateral (bottom right) views (scale is 50mm).

verse (9.5mm) and SI (9mm) measurements can be taken on each one, respectively.

The spinous process (25.9mm long) projects dorsoinferiorly at an angle of 158° relative to the coronal plane. The transverse processes (average of 17.8mm in length) form a 60° angle measured dorsally relative to the sagittal midline. Maximum and minimum inter-SAF transverse widths measure 29.6mm and 11.4mm, and maximum and minimum inter-IAF distances measure 26mm and 9.8mm, respectively.

Vertebral body transverse and DV dimensions in U.W. 88-11 fall within the overlap between chimpanzees and human subadult 95% confidence ellipses (Figure A8). Other fossil hominin T2 vertebrae (A.L. 333-81 *Au. afarensis*; KNM-WT 15000 T *H. erectus*) fall within the overlap of chimpanzees and adult and subadult humans. Vertebral body SI height measurements are short relative to SI inter-articular facet height (21.3mm) (Figure A9), in accordance with its juvenile developmental age and incomplete centrum growth. The spinal canal of U.W. 88-11 falls well within the 95% confidence ellipses of chimpanzees, whereas KNM-WT 15000 T is juxtaposed at the boundary of the extensively overlapping adult and subadult human ellipses (Figure A10). The spinous process angle of U.W. 88-11 is quite horizontal

(158°) relative to the coronal plane of the vertebra, on the high end of the human distribution, but close to the median chimpanzee value (Figure A11). Its transverse process is dorsally angled at $\sim 60^\circ$ relative to the sagittal midline, which is at the low end of the human and especially the chimpanzee distributions (see Figure A11). In both angles, the KNM-WT 15000 T processes are more extreme than U.W. 88-11, falling outside the human and chimpanzee distributions.

U.W. 88-37: Middle Thoracic Vertebra

U.W. 88-37 is a complete middle thoracic vertebra (Figure 4). Its vertebral body is crushed ventrally on the right side, probably a result of taphonomic damage. A lytic lesion is present on the right side of the spinous process and continues anteriorly into the lamina, presenting a large fossa approximately one third the length of the spinous process and one third the height of the lamina. The superior aspect of the spinous process is convex above the lesion and therefore represents remodeling. The pathology is described in detail, and differential diagnoses for the pathology are provided, in a separate study (Randolph-Quinney et al. 2016). The vertebral body lacks ring apophyses.

The vertebral body is somewhat heart-shaped from superior view (DV length of 14.6mm at the midline of the



Figure 3. U.W. 88-11 (MH1) in inferior (top left), superior (top right), dorsal (middle left), ventral (middle right), right lateral (bottom left), and left lateral (bottom right) views (scale is 50mm).

superior vertebral body, transverse width of 18.9mm across the widest point of the superior body; corresponding inferior vertebral body measurements are 15.6mm and 22.6mm, respectively). Ventral body SI height at midline measures 9.1mm and dorsal body height at midline 10.3mm.

The spinal canal is ovoid in shape (DV length of 8.7mm, 11.5mm in transverse diameter). Pedicles are taller (9mm in SI height) than they are wide (4.7mm in transverse width). Maximum inter-SAF and inter-IAF transverse widths measure 21.3mm and 23.2mm, respectively. Minimum inter-SAF and inter-IAF transverse distances are 8.3mm and 7.2mm, respectively. The spinous process (30mm in DV length) projects dorsoinferiorly at an angle of 124° relative to the coronal plane. From superior view, the transverse processes (average of 17.5mm in length) are angled at 54° relative to the sagittal midplane.

Assessment of the serial position of this vertebra is difficult in the absence of closely-associated vertebrae. Many features demonstrate characteristics common to upper mid-thoracic vertebrae (e.g., spinous and transverse pro-

cess morphology, articular facet and lamina morphology, and vertebral body and spinal canal shape); therefore, we allocate U.W. 88-37 to the T4, T5, or T6 level (see also Randolph-Quinney et al. 2016).

U.W. 88-37 produces vertebral body dimensions that fall within the human subadult 95% confidence ellipse, along with small (presumed female) *Au. afarensis* and *Au. africanus* middle thoracic vertebrae (Figure A12). Juvenile male *H. erectus* and large (presumed male) *Au. afarensis* are characterized by adult human- and chimpanzee-sized body dimensions. SI vertebral body height is short relative to SI inter-articular facet height (22.7mm) in the *Au. sediba* and *H. erectus* juveniles (KNM-WT 15000), reflecting incomplete SI vertebral body growth (Figure A13). In contrast, adult *Au. afarensis* and *Au. africanus* produce vertebral body height ratios like adult humans and chimpanzees, consistent with completed growth (Figure A14).

The spinal canal of U.W. 88-37 is fairly restricted, particularly in the DV dimension (see Figure A14). This cannot be accounted for by MH1's juvenile age since the subadult



Figure 4. U.W. 88-37 (MH1) in right lateral (top left), left lateral (top right), inferior (middle left), superior (middle right), dorsal (bottom left), and ventral (bottom right) views (scale is 50mm).

humans and chimpanzees included in this comparative sample (which includes individuals of similar developmental age to MH1) do not demonstrate shorter DV spinal canal dimensions than adults (see Figure A14). In contrast, adult *Au. sediba* U.W. 88-189 falls out closer to the adult human 95% confidence ellipse, and juvenile *H. erectus* falls within the adult and subadult human distributions. If the spinal canal dimensions are standardized by vertebral body dimensions, while U.W. 88-37 and U.W. 88-189 fall outside the range of adult human and chimpanzee variation in relative spinal canal DV length, they fall within or very near the chimpanzee and human subadult ellipses (Figure A15). In contrast, adult *Au. afarensis* and *Au. africanus* fall in or near the human and chimpanzee ellipses for relative spinal canal length, but well outside them for relative spinal canal width. Whereas *Au. afarensis* falls within or very near the human distributions for relative spinal canal DV length, only juvenile *H. erectus* falls out with humans in both rela-

tive dimensions.

The spinous process of U.W. 88-37 angles inferiorly at 124° relative to the coronal plane; the transverse process angles dorsally at 54° relative to the sagittal midplane (Figure A16). U.W. 88-37 falls within the human distribution and outside that of chimpanzees for spinous process orientation, as do Sts 14 and A.L. 288-1, whereas A.L. 333-x26 and KNM-WT 15000 plot with chimpanzees, outside the sample of modern humans. For transverse process orientation, where humans and chimpanzees overlap more extensively, nearly all fossil hominins fall within the range of humans (U.W. 88-37, Sts 14, A.L. 333-158, and KNM-WT 15000), the latter two also overlapping with the chimpanzee distribution. The transverse process angle of A.L. 288-1 is nearly perpendicular to the sagittal midplane and plots with chimpanzees outside the range of human variation recorded in this sample. Adult female *Au. sediba* U.W. 88-189, considered a T6 in this study (see below), falls outside hu-



Figure 5. U.W. 88-70 (MH1) in superior (top left), inferior (top right), right lateral (middle left), left lateral (middle right), ventral (bottom left), and dorsal (bottom right) views (scale is 50mm).

man, chimpanzee, and fossil hominin distributions.

U.W. 88-69: Lower Thoracic Vertebra

U.W. 88-69 is a partial lower thoracic vertebra (Figure 5). It is missing the right transverse process and ventrolateral aspect of the vertebral body. Much of the ventral portion of the vertebral body is missing, especially on the right side. One of each of the SAFs and IAFs are complete, the left and right, respectively, while the other sides are damaged. The distal aspect of the spinous process is nearly complete on the left side, but missing on the right.

The vertebral body measures 13mm in SI height at midline. Pedicles are tall (7.9mm in SI height) and narrow (4.1mm in transverse width). The preserved left side of the body bears a superior demifacet, but there does not appear to be an inferior one, consistent with a human T9 or T10. Vertebral body SI height is short relative to SI interarticular facet height (25.9mm), in accordance with MH1's juvenile status. The superior and inferior vertebral bodies lack ring apophyses.

The spinal canal is teardrop-shaped, longer than it is wide (DV length of 9.6mm, transverse width of 11.2mm). The complete left SAF measures 9.1mm in SI height and 6.7mm in transverse width. The complete right IAF measures 10mm SI and 8.4mm transversely. The spinous process appears to be relatively short dorsoventrally, but is

abraded distally and projects dorsoinferiorly at an angle of 139° relative to the coronal plane. The transverse process (left side: 16.6mm in length from the neural arch) angles 61° relative to the sagittal midplane and its inferior aspect arcs inferiorly between the IAFs. The transverse process does not bear a costal facet, which is not typical of human T10 vertebrae, but is consistent with morphology observed in MH2 (see below) and possibly A.L. 288-1 (Meyer et al. 2015).

Relative SI vertebral body height is short in juvenile U.W. 88-69 compared to other fossil hominin T9 or T10 vertebrae, which belong to adults (Figure A17). As with other australopiths, U.W. 88-69 produces a relatively small spinal canal, particularly in dorsoventral diameter (Figure A18). It falls closest to *Au. robustus* (SKX 41692), similar in transverse width to *Au. afarensis* specimens (A.L. 288-1ad and A.L. 333x-12) and larger than female *Au. africanus* (Sts 14l), but smaller than that of *H. naledi* (U.W. 101-855 and U.W. 102-036). All available fossil spinal canals fall outside the human distributions and within the chimpanzee 95% ellipse, except Sts 14l, which is transversely narrower. Spinous and transverse process angles of U.W. 88-69 fall out well within the human adult and subadult distributions (Figure A19). Only A.L. 288-1ad and SKX 41692 fall outside the human range of variation, the former within the chimpanzee distribution, and the latter at a low angle just outside the human range at the antepenultimate vertebral level.

U.W. 88-70: Lower Thoracic Vertebra

U.W. 88-70 is a lower thoracic vertebra fragment that preserves portions of the left side of the vertebra (Figure A20). Only the left partial body and neural arch, including transverse process, IAF, pedicle, partial SAF and spinous process are preserved. The inferior aspect of the vertebral body lacks a ring apophysis.

The partial spinous process appears to project dorsoinferiorly at an angle of approximately 145° relative to the coronal plane. The transverse process is short and does not bear a costal facet, consistent with human T11 and T12 vertebrae. Its morphology is somewhat intermediate between that observed in MH2's antepenultimate (U.W. 88-114) and penultimate (U.W. 88-43) thoracic vertebrae. The IAF is relatively flat and faces anteriorly and slightly medially. From superior view, the lateral aspect of the preserved inferior vertebral body flares laterally.

U.W. 88-90: Lower Thoracic Vertebra

U.W. 88-90 is a lower thoracic vertebra that, like U.W. 88-70, represents less than one-half of the original element (Figure A21). It preserves the right aspects of the vertebral body, pedicle, transverse process, and IAF. The vertebral body lacks ring apophyses.

The lateral wall of the vertebral body is vertical, and the inferior body does not flare laterally as in U.W. 88-70. The SAF itself is not preserved, but its base just dorsal to the superior aspect of the pedicle is present. As such, it is not possible to determine the orientation of the SAF. The



Figure 6. U.W. 88-92 (MH1) in right lateral (top left), ventral (top middle), left lateral (top right), superior (bottom left), dorsal (bottom middle), and inferior (bottom right) views (scale is 50mm).

IAF is preserved laterally and can be seen to angle ventrally and somewhat laterally. The transverse process is short, lacks a costal facet, and resembles that of U.W. 88-70 quite closely. While it is possible that U.W. 88-90 and U.W. 88-70 represent parts of the right and left sides of the same vertebra, respectively, differences in IAF orientation and aspects of lateral vertebral body morphology suggest that the two fragments are from different vertebrae. Given similarities in transverse process morphology, it is possible or even likely that U.W. 88-90 is directly subjacent to U.W. 88-70.

LUMBAR VERTEBRAE OF MH1

U.W. 88-92: Upper Lumbar Vertebra

U.W. 88-92 is an upper lumbar vertebra (Figure 6). The superior vertebral body is complete; the inferior vertebral body is missing a small amount of the lateral left side dorsally. The right lumbar transverse process is broken, though not detached, and deflected supra-medially such that the lateral end of the process is oriented supra-laterally rather than directly laterally as it would lie naturally; a crack along the middle of the transverse process is visible dorsally and especially ventrally. The left lumbar transverse process is broken distally and is preserved only at its base. The left inferior articular facet is broken and missing, but the other articular facets are minimally damaged. The spinous process is complete but lacks a distal epiphysis. Ring apophyses are not present on the superior or inferior vertebral bodies.

The superior vertebral body is somewhat heart-shaped, and measures 29.1mm in transverse width and 20.1mm in

DV length at the midline. Due to the shape of the dorsal border of the vertebral body, the spinal canal is ovoid rather than triangular in shape (14.8mm in transverse width, 9.8mm in DV length). In both of these features, U.W. 88-92 more closely resembles human upper lumbar vertebrae than those of chimpanzees. As with cervical and thoracic vertebrae of MH1, the vertebral body is superior-inferiorly short (15.7mm ventrally, 17.1mm dorsally) relative to the SI inter-articular facet height (35.8mm) (Figure A22). The vertebral body is ventrally-wedged (4.0°), which is typical of upper lumbar vertebrae (Been et al. 2012; Ostrofsky and Churchill 2015; Sanders 1995; Whitcome et al. 2007).

In lateral view, the superior vertebral body is flush with the superior margin of the pedicles and meets the SAFs at their superior-inferior mid-points, whereas the IAFs extend well below the inferior margin of the centrum. This configuration is reminiscent of human lumbar vertebrae and contrasts with those of chimpanzees, which demonstrate the opposite pattern: SAFs that extend well above the superior vertebral body and IAFs that do not protrude far below the inferior vertebral body (S.A.W., personal observation,).

Mammillary processes are identifiable as mediolateral thicknesses on the dorsolateral aspects of the SAFs. The SAFs are fully curved in a strong dorsomedial orientation, measuring 11.5mm SI and 11.8mm transversely on average. The preserved right IAF is curved and oriented ventrolaterally, measuring 13.3mm in superior-inferior height and 9.6mm in transverse width.

The spinous process is 21.3mm long and oriented horizontally relative to the coronal plane of the vertebra (angled 184°). The spinous process is relatively thin dis-



Figure 7. U.W. 88-152 (MH1) in right lateral (top left), ventral (top middle), left lateral (top right), superior (bottom left), dorsal (bottom middle), and inferior (bottom right) views (scale is 50mm).

tally (3.8mm transversely by 12.8mm SI) and bears a sharp margin inferiorly for the interspinous ligament. The pedicles are taller in SI height (12.3mm) than they are in transverse width (6.5mm).

U.W. 88-92 falls out with juvenile humans and chimpanzees in its vertebral body height relative to SI inter-articular facet height, as does D2672 (juvenile *H. erectus*), whereas those of adult *Australopithecus* fall within the distribution of adult humans and chimpanzees (see Figure A22). When vertebral body size dimensions are compared, U.W. 88-92 falls out within the chimpanzee adult and human subadult 95% confidence ellipses, as do some adult australopiths (Figure A23).

Spinal canal dimensions of U.W. 88-92 are within the chimpanzee distribution, as are those of all early hominins. *Au. africanus* specimen StW 458 falls within the 95% ellipses for both subadult humans and adult chimpanzees, and outside the adult human distribution (Figure A24). Only the Dmanisi juvenile *H. erectus* (D2672) falls within the 95% confidence ellipses for adult humans. The spinous process of U.W. 88-92 is nearly horizontally-oriented relative to the coronal plane of the vertebra, and in fact is angled slightly superiorly, outside the range of the human and chimpanzee samples included in this study (Figure A25) but similar to *Au. africanus* specimen StW8b.

U.W. 88-152: Middle Lumbar Vertebra

U.W. 88-152 is a nearly-complete middle lumbar vertebra lacking only the left transverse process, which is broken distally at its base near the pedicle, and the distal end of the spinous process, which is broken superiorly and inferiorly

as it tapers distally (Figure 7). Ring apophyses are not present on the superior or inferior vertebral bodies.

The vertebral body is slightly dorsally wedged (-1.6° : SI vertebral body height at midline is 16.3mm; dorsal height of the vertebral body is 15.7mm) in lateral view. As with U.W. 88-92, the height of the vertebral body is short relative to the SI inter-articular facet height (36.5mm) (Figure A26). The superior body measures 32.3mm in transverse width and 21.9mm in DV length at the midline. In superior view, the vertebral body is wide and heart-shaped.

The spinal canal (9.4mm DV, 14.4mm transversely) is less elliptical and more triangular in shape than that of U.W. 88-92. The SAFs are concave, slightly curved, and dorso-medially oriented. They measure 14.1mm in SI height and 11.3mm in transverse width on average (IAFs are 14.1mm and 8.6mm, respectively).

Deep laminar fossae are present on the *pars interarticularis* just inferior to the SAFs. These fossae are non-articular, mechanically-induced concavities produced by habitual hyperextension at the inter-articular facet joints, where the inferior articular facets of the superjacent vertebra impinge onto the subjacent vertebra's lamina. They are particularly marked on this vertebra, but also present to a much less pronounced degree on U.W. 88-92. The spinous process is tapered, broken distally, and bears an excavated gash, probably of taphonomic origin, that travels supra-distally along the left side from its origin at the inferior base between the IAFs.

Unlike U.W. 88-92, the pedicles are thick transversely (8.6mm) and short superior-inferiorly (9mm); this is probably related in part to the DV thickness and position of

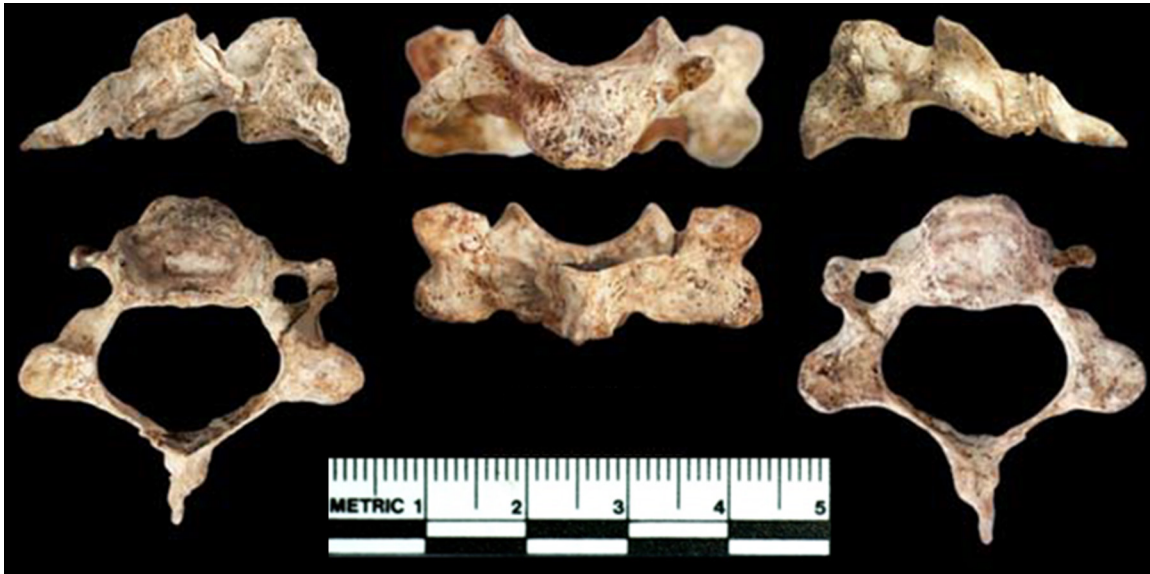


Figure 8. U.W. 88-93 (MH2) in right lateral (top left), left lateral (top right), superior (bottom left), inferior (bottom right), ventral (top middle), and dorsal (bottom middle) views (scale is 50mm).

the lumbar transverse processes in U.W. 88-152, which are somewhat more ventrally-placed than those of U.W. 88-92. The changes in mediolateral thickness of the pedicles and placement of the lumbar transverse processes are consistent with differences between non-adjacent vertebrae; the drastic change in SI height of the pedicles between U.W. 88-92 and U.W. 88-152 supports this contention.

Consistent with juvenile morphology, U.W. 88-152 presents a superior-inferiorly short vertebral body relative to its SI inter-articular facet height and falls at the low end of the subadult human distribution, far below that of adult humans (see Figure A26). In superior vertebral body dimensions, U.W. 88-152 falls within the subadult human and chimpanzee 95% ellipses along with StW 8c (*Au. africanus*) (Figure A27). Female australopiths, including Sts 14c (*Au. africanus*) and A.L. 288-1ak (*Au. afarensis*) fall within or very near the subadult ellipse, as does the juvenile SK 853 (*Au. robustus*). Larger, presumed male *Au. afarensis* A.L. 333-73 falls just inside the adult human ellipse and just outside that of chimpanzees, and also within the 95% ellipse for subadult humans. A.L. 444-7 is a very large individual that presents a transverse body width larger than the average adult human, but a DV dimension that is at the low end of adult human variation; therefore, it falls outside any of the confidence ellipses. Adult male *Au. africanus* (StW 431t) and juvenile male *H. erectus* (KNM-WT 15000 AB) lie within the overlap of all three ellipses.

In contrast with a moderately-sized vertebral body clearly larger than those of female australopiths, U.W. 88-152 presents a relatively small spinal canal (Figure A28). All australopiths fall within the chimpanzee 95% ellipse, as does KNM-WT 15000 AB, which also falls within the adult human ellipse. *Au. afarensis* is represented only by A.L. 288-1ak, which presents a large spinal canal, particularly in the DV dimension. Larger male *Au. afarensis* specimens (A.L.

333-73 and A.L. 444-7) do not preserve the spinal canal. Spinous process orientation in U.W. 88-152 is horizontal (180° relative to the coronal plane), falling at the extreme end of adult human variation (Figure A29). Other australopiths (A.L. 288-1ak, Sts 14c, and SK 853) possess more inferiorly-directed spinous processes and fall well within the human distribution. In contrast, KNM-WT 15000 AB (juvenile *H. erectus*) exhibits a spinous process that is angled superiorly, well outside the range of extant taxa.

CERVICAL VERTEBRAE OF MH2

U.W. 88-93: Upper Subaxial Cervical Vertebra

U.W. 88-93 is a nearly complete middle cervical vertebra (Figure 8). The dorsolateral aspect of the left transverse process is broken, but otherwise the vertebra is complete.

The vertebral body bears ring apophyses and measures 14.9mm in maximum transverse diameter and 10.7mm DV at midline. The ventral body measures 8.5mm in SI height, the dorsal body 8mm. The spinal canal measures 19.7mm at maximum transverse width and 14.6mm in DV length. The uncinate processes are tall, measuring approximately 8mm SI tall from the lateral aspect of the ventral body. The preserved SAF and IAF on the right side measure 8.2mm and 8.5mm in transverse width and 7.8mm and 9.8mm in SI height, respectively. The maximum inter-SAF transverse width is 36.3mm, the minimum 20.7mm, and the maximum and minimum inter-IAF widths are 37.3mm and 20mm, respectively. SI inter-facet height is 12.2mm, measured on the right side. The spinous process is 12.2mm long and is angled 144° inferiorly, measured relative to the coronal plane. The vertebral body's ventral aspect is inferiorly positioned relative to its dorsal aspect, creating a ventral slope of the body and an exaggerated inferior extension of the ventral body. This morphology is characteristic of upper subaxial

cervical vertebrae (C3 or C4) and not lower cervical vertebrae (C5-C7) (S.A.W., personal observation). Given the significantly larger size of U.W. 88-83 (see below), we follow Meyer et al. (2017) in treating U.W. 88-93 as a third cervical vertebra (C3).

U.W. 88-93 can be compared with C3 vertebrae from *Au. afarensis* (KSD-VP-1/1i) and Dmanisi *H. erectus* (D2674), as well as to the MH1 probable C3 vertebra, U.W. 88-72. In contrast with large-bodied male *Au. afarensis* and juvenile *H. erectus* from Dmanisi, which possess superior and inferior body dimensions within the range of human adult and subadult variation, *Au. sediba* specimens fall out with chimpanzees (see Figure A2, Figure A30). Although DV body length is within the range of variation of subadult humans, *Au. sediba* shows a chimpanzee-like, narrow transverse body width. In contrast, the spinal canal of U.W. 88-93 is within the range of adult and subadult humans, and along with D2674 also falls within the 95% confidence ellipse of chimpanzees (see Figure A2). Although KSD-VP-1/1i falls within the adult human ellipse, it is short in DV length relative to its wide transverse dimension. Compared to the other fossils, U.W. 88-93 has a dorsoventrally long spinal canal, but it is well within the variation observed in both humans and chimpanzees (see Figure A2).

Uncinate process height has been shown to be relatively tall in U.W. 88-93, outside the range of modern humans (where *Au. afarensis* and *H. erectus* fall) and within that of African apes and *Hyllobates* (Meyer et al. 2018). The maximum and minimum transverse widths between the SAFs and IAFs largely separate humans from chimpanzees (see Figure A3, Figure A30). U.W. 88-93 is closest to chimpanzees in both distances, but within the 95% ellipses of human subadults in the SAF metrics. The opposite pattern is true of D2674 (juvenile *H. erectus*), which falls within the human adult and subadult ellipses for IAF widths and within all three ellipses for the SAFs. KSD-VP-1/1i falls solely within the human ellipses for the SAF widths but solely within chimpanzees for the IAF widths. The length of the U.W. 88-93 spinous process falls within the range of both chimpanzees and humans but near the center of the human range (Figure A31). The U.W. 88-93 spinous process angle falls within an area of extensive overlap between humans and chimpanzees, as does D2674 (see Figure A31).

U.W. 88-83: Lower Cervical Vertebra

U.W. 88-83 is a partially complete lower cervical vertebra, missing its spinous process, left lamina and articular facets (both SAF and IAF), and the posterior aspect of the left transverse process (Figure 9). The vertebral body and right neural arch structures are nearly complete.

The vertebral body bears ring apophyses and measures 13.2mm in superior transverse width and 10.9mm in DV length, 8.2mm in SI ventral height, and 9.4mm in dorsal height at the midline. The spinal canal measures approximately 17.3mm in transverse width and 10.8mm in DV length. The left uncinat process is crushed, but the right uncinat process measures 5mm SI from the lateral aspect of the vertebral body. The preserved SAFs and IAFs on the

right side measure 9mm and 7.9mm in transverse width and 9.7mm and 10.3mm in SI height, respectively. SI interarticular facet height is 18.5mm.

U.W. 88-83 can be compared to two *Au. afarensis* specimens (A.L. 333-106 and KSD-VP-1/1i) and one specimen from Swartkrans that is thought to belong to *Au. robustus* (SKW 4776). Concerning vertebral body dimensions, whereas the *Au. afarensis* specimens falls within the human distribution, other australopiths fall within the chimpanzee 95% ellipse (Figure A32). The relative SI vertebral body height is within the range of adult humans (Figure A33). The spinal canal of U.W. 88-83 is also small, particularly in the DV dimension, and contrasts strongly with KSD-VP-1/1i, which falls at the high end of the human 95% confidence ellipse (see Figure A32). A.L. 333-106 falls between the two in DV length, but is relatively narrow in transverse dimension, similar to U.W. 88-83, and starkly distinct from KSD-VP-1/1i.

THORACIC VERTERAE OF MH2

U.W. 88-188: Upper Thoracic Vertebra

U.W. 88-188, U.W. 88-189, U.W. 88-190, and U.W. 88-191 are preserved in partial articulation in a block of breccia (Figure A34). This upper thoracic block of vertebrae was microCT scanned and segmented into 3D models of each vertebra. U.W. 88-188 is an upper thoracic vertebra (Figure 10). Its body is perpendicular to, and is held in matrix against, that of U.W. 88-189; however, these elements probably did not articulate in life. U.W. 88-188 has a complete vertebral body and left neural arch; the right side is sheared off at a ventro-inferior angle. The spinous process is not present.

The superior vertebral body of U.W. 88-188 is wide transversely, with a DV length of 11.6mm at the midline and a width of 18.8mm transversely across the widest point of the superior body (corresponding inferior body dimensions are 13.6mm and 23.4mm, respectively). The SI vertebral body height at midline measures 11.6mm ventrally and 11.9mm dorsally. Costal demifacets are visible and present on the left side of the body, as are ring apophyses both superiorly and inferiorly.

The spinal canal, although incomplete, would be ovoid in shape, with a dorsoventral length of 10.6mm and a width of 14.5mm in maximum transverse diameter. Pedicles are SI taller (8.2mm) than they are transversely wide (4.2mm). The left SAF measures 6.8mm transversely and 9.1mm SI. The relatively wide vertebral body and spinal canal, shelf-like superior aspects of the lamina/transverse process junction, relatively dorsally orientation of the transverse process, and dorso-lateral orientation of the SAF together suggest that this is an upper thoracic vertebra, but probably not the first thoracic (T1). Here, we tentatively identify U.W. 88-188 as a third thoracic vertebra (T3).

Superior and inferior vertebral body dimensions are small and fall closest to Sts 14p (*Au. africanus*) and subadult humans (Figure A35). In contrast, two juvenile *H. erectus* specimens (KNM-WT 15000U and D2721) fall within the ellipses of chimpanzees and adult and subadult humans.



Figure 9. U.W. 88-83 (MH2) in inferior (top left), superior (top right), dorsal (middle left), ventral (middle right), right lateral (bottom left), and lateral (bottom right) views (scale is 50mm).

Transverse process measures 18.1mm in length and 51° in orientation, within the human sample, outside the range of sampled chimpanzees, and between the two *H. erectus* specimens (Figure A36). *Au. africanus* specimen Sts 14p produces a higher transverse process angle, well within the range of variation in both chimpanzees and humans.

U.W. 88-189: Middle Thoracic Vertebra

U.W. 88-189 is a middle thoracic vertebra with a nearly complete vertebral body and neural arch, missing much of the spinous process (Figure 11). It is preserved in matrix between, but not in articulation with, U.W. 88-188 and U.W. 88-190. It is not directly subjacent to U.W. 88-188; instead, at least one, but perhaps two or more vertebrae are missing between the two.

The vertebral body of U.W. 88-189 is much more dorsoventrally elongate than that of U.W. 88-188, measuring 13.6mm at the dorsoventral midline and 18.4mm transversely across the widest point of the superior body. The inferior body is obscured by matrix, but the 3D model demonstrates that the inferior body is transversely flared and

very wide, measuring 26.4mm transversely by 15.2mm DV. The spinal canal is ovoid in shape, measuring 10.4mm DV and 13.4mm in transverse diameter. Maximum inter-SAF transverse width is 25.6mm; maximum inter-IAF transverse width is 24.2mm. The SAFs measure 9mm transversely and 8.1mm SI, on average.

The spinous process is inferiorly-directed at approximately 100° relative to the superior surface of the vertebral body, although it is broken distally. Pedicles are taller (8.6mm in SI height) than they are wide (3.7mm in transverse width). The transverse processes (average of 18.7mm in length along their long axis) form a 45° angle with the sagittal midline.

Like U.W. 88-37, U.W. 88-189 has a small superior vertebral body that falls out with human subadults (see Figure A12). In contrast, the spinal canal of U.W. 88-189 is substantially larger than that of U.W. 88-37 and falls within the area of overlap between chimpanzee and adult and subadult human 95% confidence ellipses, closer to juvenile *H. erectus* (KNM-WT 15000 CA and W) than to other australopiths (see Figures A14). The spinous and transverse process

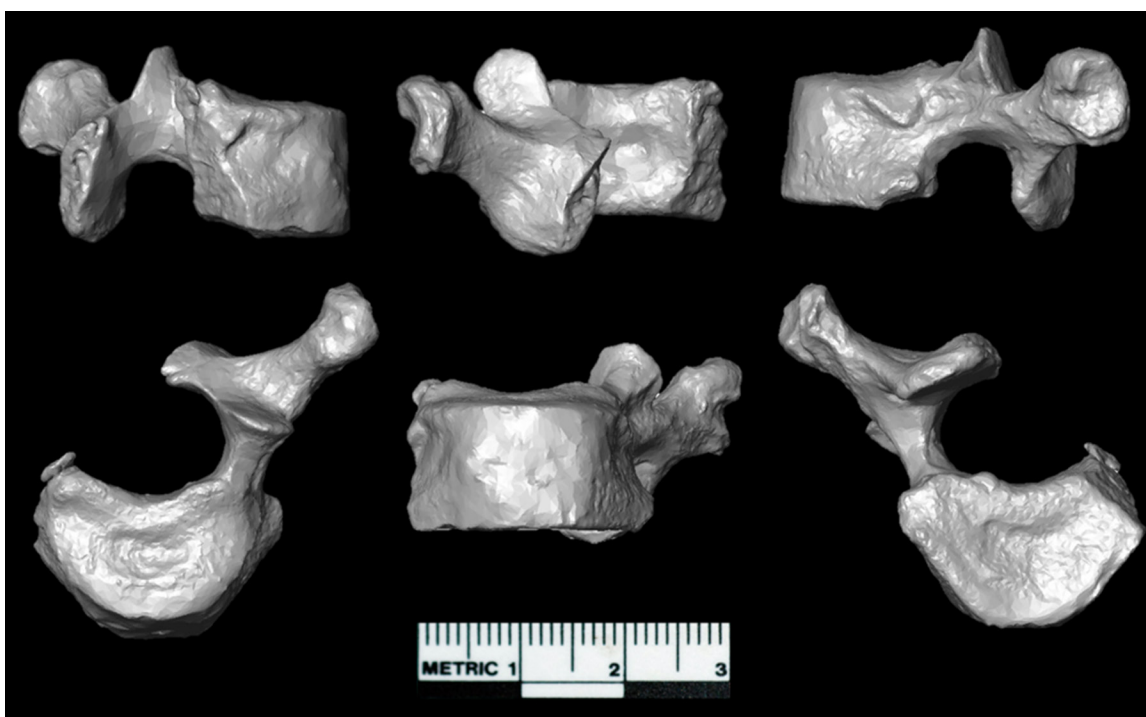


Figure 10. Model of U.W. 88-188 (MH2) isolated virtually from the upper thoracic block. Views are right lateral (top left), dorsal (top middle), left lateral (top right), superior (bottom left), ventral (bottom middle), and inferior (bottom right) (scale is 30mm).

angles produced by U.W. 88-189 are low (meaning strong inferior inclination of the spinous process and strong dorsal orientation of the transverse processes) and outside the range of variation observed in other fossil hominins and the comparative sample included in this study (see Figure

A16).

U.W. 88-190: Middle Thoracic Vertebra

U.W. 88-190 preserves the dorsal and lateral aspects of the body and a nearly complete neural arch. The left transverse

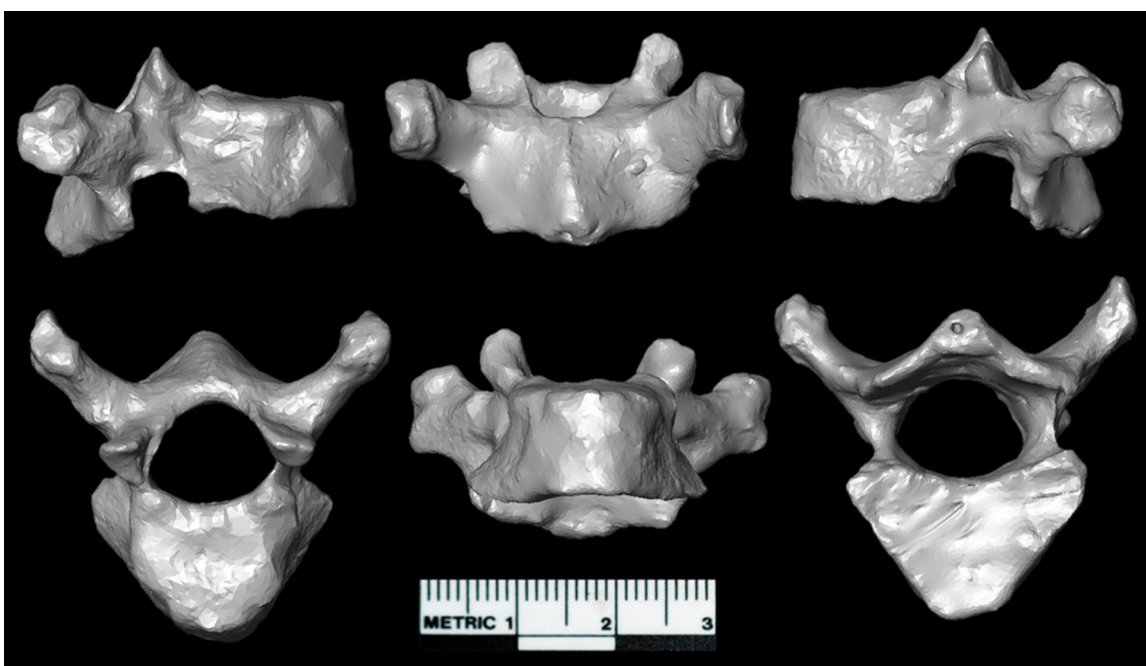


Figure 11. Model of U.W. 88-189 (MH2) isolated virtually from the upper thoracic block. Views are right lateral (top left), dorsal (top middle), left lateral (top right), superior (bottom left), ventral (bottom middle), and inferior (bottom right) (scale is 30mm).

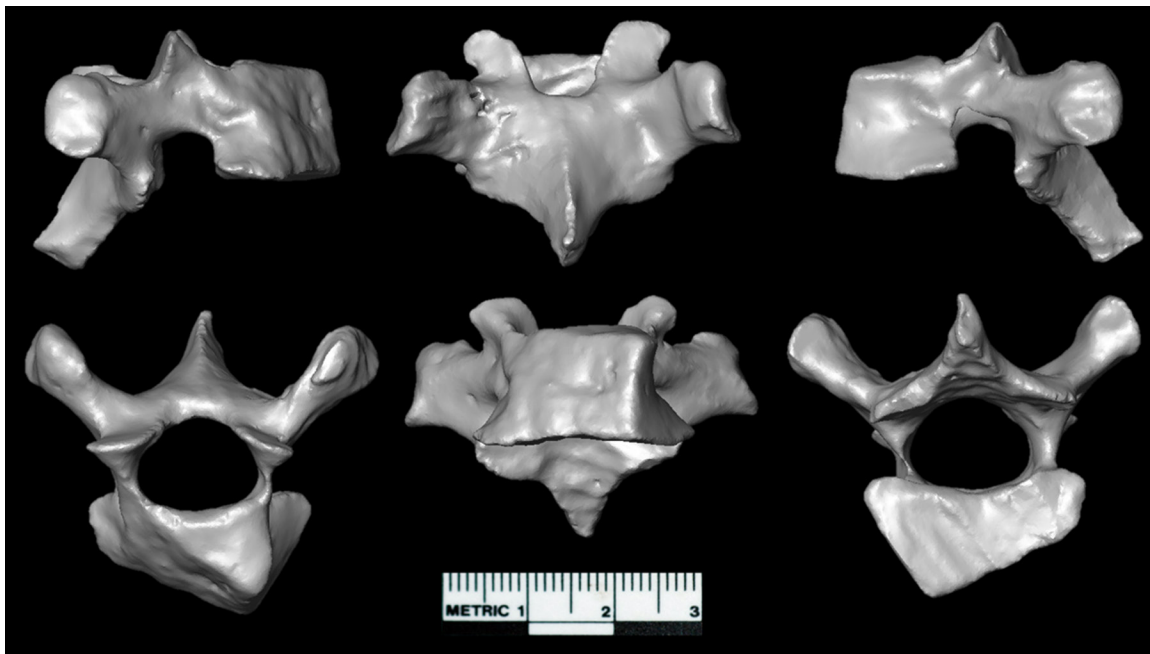


Figure 12. Model of U.W. 88-190 (MH2) isolated virtually from the upper thoracic block. Views are right lateral (top left), dorsal (top middle), left lateral (top right), superior (bottom left), ventral (bottom middle), and inferior (bottom right) (scale is 30mm).

process is obscured by matrix, but the virtual model shows that it is complete (Figure 12). The left SAF is damaged superiorly and the spinous process is broken distally.

The inferior vertebral body measures 25.7mm transversely and 12.9mm in dorsal SI height. The spinal canal is ovoid in shape (DV length of 10.9mm in sagittal diameter, transverse width of 13.9mm). The left SAF measures 9.1mm transversely and 7.4mm SI. SI inter-articular facet height is 26.9mm. Pedicles are relatively tall (9mm SI, 3.4mm in transverse width). The spinous process projects dorsoinferiorly and forms an angle of approximately 125° relative to the coronal plane. The visible (right) transverse process (20.1mm in length along its long axis) is angled dorsally at 54° relative to the sagittal midline.

The spinal canal of U.W. 88-190 is within the chimpanzee 95% confidence ellipse, falling just outside that of subadult humans (Figure A37). In contrast, the spinal canal dimensions of Sts 14l and A.L. 288-1ag are smaller, particularly in transverse diameter, and outside the 95% ellipse for chimpanzees. Both U.W. 88-190 and Sts 14l spinous process angles are well within the human range of variation (Figure A38). The U.W. 88-190 transverse process angle falls on the adult human median value and near the two available *Au. africanus* angles (Sts 14l and StW 431n) (see Figure A38). In contrast, the A.L. 288-1ag transverse process is less dorsally angled and falls outside the range of human variation and within that of chimpanzees.

U.W. 88-191: Middle or Lower Thoracic Vertebra

U.W. 88-191 is a partial vertebral body and neural arch that is largely obscured by matrix and crushed against the inferior side of the superjacent vertebra (U.W. 88-190) (see Figure A35, Figure A39). Only the transverse processes

are complete, the left of which is held in matrix superiorly. On average, the transverse processes measure 17.9mm in length and angle at 43° relative to the sagittal midline of the vertebra (see Figure A38). In this sense, it is consistent with following U.W. 88-190 inferiorly. The neural canal measures 13.4 transversely by 12.7 DV. The maximum inter-SAF distance is 22.2mm, the minimum measurement 9.7mm.

U.W. 88-96: Middle to lower thoracic vertebra

U.W. 88-96 is a fragment of a thoracic vertebra preserving only the inferior portion of the spinous process, broken distally, the right transverse process, and the upper portions of the inferior articular facets (Figure A40). The following features suggest that U.W. 88-96 is a lower or low-middle thoracic vertebra: the transverse process measures 19.1mm in length from the internal aspect of the spinal canal and is angled at 66° relative to the sagittal midplane; it is knob-like in shape and bears a small costal facet as seen in some modern human T9 or T10 vertebrae (S.A.W., personal observation); the preserved lamina is relatively flat, not convex or bulbous in shape; the inferior portion of the transverse process is DV thin (relative the superior portion); and the preserved inferior portion of the spinous process suggests a less strong caudal orientation than would be expected of middle thoracic vertebrae. Its transverse process is longer than that of the lower thoracic vertebra, U.W. 88-69 (see below), suggesting that it is cranial to it; however, U.W. 88-96 is too incomplete and damaged to determine if it is directly superjacent and consecutive with U.W. 88-69.

U. W. 88-114: Lower Thoracic Vertebra

U.W. 88-114, U.W. 88-43, and U.W. 88-44 are preserved to-

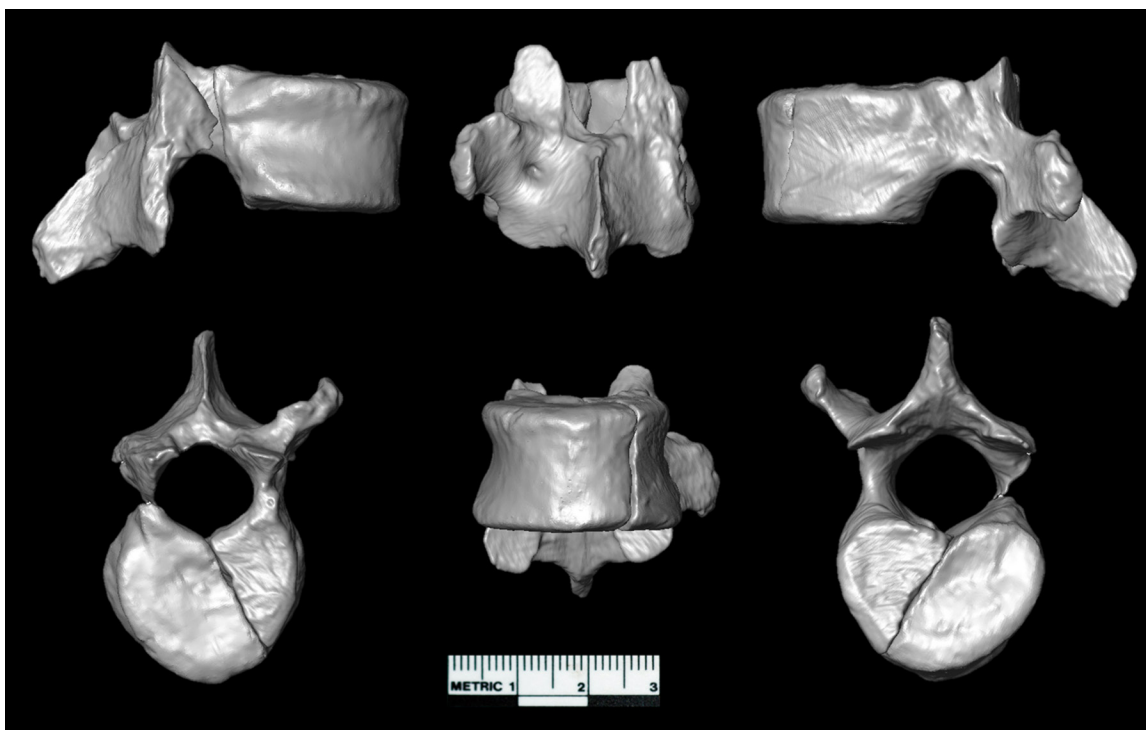


Figure 13. Model of U.W. 88-114 (MH2) isolated virtually from the lower thoracic block and refit with its detached vertebral body. Views are right lateral (top left), dorsal (top middle), left lateral (top right), superior (bottom left), ventral (bottom middle), and inferior (bottom right) (scale is 30mm).

gether in a block of matrix along with five rib fragments (U.W. 88-45, U.W. 88-46, U.W. 88-47, U.W. 88-48, U.W. 88-49) (Figures A41, A42). U.W. 88-114 is the antepenultimate thoracic vertebra, probably T10 (Figure 13). The vertebral body is nearly complete except for a small piece missing from the anterolateral superior border. Roughly two-thirds of the body is broken and detached from the block, but it refits with the rest of the vertebra. The left SAF and transverse process are partially exposed, whereas these structures on the right side are missing. The spinous process, right IAF, and distal aspect of the transverse process are obscured by matrix and rib fragments.

Because much of U.W. 88-114 is surrounded by breccia, with only the left SAF, transverse process, and approximately one-third of the vertebral body exposed (see Figures A41, A42), we segmented the three vertebrae virtually using micro-CT scans and created 3D virtual models. Measurements were estimated from the virtual models and compared to exposed morphologies. We report measurements taken from the virtual models here, although those available morphologies on the fossil itself produced nearly identical measurements.

The superior vertebral body is somewhat heart-shaped, measuring 24.9mm transversely at its maximum width (the inferior body transverse width is 27.8mm) by 19.6mm DV at the midline (the inferior body measures 19.2mm DV). The vertebral body is taller dorsally (17.6mm SI) than ventrally (16.5mm SI). SI inter-articular facet distance is approximately 27mm. The spinal canal measures 13.6mm

transversely and 13.3mm DV. The right IAF extends further inferiorly than the left side, but the right SAF is incomplete and cannot be measured. Maximum inter-SAF transverse width is 21.9mm (SAF min. width is 8.1mm) and maximum inter-IAF width is 25.5mm (IAF min. width is 9.7mm). The left SAF is dorsolaterally oriented ($\sim 104^\circ$) and its inferior aspect gives rise to a dorsolaterally-directed ($\sim 50^\circ$) transverse process. The SAFs measure 7.5mm in transverse width by 9.8mm in SI height (IAFs measure 8mm transversely by 7.9mm SI).

A costal facet is situated superiorly on the body-pedicle border on the right side; on the left, the facet is positioned similarly but is not complete. The transverse process is relatively long and thin and does not bear a costal facet. In this way, it resembles a penultimate thoracic more than it does an antepenultimate one; however, presumed T10 vertebrae from MH1 (see above), *Au. afarensis* (Meyer et al. 2015), and *H. naledi* (Hawks et al. 2017) also lack costal facets on their transverse processes. Shifted costal morphologies such as these are possibly related to a cranial border shift in *Hox* gene expression associated with the repositioning of the transitional vertebra in fossil hominins (see Williams et al. 2016). The pedicles measure 10.8mm in SI height, 3.6mm in transverse width, and 5.9mm in DV length. The lamina SI height is 15.1mm and its transverse width is 24mm.

When the superior vertebral body dimensions of U.W. 88-114 are compared to those of extant taxa and other fossil hominins, they are found to fall within the 95% confidence ellipses of adult humans and chimpanzees, along with A.L.

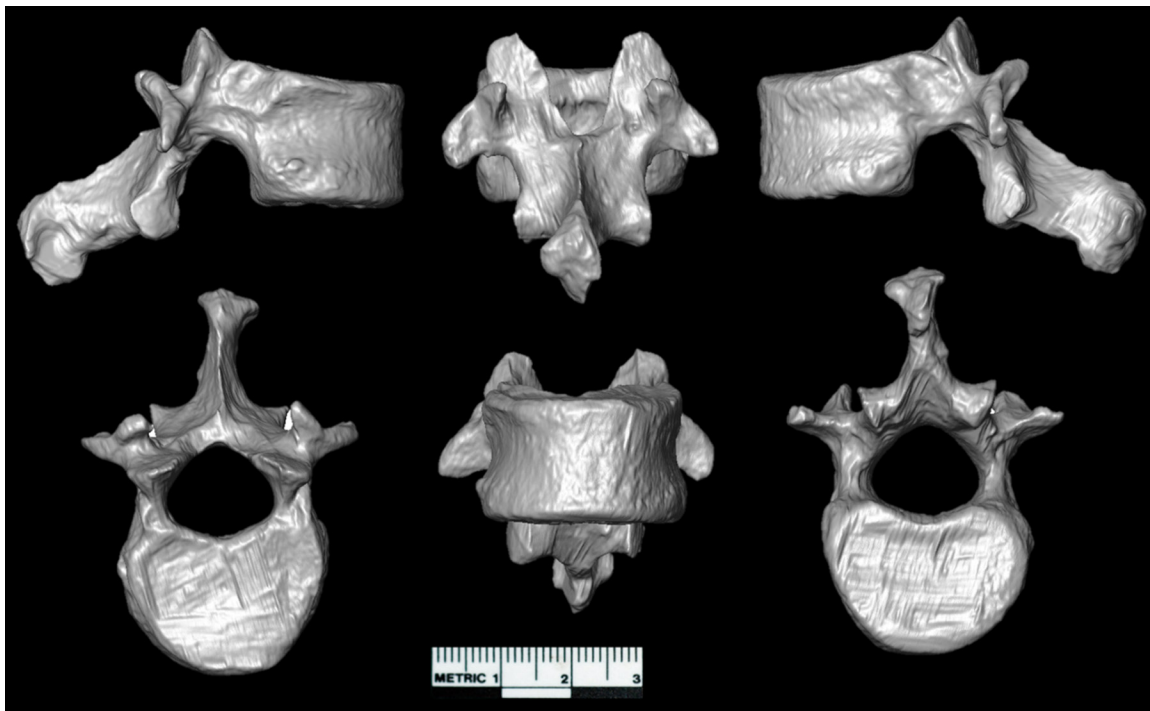


Figure 14. Model of U.W. 88-43 (MH2) isolated virtually from the lower thoracic block. Views are right lateral (top left), dorsal (top middle), left lateral (top right), superior (bottom left), ventral (bottom middle), and inferior (bottom right) (scale is 30mm).

333x-12 (*Au. afarensis*) and SKX 41692 (*Au. robustus*) (Figure A43). In contrast, the A.L. 288-1ad superior vertebral body is relatively narrow transversely, whereas that of Sts 14h is small in both transverse and DV dimensions. U.W. 88-114 produces a wedging angle of 3.2° (Figure A44). U.W. 101-855 (*H. naledi*) falls near subadult humans and just outside the chimpanzee ellipse. The SI height of the vertebral body is tall relative to the SI inter-articular facet height (see Figure A17), consistent with its completed growth. The spinal canal of U.W. 88-114 is large, falling within the human adult and subadult ellipses, in contrast with both juvenile *Au. sediba* (U.W. 88-69) and other adult early hominins (see Figure A18). Spinous and transverse process orientations fall well within the human distributions and in the middle of the fossil hominin distribution (see Figure A19).

U.W. 88-43: Penultimate Thoracic Vertebra

U.W. 88-43 is a complete lower thoracic vertebra (Figure 14). It is entrapped in breccia along with partial U.W. 88-114 above (superjacent) and U.W. 88-44 in partial articulation below (subjacent) (see Figure A42). The superior portion of the vertebral body and the dorsosuperior aspect of the neural arch are obscured by matrix and other fossils (U.W. 88-114 and rib fragment U.W. 88-48). The spinous process is visible from the right side but obscured dorsally and on the left side. The left transverse process and IAFs are obscured, but those on the right side are visible. The right IAF is in partial articulation with the SAF of the subjacent vertebra (U.W. 88-44). A virtual model of the vertebra is used in conjunction with visible morphology for the description and to estimate measurements below. The vertebra is complete,

with only a small degree of postdepositional chipping on the spinous process.

Body shape is consistent with a lower thoracic vertebra: superior transverse width of 27.4mm across the widest point of the superior body (inferior body maximum width is 28.5mm); DV length of the superior vertebral body is 18.9mm (inferior DV body length is 19.1mm). SI vertebral body height measures 16.6mm ventrally and 17.6mm dorsally. The spinal canal measures 14.8mm in transverse width and 12.8mm in DV length. The maximum inter-SAF transverse width is 25.2mm (IAF min. width is 8.4mm); maximum IAF transverse width is 18.9mm (IAF min. width is 8.4mm). The SAFs measure 8.3mm in transverse width by 8.6mm in SI height (IAFs measure 7.4mm transversely by 7.5mm SI) and are dorsolaterally oriented ($\sim 105^\circ$).

Complete costal facets are positioned high (superiorly) on the body-pedicle border and inferior demi-facets are lacking. U.W. 88-43 bears flat, posteriorly-directed SAFs and curved, laterally-directed IAFs; therefore, it is the transitional vertebra (Williams et al. 2013). The transverse processes project directly laterally ($\sim 73^\circ$) and are 14mm long, measured from the spinal canal along the long axis. It is bifurcated SI and ML as in penultimate and especially ultimate thoracic vertebrae. Pedicle dimensions are 11mm SI, 4.6mm transversely, and 4.6mm DV. The lamina SI height measures 14.5mm and its transverse width is 17mm.

Compared to extant taxa, the vertebral body dimensions of U.W. 88-43 are outside the 95% confidence ellipses of adult humans and within that of adult chimpanzees. It is most similar in size to male *Au. africanus* (StW41a) and *H. naledi* (U.W. 102-151), but smaller than the former and

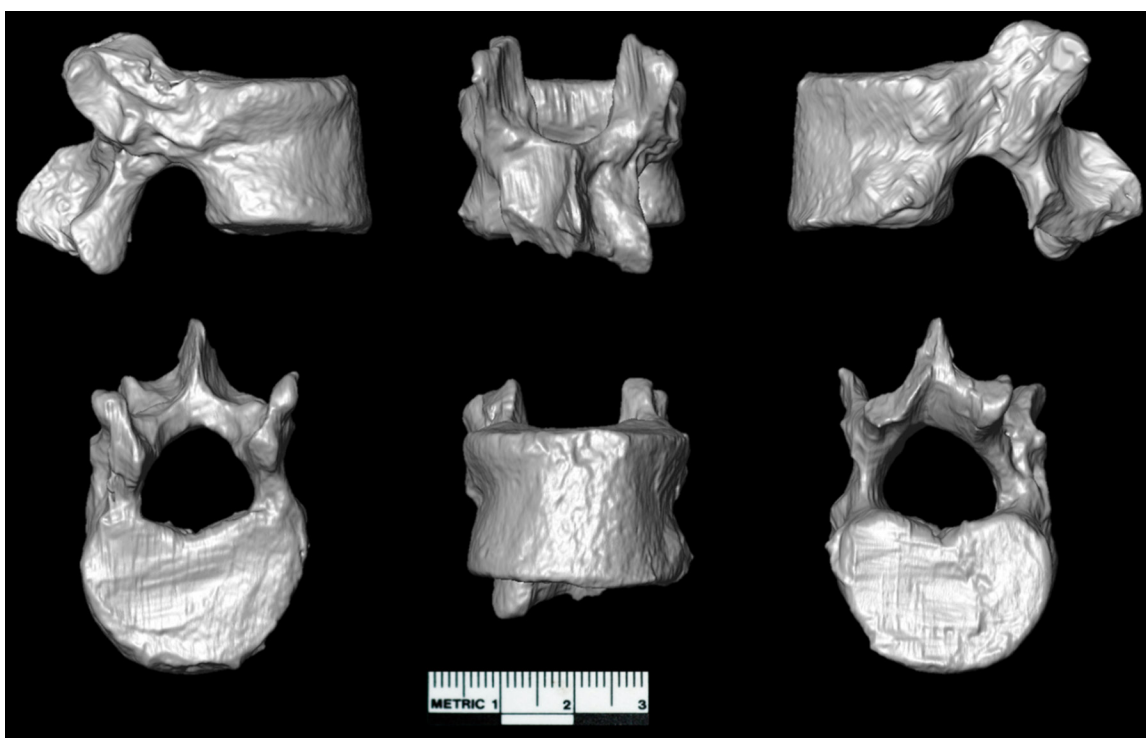


Figure 15. Model of U.W. 88-44 (MH2) isolated virtually from the lower thoracic block. Views are right lateral (top left), dorsal (top middle), left lateral (top right), superior (bottom left), ventral (bottom middle), and inferior (bottom right) (scale is 30mm).

larger than the latter (Figure A45). The spinal canal is large, falling within both adult human and chimpanzee 96% confidence ellipses (see Figure A45). Among fossil hominins, it is most similar to *H. erectus* (D2715 and KNM-WT 15000Y) in size. The vertebral body is tall relative to the SI inter-articular facet height (Figure A46). The vertebral wedging angle of the U.W. 88-43 body is 3.0° (Figure A47). The spinous process angle of U.W. 88-43 is similar to the human sample median value and falls closest to U.W. 101-1733 (*H. naledi*) among fossil hominins (Figure A48). In transverse process orientation, U.W. 88-43 falls outside the human sample and groups with other australopiths, whereas fossil members of the genus *Homo* produce lower angles (see Figure A48).

U.W. 88-44: Last Thoracic Vertebra

U.W. 88-44 is a near-complete ultimate thoracic vertebra (Figure 15). It is preserved in partial articulation with the superjacent vertebra (U.W. 88-43), both in a block of breccia, along with the antepenultimate thoracic vertebra (U.W. 88-114) and a number of rib fragments. U.W. 88-44 is obscured by matrix dorsally and inferiorly, by an unassociated rib (U.W. 88-46) on the entirety of the left side, and by U.W. 88-43 and matrix infill superiorly (see Figure A42). The spinous process is not visible as it is entirely covered in matrix. The right transverse process is represented only by a small protuberance located dorsally on the pedicle. A virtual model of the vertebra was created, from which measurements are estimated. Both the visible morphology of the fossil itself and the 3D model are used for the description below. The vertebra is mostly complete, missing much

of the left IAF, which is broken inferiorly along with the base of the spinous process on the left side. The spinous process preserves much of its base but is broken distally. The ventrosuperior border of the body is also broken at midline.

The vertebral body is transversely wider (29mm superiorly, 28mm inferiorly) than its DV diameter (18mm superiorly, 18.5mm inferiorly). The SI ventral body height measures 19.7mm, the SI dorsal body height 20.5mm, which produces a vertebral wedging angle of 2.6° (Figure A49). SI inter-articular facet height is 31mm. Maximum inter-SAF transverse width is 18.1mm (max. inter-IAF is 21mm); minimum inter-SAF is 11.3mm (min. inter-IAF is 8.7mm). The SAFs are strongly dorsomedially oriented ($\sim 24^\circ$). The average SAF SI height is 10mm (right IAF height=10.3mm); SAF transverse width is 7.8mm (right IAF width=8.2mm). From lateral view, both the superior articular process and the inferior articular process have a strong dorsal orientation, leading to the presence of a large intervertebral foramen and strong dorsal 'flare' to the inferior articular facet.

The spinous process is not complete enough to estimate its length or orientation. The lamina measures 14.9mm in SI height on the right side (the left side is incomplete due to the broken IAF) and 17.9mm in width. The pedicles measure 11.8mm in SI height and approximately 5mm in DV length. They are particularly asymmetrical in transverse width, measuring 4.5mm on the left side and approximately 6.3mm on the right (average pedicle width=5.4mm). This asymmetry is due in part to the costal facet components, which themselves are asymmetrical.



Figure 16. MH2 lower lumbar vertebrae and sacral body fragment. U.W. 88-127 (penultimate lumbar body), shown in superior (top) and dorsal, right lateral, ventral, and left lateral (middle panel, top element: left to right) views; U.W. 88-126 (ultimate lumbar vertebra) shown in the same views as U.W. 88-127 (middle pane, middle element); U.W. 88-125 (S1 body fragment) shown in the same view as above and in inferior view (bottom).

The transverse processes are essentially nonexistent and consist of a small 2.8mm projection bearing a costal demi-facet located on the base of the right superior articular process in a similar position as the transverse process of U.W. 88-43. The mammillary process is positioned dorsosuperiorly on the lateral aspect of the right superior articular process. On the left side, the mammillary process is positioned similarly, but the projection representing the inferior aspect of the transverse process is smaller than the right and does not bear an articular facet. Both sides exhibit structures on the dorsal vertebral body and pedicles that can be considered costal homologues—on the right side, a raised ridge bearing a costal demi-facet, and on the left a raised costal facet positioned at the body-pedicle border. The small facets on the raised surfaces of the right side seem to be a bifurcated costal facet for a small last rib. The left side bears a large raised costal facet at the body-pedicle border similar to that present on Sts 14f, which Haeusler et al. (2002) showed articulates with the last rib. Unfortunately, a last rib has not yet been recovered for MH2.

U.W. 88-44 has a “hybrid” appearance, combining features of thoracic and lumbar vertebrae. The morphology of the left side suggests that this vertebra bore a last rib, whereas the right side is more ambiguous in morphology. A similar combination of morphologies characterizes Sts 14f, which has been identified as either the first lumbar vertebra or the last thoracic vertebra in the Sts 14 series (Benade 1990; Haeusler et al. 2002; Robinson 1972; Rosenman 2008; Sanders 1995; Williams 2012; Williams et al. 2016). What is clear is that many early fossil hominins possess six vertebrae with curved, sagittally-oriented SAFs (i.e., the mam-

millary process is situated on the superolateral aspect of the superior articular process), including *Au. africanus* (Sts 14 and StW 431) and *H. erectus* (KNM-WT 15000) (Benade 1990; Haeusler et al. 2002, 2011; Robinson 1972; Rosenman 2008; Sanders 1995), and based on known material, is probably the case for *Au. afarensis* (Meyer et al. 2015; Ward et al. 2017) and *Au. sediba* (Williams et al. 2013). However, six post-transitional vertebrae are found in modern humans at moderate frequencies (Haeusler et al. 2011, 2012; Williams 2012b; Williams et al. 2016), so a similar degree of variation within fossil hominin species should be expected.

Compared to other fossil hominins, the superior vertebral body dimensions of U.W. 88-44 fall outside the 95% confidence ellipses of adult humans and chimpanzees but within those of subadults (Figure A50). Although adult male *H. naledi* (U.W. 102-154a) falls within the adult human confidence ellipse, it is most similar to U.W. 88-44 among fossil hominins (see Figure A50). Spinal canal dimensions of U.W. 88-44 fall outside the adult human 95% confidence ellipse but within that of adult chimpanzees and closest to *H. erectus* (KNM-WT 15000 AR/BA) among fossil hominins (see Figure A50). The vertebral body SI height is tall relative to the SI inter-articular facet height, similar to other adults (Figure A51).

LUMBAR VERTEBRAE OF MH2

U.W. 88-127 and U.W. 88-153: Penultimate Lumbar Vertebra

Two articulated lower lumbar vertebral bodies, U.W. 88-127 and U.W. 88-126, were recovered in articulation with a fragment of the first sacral body (U.W. 88-125) (Figure 16). The partial neural arches of these vertebrae (U.W. 88-153 and U.W. 88-138) were recovered in articulation with the remaining portion of the preserved sacrum (U.W. 88-137; see Churchill et al. 2018a). The rearticulated lower lumbar vertebra and sacrum are shown in Figure A52.

U.W. 88-127 is a nearly complete vertebral body, sheared from the neural arch at the pedicles, and U.W. 88-153 is the inferior aspect of the neural arch (Figure 17). These elements do not refit directly, but U.W. 88-153 articulates directly with the neural arch of the subjacent vertebra, U.W. 88-138, and the articulated lumbar vertebral bodies, U.W. 88-127 and U.W. 88-126, refit with the sacrum, and U.W. 88-138 and U.W. 88-126 refit, demonstrating the association between U.W. 88-127 and U.W. 88-153 (see Figure A52). The spinous process is preserved proximally but damaged inferiorly and missing superiorly. The superior neural arch (including the lumbar transverse processes) is missing entirely, broken at the mid-lamina on the right side and at the lower lamina on the left side. Approximately half (lateral) of the left IAF is sheared off, and the right IAF is complete.

The superior vertebral body of U.W. 88-127 is elliptical in superior view, transversely wide (31.4mm) and dorsoventrally short (22.2mm) (Figure A53). The ventral (22.1mm) and dorsal (21.5mm) SI body heights are roughly equivalent, giving this vertebra a relatively neutral wedg-

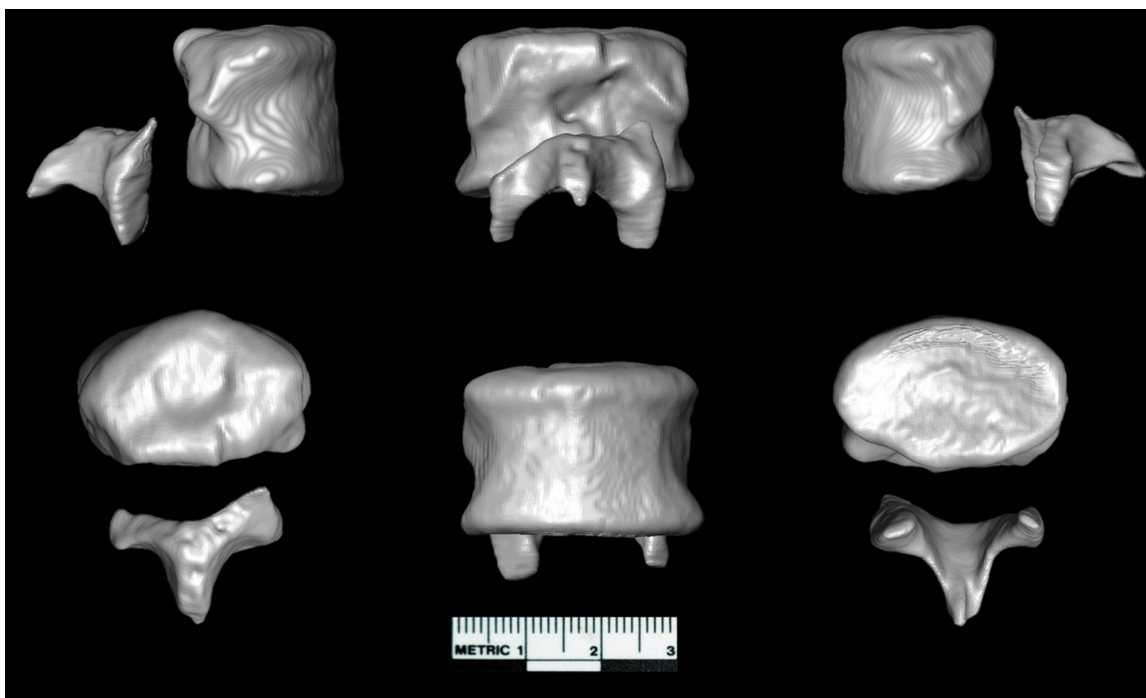


Figure 17. U.W. 88-127 and U.W. 88-153 (MH2) in right lateral (top left), dorsal (top middle), left lateral (top right), superior (bottom left), ventral (bottom middle), and inferior (bottom right) views.

ing angle of approximately -1.6° (Figure A54). The vertebral body is tall relative to the SI inter-articular facet height (approximately 32.6mm), which is consistent with other adult hominins (Figure A55). The minimum inter-IAF transverse width is 11.6mm, and the preserved right inferior articular facet is 14.7mm in SI height and 9.2mm in transverse width (the left SAF measures approximately 15.4mm SI and 13.7mm transversely).

U.W. 88-127 is somewhat dorsally wedged, but not strongly so; it falls near the human male median value and that of Sts 14 (*Au. africanus*) (see Figure A54). Although human female L4 vertebrae tend to be more dorsally wedged (Ostrowsky and Churchill 2015; Whitcome et al. 2007), U.W. 88-127 falls well within the range of variation in the human female sample presented here. However, all fossil hominins also fall within the lower range of chimpanzee penultimate lumbar vertebra wedging angles (see Figure A54).

U.W. 88-126 and U.W. 88-138: Last Lumbar Vertebra

U.W. 88-126 is the vertebral body and U.W. 88-138 the neural arch of the last lumbar vertebra of MH2 (see Figures 16, A52; Figure 18). The two specimens refit at the right pedicle-vertebral body border, shown here as a 3D model (see Figure 18). The spinous process, IAFs, and lamina are complete, as are the SAF and pedicle on the right side. The left pedicle is preserved only at its base ventrally, and the lumbar transverse process is missing its distal termination. The vertebral body itself is complete aside from a chip on the ventral-lateral inferior body and a pyramidal wedge missing at the midline of the ventral-inferior border.

The vertebral body is transversely wider (32.8mm;

21.4mm DV) and SI shorter (21mm ventrally, 17mm dorsally) than U.W. 88-127 and, like U.W. 88-127, bears a strong canal for the basivertebral vein at the middle of the dorsal aspect of the body. The spinal canal is large, measuring 23mm in transverse width by 16.3mm DV. Maximum inter-IAF transverse width measures 32.2mm; minimum inter-IAF transverse width is 15.6mm. The preserved right SAF measures 13.4mm transversely and 10.8mm DV. On average, the IAFs measure 14.4mm in SI height and 11.7mm in transverse width. The preserved right pedicle is robust, measuring 10.9mm in transverse width by 11.2mm in SI height. The lumbar transverse process is robust and oriented strongly dorsally (50°). The spinous process measures 23.6mm in DV length and is angled at 166° relative to the coronal plane of the vertebra.

When compared to extant taxa and other fossil hominins, U.W. 88-126 is a small vertebral body, outside the range of adult humans and chimpanzees (Figure A56). The vertebral body forms a strong dorsal wedging angle (-10.7°) that falls at the extreme end of human female variation in the comparative sample (see Figure A54). In contrast, other fossil hominin last lumbar vertebrae are also dorsally wedged, best approximating human males and falling at the low end of the chimpanzee distribution. The spinal canal is large, falling out near the middle of the adult human distribution, in strong contrast with the small vertebral body (see Figure A56). The spinous process angle falls out in the human comparative sample and outside that of chimpanzees (Figure A57). The transverse process angle is very dorsal and outside the range of human variation observed in the comparative sample, near the chimpanzee

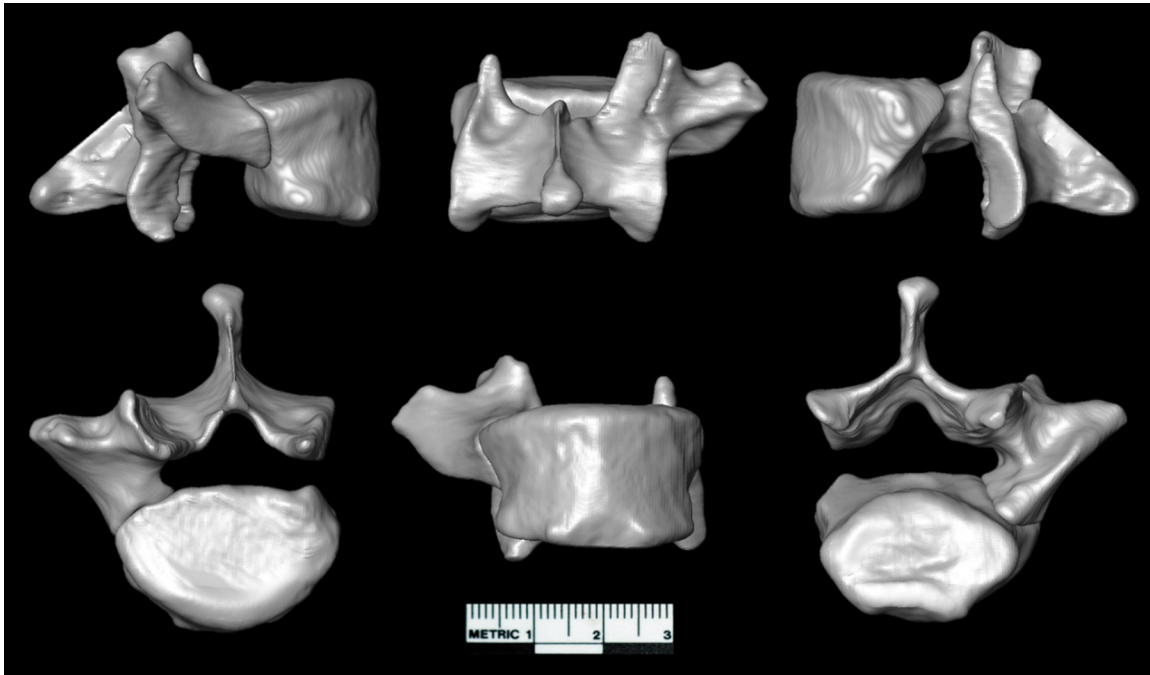


Figure 18. U.W. 88-126 (body) and U.W. 88-138 (neural arch) (MH2) in right lateral (top left), dorsal (top middle), left lateral (top right), superior (bottom left), ventral (bottom middle), and inferior (bottom right) views.

mean (see Figure A57). The SAFs are strongly sagittalized, at the extreme end of human variation sampled in this study and close to the chimpanzee median value, whereas other hominins fall well within the sampled human distribution (Figure A58).

RIBS

VERTEBROSTERNAL RIBS (1–7) OF MH1

U.W. 88-148: Right First Rib

U.W. 88-148 is a right-side 1st rib, composed of two fragments that articulate well with one another (Figure 19). The larger, proximal fragment preserves the head, neck, tubercle and proximal three-fifths of the shaft; the smaller distal fragment preserves the distal two-fifths of the shaft. The two fragments differ in their coloration on the inferior surface. A small (ca. 3.5mm diameter) patch of matrix adheres to the superior surface of the shaft in the area of the *M. scalenus medius* insertion. Small defects, perhaps representing insect damage, are visible on the inferior surface of the proximal shaft. The secondary center of ossification for the head appears to be unfused, while that of the tubercle appears fused (the appearance of these surfaces is similar before and after fusion, making it difficult to discern the state of fusion: Scheuer and Black 2000). The sternal end does not preserve the costal pit, indicating that a small amount of the distal rib may be missing.

Although the head is devoid of the articular facet, it is clear that it has a single facet for articulation with the first thoracic vertebra but not the seventh cervical vertebra. The neck is slightly flattened and ascends posterolaterally, and

measures 4.9mm (internal-external: IE) by 5.4mm (superoinferiorly: SI) at the head, 6.3mm IE by 3.4mm SI at the middle, and 7.5mm IE by 3.6mm SI at the tubercle. There is a distinct pit for the costotransverse ligament on the external aspect of the neck just medial of the tubercle. The external border of the neck is slightly constricted.

The tubercle is prominent, and as in other primates it



Figure 19. U.W. 88-148 (MH1) in superior (left), inferior (right) and dorsal (top right) perspectives. The arrow indicates the scapular tubercle, the insertion of scalenus anterior (scale is 100mm).

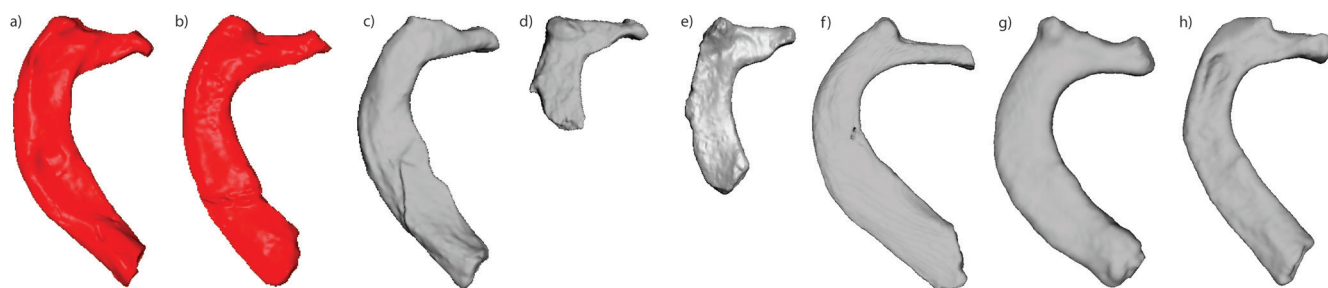


Figure 20. Superior view of 1st ribs of extant and fossil hominins where differences in axial curvature can be appreciated. a) *Au. sediba* (MH2: U.W. 88-198); b) *Au. sediba* (MH1: U.W. 88-148); c) *Au. afarensis* (A.L. 288-1ax); d) *Au. africanus* (StW 670); e) *H. naledi* (U.W. 102-250); f) juvenile *H. erectus* (KNM-WT 15000 AG-mirror image); g) *P. paniscus*; h) *H. sapiens*. Ribs scaled to approximately equal size.

coincides with the posterior angle. The tubercle has a superior-inferior height of 4.1mm and a mediolateral (ML) width of 6.1mm. The superior surface of the shaft has a shallow depression proximally for the insertion of *M. scalenus medius*, and the distolateral margin of the muscle attachment area is rugose and slightly elevated above the surrounding bone surface. The groove for the subclavian artery is shallow and indistinct, and the scalene tubercle is almost indiscernible (although a small scalene tubercle is visible close to the medial margin). Likewise the groove for the subclavian vein presents as a very shallow and indistinct sulcus. The superior surface of the distal end of the shaft shows some swelling and roughening for *M. subclavius*, suggesting that very little of the distal shaft is missing. Markings for *M. serratus anterior* or the costoclavicular ligament are not evident. The inferior surface is smooth and featureless. Both margins have edges that are rounded. The shaft measures 10.6mm IE by 4.2mm SI at the tubercle, 11.6mm IE by 3.1mm SI at the scalene tubercle, and 12.5mm IE by 4.3mm SI at the sternal end.

The apparent “univertebral pattern” of U.W. 88-148 is contrary to what is found in great apes and is also seen in

other fossil hominins (Ohman 1986; Meyer and Williams, in review) and in some other primates (Stern and Jungers 1990). Comparing 1st ribs across early hominins, U.W. 88-148 and U.W. 88-198 (MH2) are similar to *Au. afarensis* (A.L. 288-1ax) and *Au. africanus* (StW 670) (Tawane et al. 2016) in axial curvature, and to the australopiths and *H. naledi* (U.W. 102-250) in shape and orientation of the tubercle, neck, and head (Figure 20). An increase in axial curvature is observed in *H. erectus* and can also be seen in *H. sapiens*.

U.W. 88-86: Right 6th or 7th Rib

This specimen represents the proximal third (approximately) of the shaft, tubercle and distal neck of a right vertebral rib (Figure 21). This specimen was tentatively designated as the right 6th or possibly 7th rib, and thought to potentially conjoin with the distal shaft specimen U.W. 88-41 (Schmid et al. 2013). The fragment has a maximum length of 96.2mm. The specimen lacks a head but preserves the distal 8mm or so of the neck. The proximal break is in the sagittal plane, and the broken surface of the neck has adherent matrix. The distal break lies in a paracoronal plane, and also has matrix adherent to the surface of the break.



Figure 21. U.W. 88-86 (MH1) in superior (left) and inferior (right) perspectives (scale is 50mm).



Figure 22. U.W.88-41 (MH1) in superior (left) and inferior (right) perspectives (scale is 50mm).

The surface preservation is very good, although there are small areas of erosion on the inferior part of the articular tubercle and on the inferior margin of the *M. iliocostalis* insertion area at the posterior angle.

The neck is oval in cross-section, with its long axis oriented roughly superoinferiorly. The tubercle is well developed. At the position of the break, the neck measures 6.6mm IE by 9.9mm SI. The articular facet measures 9mm PD by 6.7mm SI. The facet is oval in shape and convex. The nonarticular part of the tubercle (for the attachment of the lateral costotransverse ligament) is relatively small. The nonarticular tubercle has an SI height of 8.1mm and an ML width of 9.8mm. The shaft is thick, and changes in cross-sectional shape from cylindrical (proximally) to oval (distally). The proximal shaft has a rounded superior surface and a flattened inferior surface, and measures 8.2mm IE by 7.9mm SI at the level of the tubercle. A distinct ridge, beginning about 10.5mm distal of the tubercle and extending for an additional 61.5mm, is present on the inferolateral margin of the rib, in the area of the posterior angle and *M. iliocostalis* attachment, creating a shallow costal groove on the inferior shaft (see Figure 21). The tubercle-iliocostalis line distance (TID: Franciscus and Churchill 2002) is 24.7mm. At the iliocostalis line, the shaft has an IE diameter of 10.4mm and an SI diameter of 6.2mm. At the distal break, the shaft measures 11.5mm IE by 9.2mm superoinferiorly. The curvature of the shaft is not pronounced. No torsion is visible in this proximal rib fragment.

U.W. 88-41: Right 6th or 7th Rib

This specimen preserves the distal end of a right rib fragment (Figure 22). U.W. 88-41 was tentatively designated as the right 6th or possibly 7th rib, and thought to potentially conjoin with the proximal shaft specimen U.W. 88-86 (Schmid et al. 2013). The fragment has a maximum length of 118mm, and preserves a partial shaft and sternal end

with a costal pit. The proximal break lies roughly in the coronal plane, is irregular, and is occluded with matrix. The bones have a number of small cracks, one of which encircles the shaft about 44.5mm from the break and is associated with a small (ca. 3mm diameter) pit of missing cortical bone on the superior margin of the rib. The external surface is roughened and appears to be slightly weathered.

The internal surface is smooth, with a shallow costal groove. The superior margin is rounded while the inferior margin is sharper. At the proximal break, the shaft has an IE diameter of 6.7mm and an SI diameter of 10.8mm. At the middle of the fragment, the shaft measures 6mm IE by 10.9mm SI. Towards the distal sternal end the shaft narrows SI, before thickening IE (9.8mm) and widening SI (18.7mm) at the sternal end where it terminates as the costal pit. The shaft curves internally as the sternal end is approached.

U.W. 88-86 and U.W. 88-41 are combined virtually and the refitted rib can be compared to extant and fossil middle ribs (Figure 23). U.W. 88-86/41 is qualitatively similar to chimpanzees, whereas stronger rib axial curvature is observed in *H. erectus* and particularly *H. sapiens*.

U.W. 88-15 and U.W. 88-131: Left 6th or 7th Rib

U.W. 88-15 is a proximal fragment of a left rib, preserving most of the neck, the tubercle, and about 21mm of the proximal shaft to the posterior angle (Figure A59). The maximum length of the fragment is 44.3mm. U.W. 88-131 preserves about 38mm of the proximal shaft from the posterior angle distally (Figure A60). The maximum length of the fragment is 43.2mm. The two fragments conjoin cleanly.

The proximal break in the neck of U.W. 88-15 occurs in the area in which the neck is flaring to accommodate the head. The break lies in a parasagittal plane, and the surface is infilled somewhat with matrix. The distal break in this specimen lies in a paracoronal plane, and its surface has exposed trabeculae. The surface color and lack of matrix infilling suggests the break occurred post-fossilization but not recently (i.e., it probably occurred during mining activities). The proximal break in U.W. 88-131 mirrors the distal break in U.W. 88-15, and likewise has trabeculae exposed on its surface. The distal break in this specimen lies in a parasagittal plane, and also appears to exhibit exposed trabeculae. Both specimens have many fine cracks in the surficial cortical bone, but are otherwise in a good state of preservation.

In its overall morphology, U.W. 88-15/131 is a good match for that of the right-side specimen U.W. 88-86, and it is probable the two are antimeres. The neck is oval in cross-section, with its long axis roughly superoinferiorly oriented. The neck measures 6.8mm IE by 10.1mm SI. There is a distinct crest, extending 7.4mm distally from the break in the neck, for the costotransverse ligament. There is also a sharp ridge on the superior margin adjacent to the tubercle for the attachment of the superior costotransverse ligament. The articular facet is oval in shape, convex, and measures 9.8mm PD by 7.4mm SI. As in U.W. 88-86, the nonarticular tubercle is small relative to the articular facet. The nonarticular tubercle has an SI height of 8.1mm and an

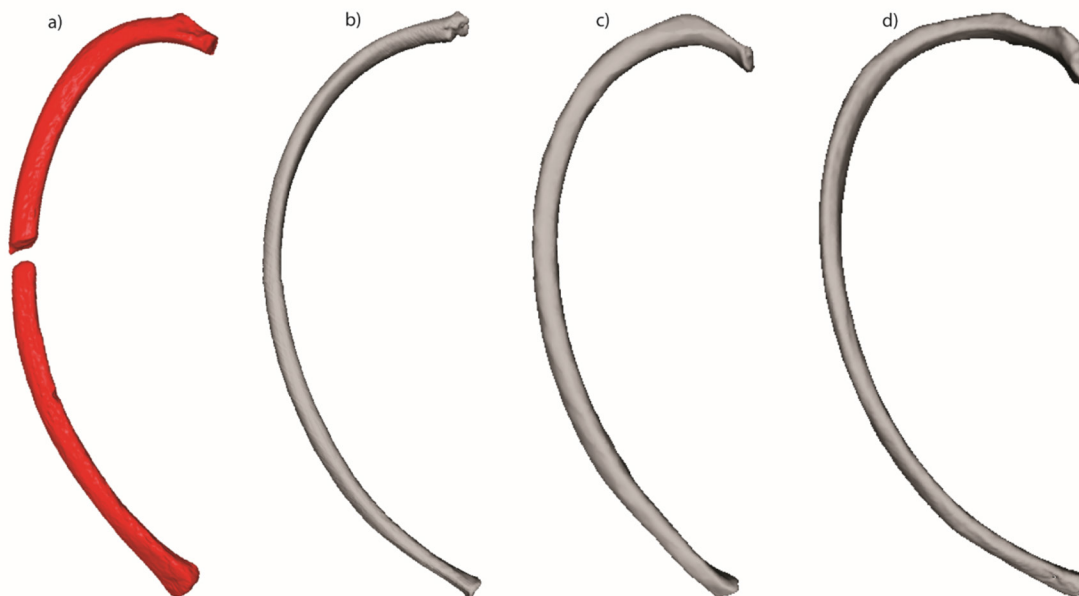


Figure 23. Superior view of middle ribs of extant and fossil hominins where differences in axial curvature can be appreciated. a) *Au. sediba* (MH1: virtual reconstruction of U.W.88-86/41); b) juvenile *H. erectus* (KNM-WT15000 AL); c) *P. troglodytes* (extant); d) *H. sapiens* (extant). Ribs scaled to approximately equal size.

ML width of 12.8mm.

The proximal shaft has a rounded superior surface and a flattened inferior surface. At the level of the tubercle, the shaft measures 8.8mm IE by 7.9mm SI. The proximal part of the *M. iliocostalis* line is visible on the external surface, inferiorly, and at the posterior angle it forms a small, inferiorly-directed crest. The tubercle-iliocostalis distance is 24.3mm. At the iliocostalis line the shaft has an IE diameter of 10.4mm and an SI diameter of 6.2mm. A shallow and wide costal groove is visible and continuous between the two fragments. At the distal break, the shaft measures 11.5mm IE by 9.6mm SI.

U.W. 88-155: Left 7th or 8th Rib

U.W. 88-155 is a 98.5mm (maximum length) fragment of the proximal shaft of a left side vertebrosteral rib, tentatively identified as a 7th or 8th rib (Schmid et al. 2013) (Figure A61). The specimen is preserved from immediately distal of the tubercle up to the midshaft area of the rib. Proximally the shaft is broken in the sagittal plane, and the fracture surface is occluded with matrix. Distally the rib is fractured in the coronal plane, and the surface of the fracture exposes trabeculae. The surface is weathered (more so on the external than internal surface) and has multiple fine cracks. A small (diameter=ca. 5mm) piece of matrix still adheres to the external surface adjacent to the break.

The incompleteness of the specimen makes it difficult to sequence this fragment, and relatively little can be said about its morphology. The iliocostalis line is visible on the external surface and a small ridge of bone projects inferiorly from the external inferior surface in the area of the posterior angle. At the level of the iliocostalis line, the shaft

has an IE diameter of 9.4mm and an SI diameter of 6.4mm. The internal surface is smooth and exhibits a wide but shallow costal groove. At the distal break the shaft measures 10.1mm IE by 5.2mm SI.

ASTERNAL RIBS (8–10) OF MH1

U.W. 88-165: Right 7th–9th Rib

This fragment represents a portion of the shaft of a right lower vertebrosteral rib or, more likely, an asternal rib (Figure A62). This specimen was misidentified as a left-side rib and was tentatively identified as belonging to the same rib as the distal left-side fragment U.W. 88-74 (Schmid et al. 2013). This attribution appears to have been in error as this specimen seems to be a right rib. The fragment has a maximum length of 72.8mm. It has a complete fracture through the shaft about 26mm proximal of the distal break, and the resulting two fragments are displaced relative to one another but held together by matrix. The proximal break falls roughly in the coronal plane, while the distal break lies roughly in the sagittal plane. The specimen exhibits a small amount of crushing at both its proximal and distal ends, as well as a few small cracks in the surface, but otherwise the surface preservation is very good.

Little can be said about the morphology of this specimen. The shaft has a maximum superoinferior diameter of 10.2mm (obtained at the distal end of the fragment). The IE diameter at the same location (distal end) is 4.8mm. A shallow costal groove is evident.

U.W. 88-74: Left 7th–9th Rib

This fragment represents a portion of a left lower vertebro-

sternal rib or, more likely, an asternal rib (Figure A63). This specimen was tentatively identified as belonging to a rib in the series 7–9 (Schmid et al. 2013), and to possibly represent the same rib as the shaft fragment U.W. 88-165. The proposed association of the two specimens appears to have been in error, as U.W. 88-165 appears to represent a right-side rib. U.W. 88-74 is a distal rib fragment (maximum length 33.8mm) that preserves 30.9mm of the distal shaft and the sternal end with a costal pit. The shaft is fractured in a paracoronal plane, and the fracture surface has matrix penetrating into the trabeculae. The surface preservation of the specimen is quite good.

Little can be said about the morphology of this specimen. At the proximal end the shaft measures 4.6mm IE by 9.5mm SI. Towards the sternal end, the shaft widens and produces a costal pit that is elliptical in shape. Here the shaft is 6.1mm IE by 16.4mm SI. There is an internal curvature of the shaft as it approaches the sternal end at the costal pit.

FLOATING RIBS (11–12) OF MH1

U.W. 88-17: Left 11th or 12th Rib

U.W. 88-17 is a 29.8mm-long (maximum length) fragment that appears to represent the distal end of an 11th or 12th rib from the left side (Figure A64). Surface preservation is poor and there is a large area of matrix adherent to the external surface. At the proximal end the shaft measures 3.8mm IE by 7.9mm SI. The distal tip of the rib is preserved and there is no costal pit. The distal dimensions of the shaft are 3.5mm IE by 4.5mm SI. The internal surface is relatively smooth.

INDETERMINATE RIB FRAGMENTS OF MH1

U.W. 88-13: Indeterminate Rib Fragment

U.W. 88-13 is a rib fragment from the right side that preserves the distal shaft and sternal end with the costal pit (Figure A65). The fragment has a maximum length of 50.2mm. The proximal break is irregular, lies largely in the coronal plane, and is occluded with matrix. At the proximal break, the shaft measures 3.7mm IE by 7.6mm SI. The surface is weathered and has a few small pits. The shaft is mildly curved, and no portion of the costal groove is present. The costal pit is oval in shape. At the distal end the shaft is 4.9mm IE by 10.7mm SI.

U.W. 88-141: Indeterminate Rib Fragment

This 35.9mm-long (maximum length) specimen is a rib fragment from the right side (Figure A66). It is composed of multiple sub-fragments that are held together by matrix. It appears to be a distal part of the shaft approaching the sternal end of the rib. No morphological features are evident. The fragmentary and distorted nature of the specimen precludes measurement.



Figure 24. Virtual model (obtained from micro-CT scanning; Schmid et al., 2013) of U.W. 88-198 (MH2). From top to bottom: lateral, dorsal, superior (left), inferior (right), ventral, and medial perspectives (scale is 50mm).

VERTEBROSTERNAL RIBS (1–7) OF MH2

U.W. 88-198: right 1st Rib

U.W. 88-198 is the complete 1st rib from the right hand side. It preserves the head, neck, tubercle, corpus of the rib, and intact sternal end. The specimen is embedded in matrix in contact with the dorsal surface of the manubrium, making its physical removal from the matrix impossible at this time. Thus the specimen was rendered virtually from micro-CT scans (Figure 24). Slight taphonomic damage is evident on both the superior and inferior surfaces. At about midshaft, a rectangular chip measuring roughly 5mm by 2.5mm is missing from the superior surface of the specimen, and a small U-shaped fracture line extends medially from this damaged area. The fracture line continues around to the inferior surface, where it joins a ca. 31mm-long fracture that runs (PD) along the inferior surface of the mid- to distal-shaft. All of this damage is slight and in no way affects the discernible morphology or metric dimensions of the specimen. There are also two small oval defects on the external surfaces of the specimen. One appears as a small

(4mm by 2mm) oval pit on the superior surface, roughly 12mm from the distal (sternal) end. From the virtual model, this appears to represent a small, probably post-mortem fracture surface. The other defect is an oval pit, roughly 5mm by 2.5mm, on the inferior surface near the external margin of the bone, near midshaft. It is not possible to discern from the virtual model whether this defect represents an antemortem or postmortem condition.

The head exhibits a single facet for the articulation with the complete costal facet of the first thoracic vertebra. The head measures 8mm in internal-external (IE) diameter, and 7.3mm in SI diameter. The neck is narrow and rounded proximally, but widens dorsoventrally and flattens superior-inferiorly as it approaches the corpus. Adjacent to the head, the neck measures 5.3mm IE by 4.2mm SI, while at the proximodistal midpoint the neck is 7.6mm IE by 4.5mm SI. Just proximal of its union with the corpus, the neck measures 11.4mm IE by 4.6mm SI. When the corpus is held horizontally, the neck deflects slightly inferiorly, such that the head of the rib lies below the plane of the body.

The tubercle is well-developed, and coincides with the posterior angle. As in MH1, there is a distinct pit on the external surface of the neck just medial of the tubercle, for the costotransverse ligament. The articular facet measures 8mm IE by 6.9mm SI.

The shaft of the corpus is superior-inferiorly flattened, measuring 13.9mm IE by 5.6mm SI at its proximal end (adjacent to the tubercle) and 16.5mm IE by 5.1mm SI at midshaft. Distally, the shaft becomes compressed in its IE dimension (to 11.9mm at its distal end), while flaring in its SI dimension (to 8.1mm). The specimen has a tuberculoventral chord and subtense (Franciscus and Churchill 2002) of 69mm and 21.1mm, respectively.

The superior surface bears a shallow fossa just distal of the tubercle for the insertion of *M. scalenus medius*, and shallow grooves for the subclavian vasculature. Other muscle and ligament attachment areas are not discernible on the virtual model. The inferior surface is relatively smooth and featureless. The costal pit measures 11.8mm IE by 6.7mm SI, and is shallow.

As with U.W. 88-148, the head of U.W. 88-198 exhibits the univertebral pattern, in which it articulates solely with the T1 vertebra and not the C7 vertebra. As with U.W. 88-148, the head of U.W. 88-198 exhibits the univertebral pattern, in which it articulates solely with the T1 vertebra and not the C7 vertebra. It is again most similar in morphology to A.L. 288-1ax, StW 670, and U.W. 102-250 (see Figure 20).

U.W. 88-187: Left 1st Rib

U.W. 88-187 is the proximal end of the 1st rib from the left side (Figure A67). It preserves the head, neck and the proximal portion of the tubercle. Hairline cracks are evident on the surface of the specimen, but otherwise the surface preservation is good.

The head has of a single facet (univertebral pattern, see above) that is oval in shape, measuring 6.9mm IE by 5.1mm SI. The margin of the head appears to be thickened for the attachment of the radiate ligament. The neck is flattened



Figure 25. Views of U.W. 88-58 (MH2) in superior (left) and inferior (right) views (scale is 50mm).

in the SI plane. Just distal of the head, the neck measures 5.7mm IE by 3.2mm SI, while adjacent to the tubercle it is 9.9mm IE by 4.4mm SI. Both the superior and inferior surfaces are smooth and exhibit slight concavities. Only the proximal part of the articular facet is visible, and has an SI height of 3.8mm.

U.W. 88-58: Right 2nd Rib

This fragment lacks the head but preserves most (or all) of the neck, the tubercle, the posterior angle, and the proximal shaft (Figure 25). The shaft appears to be broken at the proximal end of the tuberosity (for the attachment of *M. serratus anterior*), although none of the tuberosity itself is preserved. The maximum length of the fragment is ca. 57mm. Surface preservation is generally good, although some small cracks are evident on both the superior and inferior surfaces. The neck is slightly damaged (missing some bone on its inferior surface) at its proximal end (adjacent to the head).

The neck is slightly rounded on its superior surface and flattened on its inferior surface. It is elongate, narrower proximally than distally. At the proximal end (but distal of the area of damage) the neck measures 4.4mm IE by 3.9mm SI. The external (dorsal) margin of the neck is straight, whereas the internal (ventral) margin of the neck is angled such that the neck widens distally: adjacent to the tubercle the neck has an IE dimension of 6mm and an SI height of 4.1mm. The neck has a slight inferiorward inflection, such that if the corpus were held horizontally the head of the rib would have lain below the plane of the corpus. Although the head is missing (and thus the length of the intact neck is not certain), as preserved the neck has a length of 11.4mm.

The tubercle is prominent and projects dorsally from the external surface of the rib. Its articular facet is well preserved, faces dorsomedially, and measures 4.5mm IE by

4.1mm SI. The non-articular portion of the tubercle (for the lateral costotransverse ligament) is relatively small. The insertion of the iliocostalis muscle presents as a small rugose area on the external margin of the rib adjacent to the tubercle, extending 17mm distally, where it terminates as a small, inferiorly-projecting crest (the inferior costal point).

The shaft is flattened in a SI plane. The superior surface of the shaft preserves ill-defined roughened attachment areas for the *Mm. serratus posterior superior* and *scalenus posterior*. The distal shaft at the position of the break appears to exhibit slight swelling in the superoinferior direction on its lateral margin, and thus appears to be marking the proximal extent of the tuberosity for *M. serratus anterior* (and specifically, the second digitation of that muscle). The lateral/external margin of the shaft is sharp whereas the internal/medial margin appears more rounded. There is a shallow sulcus on the inferior surface just distal of the tubercle, created by the sharp (and slightly inferiorly-projecting) margin of the *M. iliocostalis* attachment. The shaft has proximal (just distal of the tubercle) dimensions of 9.8mm IE by 4.8mm SI, while adjacent to the distal break the shaft is 8.2mm IE by 4.3mm.

U.W. 88-178: Left 2nd Rib

U.W. 88-178 is the proximal end of the 2nd rib from the left side (see Figure A67). It preserves a head, neck, tubercle and the proximal ca. 7mm of the shaft. There is a small amount of matrix that still adheres to the head, but otherwise the surface is clean and well-preserved. The total length of the fragment is ca. 30mm.

The head bears two demifacets, separated by a well-defined crest of the head for the intra-articular ligament. The superior demifacet has an IE width of 5.4mm and an SI height of 3.2mm, while the inferior demifacet has an IE width of 5.4mm and an SI height of 4.4mm. The neck is rounded and elongate. The superior surface is slightly convex while the inferior surface is mildly concave. Adjacent to the head, the neck measures 4.8mm IE by 3.6mm SI, while at its distal extent (adjacent to the tubercle) it measures 4.1mm IE by 4.8mm SI.

The tubercle is complete and exhibits an oval convex articular facet that is 4.2mm IE by 6.1mm SI. The articular facet is orientated dorsomedially. The non-articular portion of the tubercle (for the lateral costotransverse ligament) is relatively small.

U.W. 88-166: Right 3rd Rib

U.W. 88-166 is a 3rd rib fragment from the right side (Figure 26). The specimen preserves the head, neck, and tubercle, the posterior angle, and a portion of proximal shaft. The neck is separated from the corpus by a fracture, and is affixed to the shaft (with very slight displacement) by adherent matrix. Although the tubercle is present, the articular facet is not preserved. The inferior surface from the area of the tubercle to the middle of the preserved shaft evinces areas of minor crushing and slight displacement of surface bone. Two small cracks traverse the inferior surface towards the distal end of this area of damage. The maxi-



Figure 26. U.W.88-166 (MH2) in superior (left) and inferior (right) views (scale is 50mm).

imum length of the fragment is ca. 57mm.

The head is oval in shape and exhibits two articular demifacets separated by a well-developed crest for the intra-articular ligament. The superior facet is the smaller of the two, measuring 3.3mm IE by 4.9mm SI, while the inferior facet measures 4.6mm IE by 5.7mm SI. The angle between the facets is obtuse, producing a head that is very similar in shape to that seen in the ribs of most extant primates (including modern human), but not in chimpanzees, which possess a more pointed, arrow-shaped head.

The neck is flattened dorsoventrally. The neck attains its greatest SI diameter adjacent to the head, where it measures 3.1mm IE by 8.4mm SI. At the distal end (adjacent to the tubercle) the neck measures 5.7mm IE by 7.7mm SI. There is a well-defined crest of the neck (*crista colli costae*) for the anterior costotransverse ligament on the superior margin. The external surface of the neck has a deep, oval-shaped depression (similar to that observed on U.W. 88-61: see below), roughly 3.5mm PD by 2mm SI in dimension. This depression may mark the insertion site of the lateral costotransverse ligament, or perhaps some distal slips of the radiate ligament.

The ligamentous portion of the tubercle is prominent and well-defined. The shaft is superior-inferiorly flattened proximally, but begins to twist slightly beginning in the area of the posterior angle. Just distal of the tubercle the shaft has an IE dimension of 9.3mm and an SI diameter of 5.2mm. Distal to the tubercle is the roughened attachment point of the *M. iliocostalis*. Although the articular tubercle is missing, the tuberculo-iliocostalis distance (TID: Francis and Churchill 2002) can be estimated at 22mm. The dis-



Figure 27. U.W. 88-61 (MH2) in superior (left) and inferior (right) views (scale is 50mm).

tal shaft is triangular in cross-section, and measures 8.8mm IE by 5.5mm SI. There is a shallow costal groove visible on the inferior surface, running parallel to the external margin of the rib.

U.W. 88-61: Right 4th Rib

U.W. 88-61 is a nearly complete right vertebrosteral rib that was recovered adjacent to (and on top of) the right upper limb remains of MH2 (Figure 27). The size of the rib, along with its torsion, position of the *M. iliocostalis* line, and shaft cross-sectional morphology all suggest that the rib derives from the middle of the vertebrosteral rib series, most likely representing a 4th, 5th, or 6th rib. Consideration of the inclination of the rib, its curvature, the degree of torsion evident in the body, and the rugosity and position of the iliocostalis line (all relative to the preserved morphology evident in the right 3rd rib fragment U.W. 88-166) led to a provisional identification of this specimen as a 4th rib (Schmid et al. 2013). The specimen is composed of two large fragments that articulate well to form an almost complete rib. Although the head is lacking, it preserves a partial neck, tubercle, a complete shaft, and the costal pit. A transverse fracture near midshaft separates the rib into two pieces. The two fragments do not refit cleanly, although there does appear to be a contact surface on the superior margin, and it is apparent that about 5–6mm of the shaft is missing between the two surfaces of the inferior margin of the rib. Overall the surface preservation is good, although there is an area of slight exfoliation of surface bone, primarily on the external surface but also extending a few mil-

limetres onto the internal surface, on the superior margin of the distal shaft (roughly 30mm proximal of the anterior angle). Two cracks can be seen in the inferior surface of the proximal rib, roughly 18mm and 31mm distal of the tubercle, respectively. Likewise, a crack appears on the external surface of the distal rib, roughly 32mm proximal to the sternal end, with some slight displacement of the surficial bone distal of the crack.

The neck appears to have been flattened dorsoventrally, and to have an internal surface that is inclined slightly inferiorly. Adjacent to the tubercle, the neck measures 4.2mm IE by 5.8mm SI. The superior margin is sharp and exhibits a well-developed crest of the neck (crista colli costae) for the anterior costotransverse ligament. This crest continues onto the internal margin of the shaft of the rib.

The tubercle has an oval and convex articular facet that faces dorsosuperiorly and medially. The articular facet measures 4.6mm IE by 6.3mm SI. The ligamentous portion of the tubercle is prominent and well-defined. The proximal part of the shaft is triangular in cross-section, with three surfaces (inferior, dorsosuperior, and ventrosuperior). The proximal IE diameter is 8.6mm and the SI diameter is 5.1mm. The dorsosuperior surface bears the roughened elevation for the *M. iliocostalis* that corresponds with the external angle of the rib. The tubero-iliocostalis distance (TID: Franciscus and Churchill 2002) is 27.7mm. At the posterior angle (iliocostalis line), the shaft measures 9.7mm IE by 5.4mm SI. Progressing further distally the shaft flattens (superolaterally to inferomedially), producing two surfaces (internal and external). The shaft lies at an oblique angle to the SI plane. The internal surface is smooth compared to the external surface, and preserves a shallow costal groove on the proximal one quarter of the shaft. The superior margin is rounded while the inferior margin is sharper. Distally the rib flares at the anterior angle, producing a maximum diameter (superomedial by inferolateral) of 11.1mm and a thickness (superolateral to inferomedial) of 3.8mm. The rib has a tuberculoventral chord and subtense (Franciscus and Churchill 2002) of 176mm and 56.8mm, respectively. The costal pit is elliptical in shape, measuring 12.8mm by 5.2mm.

When viewed alongside chimpanzees and humans, it can be seen qualitatively that the axial curvature of U.W. 88-61 is more similar to that of chimpanzees than humans, which show a much higher degree of axial curvature (Figure 28).

U.W. 88-167 and U.W. 88-154: Right 5th Rib

U.W. 88-167 is the proximal part of a right rib, preserving a partial neck, tubercle, and proximal shaft (Figure A68). U.W. 88-154 is the distal part of the shaft of a right rib (Figure A69). It is composed of three fragments; a long fragment that is made up of two parts and a distal segment that was broken during the removal of the specimen from the surrounding matrix. The two specimens do not conjoin, but based on size and morphology they appear to represent the proximal and distal portions of the same rib. Based on the inclination of the rib, its curvature, the degree of torsion

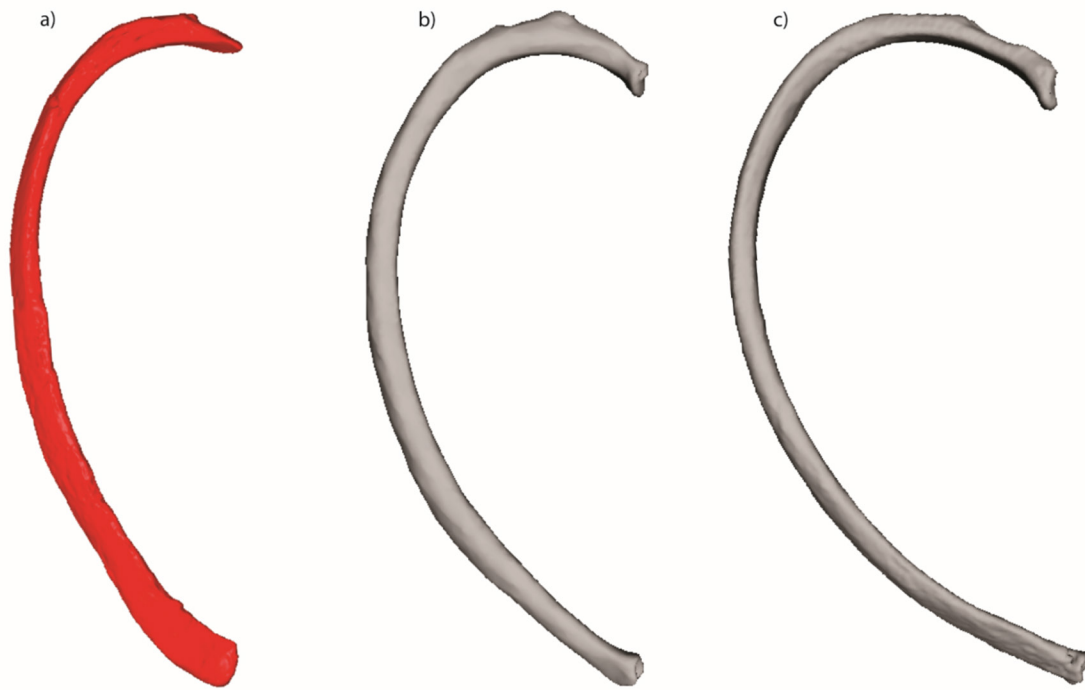


Figure 28. Superior view of 4th ribs of extant and fossil hominids where differences in axial curvature can be appreciated. a) *Au. sediba* (MH2: virtual model of U.W. 88-61); b) *P. troglodytes* (extant); c) *H. sapiens* (extant). Ribs scaled to approximately equal size.

evident in the body, and the rugosity of its iliocostal line (all relative to the morphology the right 4th rib U.W. 88-61), we have provisionally identified this as a 5th rib.

Too little of the neck is preserved to allow anything to be said about its morphology, beyond that it appears to have had a well-developed crest of the neck (still evident on the proximal shaft adjacent to the tubercle) for the anterior costotransverse ligament. The tubercle has an oval and convex articular facet, 5.9mm IE by 6.5mm SI that faces inferiorly and medially. The non-articular attachment of the lateral costotransverse ligament is well developed.

The proximal part of the shaft is triangular in cross-section with three surfaces (inferior, dorsosuperior, and ventrosuperior), measuring 7.9mm IE by 4.8mm SI. The dorsosuperior surface bears the pronounced roughened elevation for the attachment of the *M. iliocostalis*, corresponding with the posterior angle of the rib. The tuberoiliocostalis distance (TID: Franciscus and Churchill 2002) is 32.1mm. At the posterior angle (iliocostalis line), the shaft measures 9.7mm IE by 5.1mm SI. The internal surface is smooth compared to the external surface, but proximally it bears a shallow costal groove. Distally the shaft is elliptical in cross-section, being more rounded in the area around midshaft and becoming progressively flattened distally. Around midshaft the corpus measures 6.2mm IE by 10.1mm SI, while distally the shaft measures 4.1mm IE by 8.4mm SI. The superior margin is rounded as compared to the inferior margin, which is sharp.

ASTERNAL RIBS (8–10) OF MH2

U.W.88-60: Right 9th or 10th Rib

U.W.88-60 is a distal fragment of a 9th (or 10th) right rib shaft (Figure A70). The fragment is 85mm long and appears to derive from the vicinity of the anterior angle.

The internal/medial surface is smooth compared to the textured external/lateral surface. The superior margin is rounded. The inferior margin is sharp due to the presence of a costal groove. On the inferior border the costal groove disappears and blends into the distal inferior margin. At what appears to be the anterior angle, the rib measures 8.3mm SI by 5.1mm IE.

This rib is slenderer than the more superior fragments, a condition very different from that of the inferior ribs of chimpanzees and other great apes (which are the largest and longest in the series). In addition, it appears to show distinct torsion along its body, which is characteristic of the reduced last ribs of humans (but not great apes).

U.W. 88-145: Right 9th or 10th Rib

This fragment appears to be from the shaft immediately distal to the posterior angle (Figure A71). There is a roughened line visible on the external surface of the fragment, proximally. In modern human typical ribs, this would indicate the attachment of *Mm. external oblique* and *serratus anterior* (or *M. latissimus dorsi*, in 9th and 10th ribs). The maximum length is 51.4mm, SI height is 10.9mm (proxi-

mally) and 11.3mm (distally), and the mediolateral width is 8.4mm (proximally) and 6.3mm (distally). At its middle, the shaft measures 7.1mm IE by 9.3mm SI. The cross-section appears mediolaterally flattened distally as compared to the proximal section which appears more cuboidal. A clearly defined costal groove is visible on the medial (inner) aspect of the fragment. The inferior margin of the fragment is not as sharp as compared to the superior edge. There are no diagnostic features present to determine the specific rib level from which it originates.

U.W. 88-59: Indeterminate Vertebrosteral Rib

U.W. 88-59 is a ca. 87mm-long fragment of the distal shaft of a vertebrosteral rib, preserving the anterior angle (Figure A72). No costal groove is present and the rib side cannot be determined. Breaks at both ends are angular (oblique to the long axis of the shaft), and the break at one end is occluded with matrix. At the anterior angle, the shaft measures 12.5mm SI by 6.9mm IE.

INDETERMINATE RIB FRAGMENTS OF MH2

U.W. 88-143: Indeterminate Rib Fragment

This specimen preserves a portion of the shaft of a rib, but the rib number and side are indeterminate (Figure A73). The fragment measures ca. 64mm in length. No costal groove is visible. A nearly transverse break (at a right angle to the rib shaft) occurs at one end, and a more oblique (and eroded or abraded) fracture can be seen at the other. At its middle, the shaft measures 11.9mm SI by 7.3mm IE.

U.W. 88-144: Indeterminate Rib Fragment

This specimen is a ca. 51.5mm-long fragment of rib shaft most likely from the area of the anterior angle (Figure A74). The side is indeterminate. The shaft has been crushed at one end and broken, and the two broken pieces have been secondarily cemented together by matrix, with several millimeters of displacement between the adjoining surfaces.

U.W. 88-147: Indeterminate Rib Fragment

This specimen is a ca. 51mm long fragment of right rib shaft, preserving the distal portion of the iliocostalis line and posterior angle (Figure A75). A wide, distinct costal groove is evident the entire length of the specimen. Just distal of the posterior angle the shaft measures 10.5mm SI by 5.9mm IE.

U.W. 88-192: Indeterminate Rib Fragment (Left Side)

Fragment of the shaft of a left rib, about 20mm long. The specimen preserves no features that allow for the determination of the rib's position in the sequence.

U.W. 88-193: Indeterminate Rib Fragment (Left Side)

Small fragment from a left rib shaft, about 10mm long. The specimen preserves no identifiable features to sequence the rib from which it originates.

U.W. 88-199: Indeterminate Rib Fragment

This specimen is a ca. 47mm-long shaft fragment, with a



Figure 29. U.W. 88-172 (MH2) in superior (top), ventral (bottom), and left lateral (right) views (scale is 50mm).

transverse break at one end and an oblique break at the other. The specimen is abraded along one of its (superior or inferior) margins. This specimen was assigned to MH2 in Nalla (2013). At the middle of the fragment, the shaft measures 10.4mm SI by 4.3mm IE.

STERNUM

MANUBRIUM STERNI OF MH2

UW88-172: Manubrium

The manubrium is complete and almost undamaged (Figure 29). It is attached to matrix in the block also containing MH2's right first rib (U.W. 88-198) and scapula (U.W. 88-28 and U.W. 88-56) (the latter described in Churchill et al. 2018b). There are three circular depressions in a triangle shape close to the center of the ventral face, and a lump extends from the surface on the right side of these depressions, probably all of which are due to postmortem damage.

The manubrium is almost square in shape but the superior edge is longer than the inferior one. The lateral borders are roughly equal in length to the superior edge, creating a square shape whose lateral sides converge slightly inferiorly, similar to a trapezoid. The manubrium thins in lateral width inferiorly in order to articulate with the sternebra below (not present), which would be thinner than the superior breadth of the manubrium. The ventral face is not bowed outwards as is normally seen in humans, but is instead concave. The posterior side is also concave, but only slightly. The surface itself is almost flat, but the edges of the articular surfaces for the clavicles and the first ribs extend dorsally which makes the face seem more concave than it is. The dorsal surface is smooth, unlike the ventral surface.

In shape, the manubrium is dissimilar to other hominoids superiorly. Ape and human manubria generally extend laterally from the clavicular articulations to either side

of the superior surface, making the superior section of the manubrium much wider than the inferior section. The clavicular articular facets on the superior edge are flat with rounded edges, and slope inferiorly. Dorsally they extend to points, but do not ventrally. The jugular notch is shallow and measures 13.5mm in breadth. The 1st rib articulates underneath with a 5.2mm long section of fossil on the left and a 7.4mm long section on the right separating the first rib facet from that of the clavicle. The first rib facets are dish-shaped and wider superiorly than inferiorly. There is a longer section of bone (9.7mm in length) inferior to the first rib articular surfaces and superior to the second rib articular surfaces. The facets for the second ribs are lightly marked and are also wider inferiorly than superiorly.

Manubrium SI length measures 30.9mm, its maximum transverse manubrial breadth 38.2mm. Manubrial transverse breadth measured between the centers of the first rib articular facets measures 32.7mm. U.W. 88-172 is small in size, falling outside the range of adult humans and chimpanzees (Figure A76). It is nearly as SI long as it is transversely wide, and although humans and chimpanzees overlap extensively in an index of SI length to transverse breadth, U.W. 88-172 falls on the human median value (see Figure A76).

DISCUSSION AND CONCLUSIONS

This manuscript serves to provide detailed descriptions of the ~2.0 Ma vertebra, rib, and sternum fossils from Malapa attributed to *Australopithecus sediba*. Analyses of functional and evolutionary morphology of this material has been published previously (Arlegi et al. 2017; Meyer et al. 2017, 2018; Schmid et al. 2013; Williams et al. 2013) and is ongoing. Here, we discuss changes in the seriation of vertebrae and ribs from those previously published and briefly address a critique that the lumbar vertebrae of MH1 and MH2 represent two different species that became intermingled at Malapa (Been and Rak 2014).

UPDATED ASSOCIATION AND SERIATION OF VERTEBRAE AND RIBS

The fossil hominin vertebra, rib, and sternum material from Malapa belong to a minimum of two individuals (MNI=2), one adult and one juvenile (Berger et al. 2010; Schmid et al. 2013; Williams et al. 2013), whereas the totality of skeletal elements indicate an MNI of six hominins (Val et al. 2015). Given similarities in size, epiphyseal fusion, and association of the postcranial axial material, it is probable that it belongs to the two known partial skeletons, juvenile male MH1 and adult female MH2 (Berger et al. 2010; Cameron et al. 2017; Schmid et al. 2013; Val et al. 2015; Williams et al. 2013). Ten vertebrae are associated with MH1 (41.7% of the probable total number of vertebrae) and nine ribs (37.5% of the probable total number of ribs). Eleven vertebrae (45.8% of the probable total number of vertebrae) and 16 ribs (66.7% of the probable total number of ribs) are associated with MH2, along with a sternum and sacrum. Therefore, the axial skeletons of MH1 and MH2 are approximately 38% and 58% preserved, respectively. Tables 1–4 provide

updated lists of hominin vertebra and rib fossils from Malapa, and in some cases, their revised anatomical positions (compare to Schmid et al. 2013; Williams et al. 2013). Note that these are provisional identifications subject to change with recovery of additional elements and future study.

DIFFERENCES BETWEEN MH1 AND MH2: AGE OR SPECIES INTERMINGLING?

Though never fully published in a peer-reviewed journal, we briefly address Been and Rak's (2014) critiques levied at the validity of the species *Au. sediba* at the Paleoanthropology Society Meetings (the abstract of which was published in this journal). Been and Rak (2014) identified three ratios that purportedly separate *Homo erectus* from *Australopithecus* and ally MH1 with the former and MH2 with the latter. Based on these results, Been and Rak (2014) suggested that the MH1 vertebrae belong to a member of the genus *Homo* and those of MH2 belong to an *Australopithecus* individual, therefore questioning the hypodigm of *Australopithecus sediba*. Here, we test their hypothesis by examining the three indices in a comparative, age-structured context.

Their first index, "ventrodorsal length of the vertebral bodies that is relatively short when compared to the height of the vertebrae (their craniocaudal length) (Been and Rak 2014: A2)," is straightforward. In humans, marked SI (craniocaudal) vertebral body growth occurs until approximately ten years of age, whereupon incremental growth continues until the ring apophyses fuse at ~25 years of age (Dickson and Deacon 1987). When ratios of DV body length to SI body height are taken, MH1 (U.W. 88-92 and U.W. 88-152) does group with *H. erectus* (KNM-WT 15000 and D2762) to the exclusion of MH2 (U.W. 88-127 and U.W. 88-126), which groups with australopiths (Figure 30). However, like MH1 (Cameron et al. 2017), both *H. erectus* individuals are juveniles (Dean and Smith 2009), and, like MH2, all of the australopiths are at or near adulthood. The presence of fused ring apophyses on MH2 vertebrae and absence on MH1 vertebrae demonstrate that SI vertebral body growth had ceased in MH2 but would have continued in MH1. When a better, less age-influenced variable representing vertebral SI height is chosen for the denominator of the ratio (SI inter-articular facet height), MH1 lumbar vertebrae fall within the *Au. africanus* distribution to the exclusion of D2672, whereas MH2 lumbar vertebrae fall between two *Au. africanus* specimens and *H. erectus* (Figure 31).

Been and Rak's (2014) second index is spinal canal size relative to DV vertebral body length. We calculate ratios of the measured area of the spinal canal (using ImageJ) over DV body length. All fossil hominins, including MH1 and MH2, fall well within the modern human distributions at each vertebral level (L1–L5), and no separation between *H. erectus* and australopiths or MH1 and MH2 is found (Figure 32). Their final observation is that the articular processes are relatively large in MH2 (and australopiths) compared to MH1 (and *H. erectus*). We use a ratio of the calculated articular facet area (average SAF and IAF SI height X transverse width) over SI inter-articular facet height. While we find significant differences among levels of lumbar vertebrae

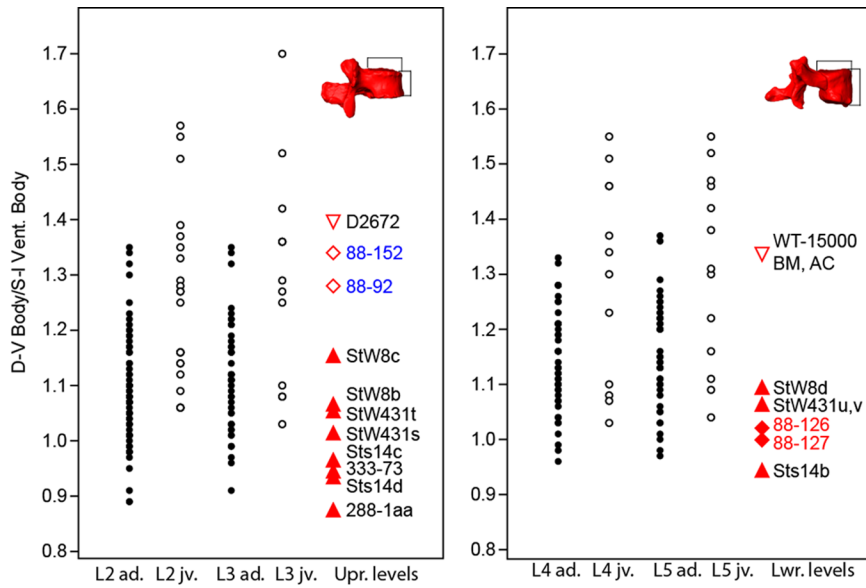


Figure 30. Been and Rak’s vertebral body index (DV body length/SI body height) in *Au. sediba*, other fossil hominins, and modern humans. Note that adults and juveniles separate (in modern humans, adults and juveniles are significantly different from each other; $p < 0.001$); therefore, juvenile MH1 (U.W. 88-92 and U.W. 88-152) vertebrae fall close to juvenile *H. erectus* (D2672), and MH2 (U.W. 88-127/153/234 and U.W. 88-126/138) clusters with other adult australopiths. This disparity is due to the incomplete SI vertebral body growth in juveniles, including MH1. Open symbols represent juveniles (“Jv”), closed symbols adults (“Ad”) of modern humans (circles), *Au. africanus* and *Au. africanus* (triangles), *H. erectus* (inverted triangles), and *Au. sediba* (diamonds).

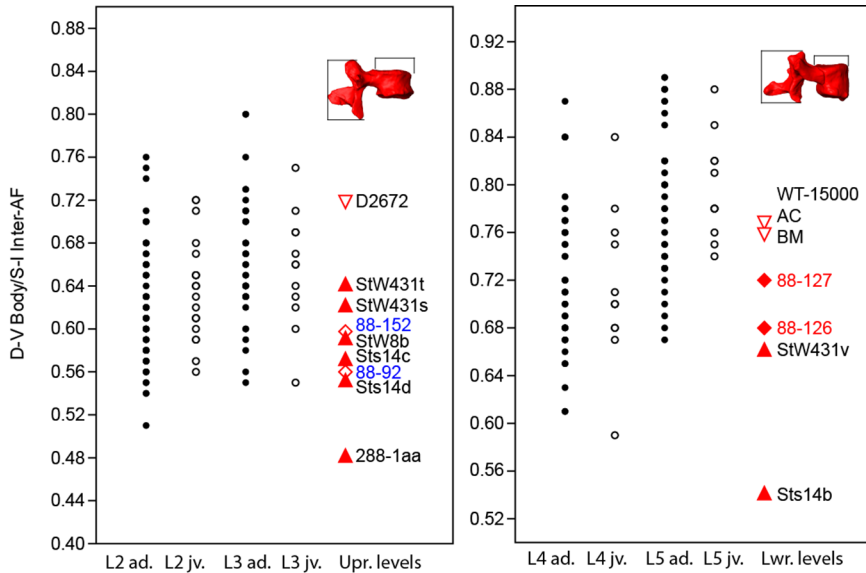


Figure 31. Vertebral body DV length standardized by SI inter-articular facet height in *Au. sediba*, other fossil hominins, and modern humans. Significant differences between adult and juvenile modern humans are not found; likewise, MH1 falls out with *Au. africanus*, not *H. erectus*, and MH2 falls out in between *Au. africanus* and *H. erectus*. This index is better than Been and Rak’s (2014) because it is not influenced by the age differences between MH1 and MH2. Symbols follow Figure 30.

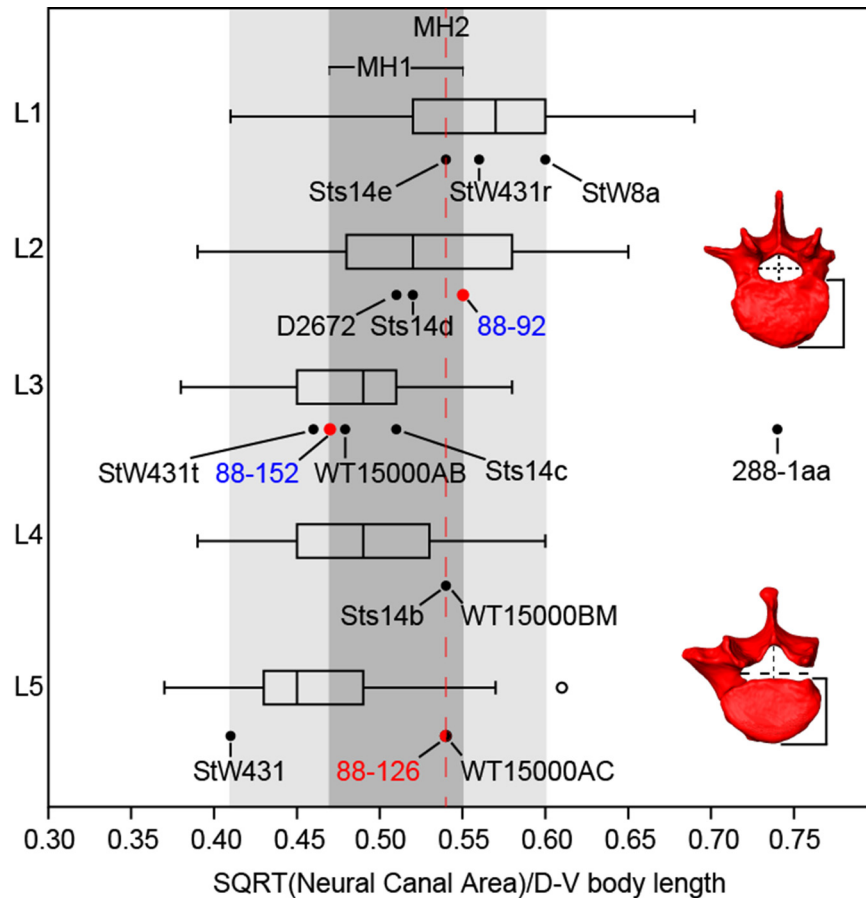


Figure 32. Index of spinal canal area relative to the DV length of the vertebral body. Data on modern human adults and juveniles are not statistically different so are pooled and are shown as box plots (with one outlier for L5, shown in an open circle). Fossils corresponding to each level are shown below the modern human data, with *Au. sediba* in red circles and other fossil hominins in closed black circles. Specimens producing an identical index are shown as a single point and labelled accordingly (i.e., Sts 14b and KNM-WT 15000 BM, U.W. 88-126 and KNM-WT 15000 AC). A light grey box encloses the observed range of variation across vertebral levels in *Au. africanus* and *H. erectus* (note that A.L. 288-1 is an outlier). *Au. sediba* specimens are enclosed in a dark grey box. MH2 (U.W. 88-126) is highlighted with a dashed red line and falls between the two MH1 specimens (U.W. 88-92 and U.W. 88-152). Spinal canal area is measured using ImageJ (as opposed to calculated using the area of an oval) due to its unusual shape in lumbar vertebrae.

(L1–L5), we fail to identify any consistent pattern of separation between australopiths and *H. erectus* (or between these fossil groups and modern humans), results that may be due in part to methodology (i.e., measurement choice). Rather, we find that differences between MH1 (upper-middle lumbar levels) and MH2 (lower lumbar levels) are consistent with change expected across vertebral levels (Figure 33).

Overall, these results are consistent with other recent work that supports conspecific partial skeletons of a single species, *Au. sediba*, at the ca 2.0 Ma site of Malapa (e.g., Ritzman et al. 2016; de Ruiter et al. 2013, 2018).

ACKNOWLEDGEMENTS

The authors thank Jeremy DeSilva and Karen Rosenberg for their help and feedback, and two anonymous reviewers, whose comments and suggestions improved the manuscript. We are grateful to Kris Carlson and Kudakwashe Jakata for assistance with microCT scanning at Wits and Charles Woodward for helping create Figure 1. We thank

the University of the Witwatersrand and the Evolutionary Studies Institute, as well as the South African National Centre of Excellence in Palaeosciences and Bernhard Zipfel and Sifelani Jirah for curating the *Au. sediba* material and allowing us access to it and to fossil comparative material in the Phillip V. Tobias Fossil Primate and Hominid Laboratory. We thank the following individuals for curating and providing access to comparative materials in their care: Stephany Potze and Lazarus Kgasi (Ditsong Museums); Yonas Yilma, Tomas Getachew, Jared Assefa, and Getachew Senishaw (National Museum of Ethiopia and Authority for Research and Conservation of Cultural Heritage); Wim Wendelen and Emmanuel Gilissen (RMCA); Lyman Jellema and Yohannes Haile-Selassie (Cleveland Museum of Natural History); and Eileen Westwig, Eleanor Hoeger, Aja Marcato, Brian O'Toole, and Neil Duncan (American Museum of Natural History). We thank Emma Mbua, Fred Spoor, and the National Museums of Kenya Earth Science Department for providing CT scans of the KNM WT-15000 axial skele-

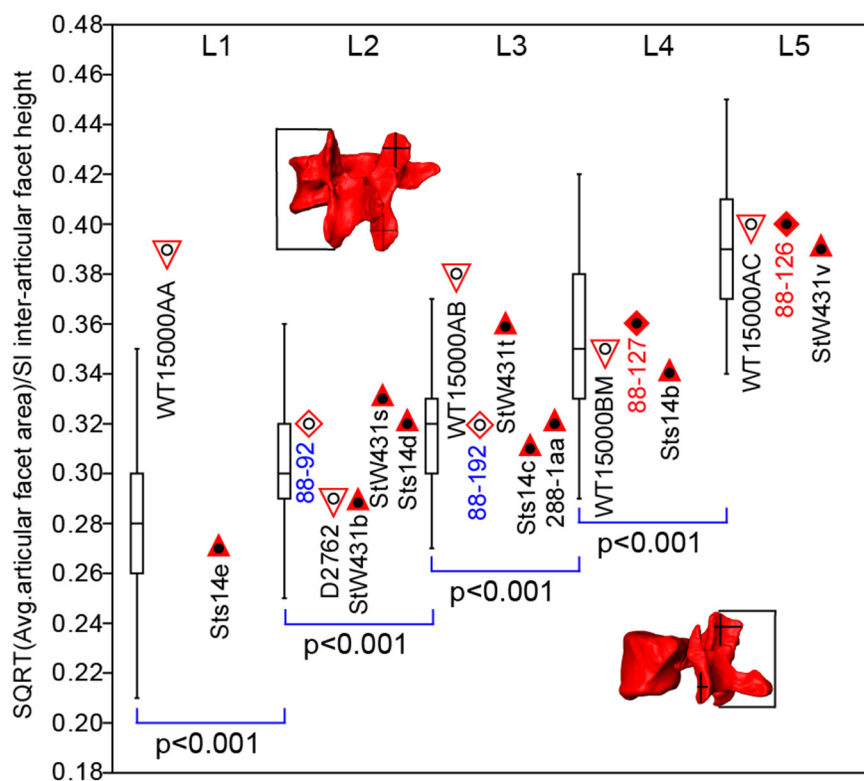


Figure 33. Index of articular facet area relative to SI inter-articular facet height. Modern human data are shown in box plots, with fossil hominins plotted to the right at each vertebral level. Note that modern humans differ significantly across levels and fossil hominins generally conform to those patterns. Additionally, there are no discernable differences in pattern detected between MH1 (U.W. 88-92 and U.W. 88-152) and MH2 (U.W. 88-127/153/234 and U.W. 88-126/138) or between *Au. africanus* (Sts 14 and StW 431 specimens) and *H. erectus* (D2762 and KNM-WT 15000 specimens). Human adults and juveniles are not statistically different from each other, so they are pooled. Articular facet area is calculated as the average transverse width multiplied by the average SI height of superior and inferior articular facets.

ton. We thank the South African Heritage Resource agency for the permits to work at Malapa and the Nash family for granting access to the site and continued support of research on their reserve, along with the South African Department of Science and Technology, the Gauteng Provincial Government, the Gauteng Department of Agriculture, Conservation and Environment and the Cradle of Humankind Management Authority, the South African National Research Foundation and the African Origins Platform, the National Geographic Society, the Palaeontological Scientific Trust, and the University of Witwatersrand's Schools of Geosciences and Anatomical Sciences and the Bernard Price Institute for Paleontology for support and facilities, as well as our respective universities. We acknowledge the Spanish Ministry of Economy and Competitively (MINEO CGL2012-37279 and CGL2015-63648-P) and the New York University Research Challenge Fund for support.

REFERENCES

- Abitbol, M.M. 1987. Evolution of the lumbosacral angle. *American Journal of Physical Anthropology* 72, 361–372.
- Arlegi, M., Gómez-Olivencia, A., Albessard, L., Martínez, I., Balzeau A., Arsuaga, J.L., and Been, E. 2017. The role of allometry and posture in the evolution of the hominin subaxial cervical spine. *Journal of Human Evolution* 104, 80–99.
- Barnes, E. 1994. *Developmental Defects of the Axial Skeleton in Paleopathology*. University of Colorado Press, Boulder.
- Barnes, E. 2012. *Atlas of Developmental Field Anomalies of the Human Skeleton: A Paleopathological Perspective*. Wiley-Blackwell, Hoboken, NJ.
- Bastir, M., García-Martínez, D., Williams, S.A., Nalla, S., Eyre, J., Oishi, M., Ogihara, N., Churchill, S.E., Berger, S.E., and Schmid, P. 2016. *PaleoAnthropology* 2016 A2–A3 (meeting abstract). doi:10.4207/PA.2016.ABS14
- Been, E. and Rak, Y. 2014. The lumbar spine of *Australopithecus sediba* indicates two hominid taxa. *PaleoAnthropology* 2014, A2 (meeting abstract). doi:10.4207/PA.2014.ABS12.
- Been, E., Gómez-Olivencia, A., and Kramer, P.A. 2012. Lumbar lordosis of extinct hominins. *American Journal of Physical Anthropology* 147, 64–77.
- Been, E., Gómez-Olivencia, A., and Kramer, P.A. 2014. Lumbar lordosis in extinct hominins: implications of the pelvic incidence. *American Journal of Physical Anthropology* 154, 307–314.
- Benade, M.M. 1990. *Thoracic and Lumbar Vertebra of African Hominids Ancient and Recent: Morphological and Func-*

- tional Aspects with Special Reference to Upright Posture. Master's Thesis, University of the Witwatersrand.
- Berger, L.R., de Ruiter, D.J., Churchill, S.E., Schmid, P., Carlson, K.J., Dirks, P.H.G.M., and Kibii, J.M. 2010. *Australopithecus sediba*: A new species of Homo-like australopithecine from South Africa. *Science* 328, 195–204.
- Berger, L.R., Hawks, J., de Ruiter, D.J., Churchill, S.E., Schmid, P., Delezene, L.K., Kivell, T.L., Garvin, H.M., Williams, S.A., DeSilva, J.M., Skinner, M.M., Musiba, C.M., Cameron, N., Holliday, T.W., Harcourt-Smith, W., Ackermann, R.R., Bastir, M., Bogin, B., Bolter, D., Brophy, J., Cofran, Z.D., Congdon, K.A., Deane, A.S., Dembo, M., Drapeau, M., Elliott, M.C., Feuerriegel, E.M., Garcia-Martinez, D., Green, D.J., Gurtov, A., Irish, J.D., Kruger, A., Laird, M.F., Marchi, D., Meyer, M.R., Nalla, S., Negash, E.W., Orr, C.M., Radovicic, D., Schroeder, L., Scott, J.E., Throckmorton, Z., Tocheri, M.W., VanSickle, C., Walker, C.S., Wei, P., and Zipfel, B. 2015. *Homo naledi*, a new species of the genus *Homo* from the Dinaledi Chamber, South Africa. *eLife* 4, e09560.
- Bonmati, A., Gómez-Olivencia, A., Arsuaga, J.L., Carretero, J.M., Gracia, A., Martínez, I., Lorenzo, C., Bértudez de Castro, J.M., and Carbonell, E. 2010. Middle Pleistocene lower back and pelvis from an aged human individual from the Sima de los Huesos site, Spain. *Proceedings of the National Academy of Sciences USA* 107, 18386–18391.
- Bräuer, G. 1988. Osteometrie. In *Anthropologie. Handbuch der vergleichenden Biologie des Menschen*, Knussmann, R. (ed.). Gustav Fischer, Stuttgart, pp. 160–232.
- Cameron, N., Bogin, B., Bolter, D., and Berger, L.R. 2017. The postcranial skeletal maturation of *Australopithecus sediba*. *American Journal of Physical Anthropology* 163, 633–640.
- Churchill, S.E., Holliday, T.W., Carlson, K.J., Jashashvili, T., Macias, M.E., Mathews, S., Sparling, T.L., Schmid, P., de Ruiter, D.J., and Berger, L.R. 2013. The upper limb of *Australopithecus sediba*. *Science* 340, 1233477.
- Churchill, S.E., Green, D.J., Feuerriegel, E.M., Macias, M.E., Mathews, S., Carlson, K.J., Schmid, P., and Berger, L.R. 2018b (this volume). The shoulder, arm, and forearm of *Australopithecus sediba*. *PaleoAnthropology* 2018, 234–281.
- Churchill, S.E., Kibii, J. M., Schmid, P., Reed, N.D., and Berger, L.R. 2018a (this volume). The pelvis of *Australopithecus sediba*. *PaleoAnthropology* 2018, 334–356.
- Cook, D.C., Buikstra, J.E., Buikstra, J.E., DeRousseau, C.J., and Johanson, D.C. 1983. Vertebral pathology in the Afar australopithecines. *American Journal of Physical Anthropology* 60, 83–101.
- Dean, M.C. and Smith, B.H. 2009. Growth and development of the Nariokotome Youth, KNM-WT 15000. In *The First Humans: Origin and Early Evolution of the Genus Homo*, Grine, F.E., Fleagle, J.G., and Leakey, R.E. (eds.). Springer, pp. 101–120.
- de Ruiter, D.J., Carlson, K.B., Brophy, J.K., Churchill, S.E., Carlson, K.J., and Berger, L.R. 2018 (this volume). The skull of *Australopithecus sediba*. *PaleoAnthropology* 2018, 56–155.
- de Ruiter, D.J., DeWitt, T.J., Carlson, K.B., Brophy, J.K., Schroeder, L., Ackermann, R.R., Churchill, S.E., and Berger, L.R., 2013. Mandibular remains support taxonomic validity of *Australopithecus sediba*. *Science* 340, 1232997.
- DeSilva, J.M., Holt, K.G., Churchill, S.E., Carlson, K.J., Walker, C.S., Zipfel, B., and Berger, L.R. 2013. The lower limb and mechanics of walking in *Australopithecus sediba*. *Science* 340, 1232999.
- DeSilva, J.M., Carlson, K.J., Claxton, A., Harcourt-Smith, W.E.H., McNutt, E.J., Sylvester, A.D., Walker, C.S., Zipfel, B., Churchill, S.E., and Berger, L.R. 2018 (this volume). The anatomy of the lower limb skeleton of *Australopithecus sediba*. *PaleoAnthropology* 2018, 357–405.
- Dickson, R.A. and Deacon, P. 1987. Spinal growth. *Journal of Bone and Joint Surgery* 69, 690–692.
- DiGiovanni, B.F., Scoles, P.V., and Latimer, B.M. 1989. Anterior extension of the thoracic vertebral bodies in Scheuermann's kyphosis: an anatomic study. *Spine* 14, 712–716.
- Dirks, P.H.G.M., Kibii, J.M., Kuhn, B.F., Steininger, C., Churchill, S.E., Kramers, J.D., Pickering, R., Farber, D.L., Mériaux, A.-S., Herries, A.I.R., King, G.C.P., and Berger, L.R. 2010. Geological setting and age of *Australopithecus sediba* from southern Africa. *Science* 328, 205–208.
- Franciscus, R.G. and Churchill, S.E. 2002. The costal skeleton of Shanidar 3 and a reappraisal of Neandertal thoracic morphology. *Journal of Human Evolution* 42, 303–356.
- Gómez-Olivencia, A., Been, E., Arsuaga, J.L., and Stock, J.T. 2013. The Neandertal vertebral column1: the cervical spine. *Journal of Human Evolution* 64, 608–630.
- Haeusler, M., Martelli, S.A., and Boeni, T. 2002. Vertebrae numbers of the early hominid lumbar spine. *Journal of Human Evolution* 43, 621–643.
- Haeusler, M., Schiess, R., and Boeni, T. 2011. New vertebral material point to a modern bauplan of the Nariokotome *Homo erectus* skeleton. *Journal of Human Evolution* 61, 575–582.
- Haeusler, M., Schiess, R., and Boeni, T. 2012. Modern or distinct axial bauplan in early hominins? A reply to Williams (2012). *Journal of Human Evolution* 63, 557–559.
- Haile-Selassie, Y., Latimer, B.M., Alene, M., Deino, A.L., Gibert, L., Melillo, S.M., Saylor, B.Z., Scott, G.R., and Lovejoy, C.O. 2010. An early *Australopithecus afarensis* postcranium from Woranso-Mille, Ethiopia. *Proceedings of the National Academy of Sciences USA* 107, 12121–12126.
- Hawks, J., Elliott, M., Schmid, P., Churchill, S.E., de Ruiter, D.J., Roberts, E.M., Hilbert-Wolf, H., Garvin, H.M., Williams, S.A., Delezene, L.K., Feuerriegel, E.M., Randolph-Quinney, P., Kivell, T.L., Laird, M.F., Tawane, G., DeSilva, J.M., Bailey, S.E., Brophy, J.K., Meyer, M.R., Skinner, M.M., Tocheri, M.W., VanSickle, C., Walker, C.S., Campbell, T.L., Kuhn, B., Kruger, A., Tucker, S., Gurtov, A., Hlophe, N., Hunter, R., Morris, H., Peixotto, B., Ramalepa, M., van Rooyen, D., Tsikoane, M., Boschhoff, P., Dirks, P.H.G.M., and Berger, L.R. 2017.

- New fossils of *Homo naledi* from the Lesedi Chamber, South Africa. *eLife* e24232.
- Irish, J.D., Guatelli-Steinberg, D., Legge, S., Berger, L.R., and de Ruiter, D.J. 2013. Dental morphology and the phylogenetic 'place' of *Australopithecus sediba*. *Science* 340, 1233062.
- Jellema, L.M., Latimer, B., Walker, A. 1993. The rib cage. In *The Nariokotome Homo erectus Skeleton*, Walker, A. and Leakey, R. (eds.), Harvard University Press, Cambridge, pp. 294–325.
- Johanson, D.C., Lovejoy, C.O., Kimbel, W.H., White, T.D., Ward, S.C., Bush, M.E., Latimer, B.M., and Coppens, Y. 1982. Morphology of the Pliocene partial hominid skeleton (A.L. 288-1) from the Hadar Formation, Ethiopia. *American Journal of Physical Anthropology* 57, 403–451.
- Kibii, J.M., Churchill, S.E., Schmid, P., Carlson, K.J., Reed, N.D., de Ruiter, D.J., and Berger, L.R. 2011. A partial pelvis of *Australopithecus sediba*. *Science* 333, 1407–1411.
- Kivell, T.L., Churchill, S.E., Kibii, J.M., Schmid, P., and Berger, L.R. 2018 (this volume). The hand of *Australopithecus sediba*. *PaleoAnthropology* 2018, 282–333.
- Kivell, T.L., Kibii, J.M., Churchill, S.E., Schmid, P., and Berger, L.R. 2011. *Australopithecus sediba* hand demonstrates mosaic evolution of locomotor and manipulative abilities. *Science* 333, 1411–1417.
- Latimer, B.M., Lovejoy, C.O., Spurlock, L., and Haile-Selassie, Y. 2016. The thoracic cage of KSD-VP-1/1. In *The Postcranial Anatomy of Australopithecus afarensis: New Insights from KSD-VP-1/1*, Haile-Selassie, Y. and Su, D.F. (eds.). Springer, Dordrecht, pp. 143–154.
- Latimer, B. and Ward, CV. 1993. The thoracic and lumbar vertebrae. In *The Nariokotome Homo erectus Skeleton*, Walker, A. and Leakey, R. (eds.). Harvard University Press, Cambridge, pp. 266–293.
- Leakey, R.E., Leakey, M.G., and Behrensmeyer, A.K. 1978. The hominid catalogue. In *Koobi Fora Research Project, Volume 1: The Fossil Hominids and an Introduction to Their Context, 1968-1974*, Leakey, M.G. and Leakey, R.E. (eds.). Clarendon Press, Oxford, pp. 86–182.
- Lovejoy, C.O., Johanson, D.C., and Coppens, Y. 1982. Elements of the axial skeleton recovered from the Hadar formation: 1974-1977 Collections. *American Journal of Physical Anthropology* 57, 631–635.
- Meyer, M.R. 2005. *Functional biology of the Homo erectus axial skeleton from Dmanisi, Georgia*. Ph.D. Dissertation, University of Pennsylvania.
- Meyer, M.R. 2016. The cervical vertebrae of KSD-VP-1/1. In *The Postcranial Anatomy of Australopithecus afarensis: New Insights from KSD-VP-1/1*, Haile-Selassie, Y. and Su, D.F. (eds.). Springer, Dordrecht, pp. 63–111.
- Meyer, M.R. and Haeusler, M. 2015. Spinal cord evolution in early *Homo*. *Journal of Human Evolution* 88, 43–53.
- Meyer, M.R. and Williams, S.A. in review. Earliest axial remains from the genus *Australopithecus*: vertebrae of *A. anamensis* from Asa Issie. *Journal of Human Evolution*.
- Meyer, M.R., Williams, S.A., Schmid, P., Churchill, S.E., and Berger, L.R. 2017. The cervical spine of *Australopithecus sediba*. *Journal of Human Evolution* 104, 32–49.
- Meyer, M.R., Woodward, C., Tims, A., and Bastir, M. 2018. Neck function in early hominins and suspensory primates: insights from the uncinated process. *American Journal of Physical Anthropology* 166, 613–637.
- Meyer, M.R., Williams, S.A., Smith, M.P., and Sawyer, G.J. 2015. Lucy's back: reassessment of fossils associated with the A.L. 288-1 vertebral column. *Journal of Human Evolution* 85, 174–180.
- Nalla, S. 2013. *The Morphology of the Upper Thorax of Australopithecus sediba within the Context of Selected Hominoids*. Ph.D. dissertation, University of the Witwatersrand.
- Nalley, T.K. and Grider-Potter, N. 2015. Functional morphology of the primate head and neck. *American Journal of Physical Anthropology* 156, 531–542.
- Ohman, J.C. 1986. The first rib of hominoids. *American Journal of Physical Anthropology* 70, 209–229.
- Ostrofsky, K.R. and Churchill, S.E. 2015. Sex determination by discriminant function analysis of lumbar vertebrae. *Journal of Forensic Science* 60, 21–28.
- Pickering, R., Dirks, P.H.G.M., Jinnah, Z., de Ruiter, D.J., Churchill, S.E., Herries, A.I.R., Woodhead, J.D., Hellstrom, J.C., and Berger, L.R. 2011. *Australopithecus sediba* at 1.977 Ma and implications for the origins of the genus *Homo*. *Science* 333, 1421–1423.
- Rak, Y. and Been, E. 2014. Two hominid taxa at Malapa: the mandibular evidence. *PaleoAnthropology* 2014, A20 (meeting abstract). doi:10.4207/PA.2014.ABS12.
- Randolph-Quinney, P.S., Williams, S.A., Steyn, M., Meyer, M.R., Smilg, J.S., Churchill, S.E., Odes, E.J., Augustine, T., Tafforeau, P., and Berger, L.R. 2016. Osteogenic tumour in *Australopithecus sediba*: earliest hominin evidence for neoplastic disease. *South African Journal of Science* 112 (7/8), 1–7.
- Ritzman, T.B., Terhune, C.E., Gunz, P., and Robinson, C.A. 2016. Mandibular ramus shape of *Australopithecus sediba* suggests a single variable species. *South African Journal of Science* 100, 54–64.
- Robinson, J.T. 1972. *Early Hominid Posture and Locomotion*. University of Chicago Press, Chicago.
- Rosenman, B.A. 2008. *Triangulating the Evolution of the Vertebral Column in the Last Common Ancestor: Thoracolumbar Transverse Process Homology in the Hominoidea*. Ph.D. dissertation, Kent State University.
- Russo, G.A. and Williams, S.A. 2015. "Lucy" (A.L. 288-1) had five sacral vertebrae. *American Journal of Physical Anthropology* 156, 295–303.
- Sanders, W.J. 1995. *Function, Allometry, and Evolution of the Australopithecine Lower Precaudal Spine*. Ph.D. Dissertation, New York University.
- Sanders, W.J. 1998. Comparative morphometric study of the australopithecine vertebral series Stw-H8/H41. *Journal of Human Evolution* 34, 249–302.
- Scheuer, L. and Black, S. 2000. *Developmental Juvenile Osteology*. Elsevier Academic Press, Amsterdam.
- Schmid, P., Churchill, S.E., Nalla, S., Weissen, E., de Ruiter, D.J., and Berger, L.R. 2013. Mosaic morphology in the thorax of *Australopithecus sediba*. *Science* 340, 1234598.

- Stern, J.T. and Jungers, W.L. 1990. The capitular joint of the first rib in primates: a re-evaluation of the proposed link to locomotion. *American Journal of Physical Anthropology* 82, 431–439.
- Tardieu, C., Bonneau, N., Hecquet, J., Boulay, C., Marty, C., Legaye, J., and Duval-Beaupère, G. 2013. How is sagittal balance acquired during bipedal gait acquisition? Comparison of neonatal and adult pelvis in three dimensions: evolutionary implications. *Journal of Human Evolution* 65, 209–222.
- Tawane, G., García-Martínez, D., Eyre, J., Bastir, M., Berger, L., Schmid, P., Nalla, S., and Williams, S.A. 2016. A hominin first rib discovered at the Sterkfontein Caves, South Africa. *South African Journal of Science* 112, 5/6.
- Thompson, N.E. and Almécija, S. 2017. The evolution of vertebral formulae in Hominoidea. *Journal of Human Evolution* 110, 18–36.
- Val, A., Dirks, P.H.G.M., Backwell, L.R., d’Errico, F., and Berger, L.R. 2015. Taphonomic analysis of the faunal assemblage associated with the hominins (*Australopithecus sediba*) from the Early Pleistocene Cave Deposits of Malapa, South Africa. *PLoS One* 10, e0126904.
- Ward, C.V., Kimbel, W.H., Harmon, E.H., and Johanson, D.C. 2012. New postcranial fossils of *Australopithecus afarensis* from Hadar, Ethiopia (1990–2007). *Journal of Human Evolution* 63, 1–51.
- Ward, C.V., Nalley, T.K., Spoor, F., Tafforeau, P., and Alemseged, Z. 2017. Thoracic vertebral count and thoracolumbar transition in *Australopithecus afarensis*. *Proceedings of the National Academy of Sciences USA* 114, 6000–6004.
- Whitcome, K.K., Shapiro, L.J., and Lieberman, D.E. 2007. Fetal load and the evolution of lumbar lordosis in bipedal hominins. *Nature* 450, 1075–1078.
- White, T.D., Black, M.T., and Folkens, P.A. 2011. *Human Osteology*, Third Edition. Academic Press, New York.
- Williams, S.A. 2011a. *Evolution of the Hominoid Vertebral Column: The Long and Short of it*. Ph.D. Dissertation, University of Illinois at Urbana-Champaign.
- Williams, S.A. 2011b. Variation in anthropoid vertebral formulae: implications for homology and homoplasy in hominoid evolution. *Journal of Experimental Zoology B (Molecular and Developmental Evolution)* 318, 134–147.
- Williams, S.A. 2012a. Placement of the diaphragmatic vertebra in catarrhines: implications for the evolution of dorsostability in hominins and bipedalism in hominins. *American Journal of Physical Anthropology* 148, 111–122.
- Williams, S.A., 2012b. Modern or distinct axial bauplan in early hominins? Comments on Haeusler et al. (2011). *Journal of Human Evolution* 63, 552–556.
- Williams, S.A., DeSilva, J.M., and De Ruiter, D.J. 2018 (this volume). Malapa at 10: Introduction to the Special Issue on *Australopithecus sediba*. *PaleoAnthropology* 2018, 49–55.
- Williams, S.A., García-Martínez, D., Bastir, M., Meyer, M.R., Nalla, S., Hawks, J., Schmid, P., Churchill, S.E., and Berger, L.R. 2017. The vertebrae and ribs of *Homo naledi*. *Journal of Human Evolution* 104, 136–154.
- Williams, S.A., Middleton, E.R., Villamil, C.I., and Shattuck, M.R. 2016. Vertebral numbers and human evolution. *Yearbook of Physical Anthropology* 159, S19–S36.
- Williams, S.A., Ostrofsky, K.R., Frater, N., Churchill, S.E., Schmid, P., and Berger, L.R. 2013. The vertebral column of *Australopithecus sediba*. *Science* 340, 1232996.
- Williams, S.A. and Russo, G.A. 2015. Evolution of the hominoid vertebral column: the long and the short of it. *Evolutionary Anthropology* 24, 15–32.
- Williams, S.A. and Russo, G.A. 2016. The fifth element (of Lucy’s sacrum): reply to Machnicki, Lovejoy, and Reno. *American Journal of Physical Anthropology* 161, 374–378.
- Zipfel, B., DeSilva, J.M., Kidd, R.S., Carlson, K.J., Churchill, S.E., and Berger, L.R. 2011. The foot and ankle of *Australopithecus sediba*. *Science* 333, 1417–1420.

APPENDIX I
Supplementary figures of *Au. sediba* axial skeletal material.

This appendix contains information about the segmentation protocol of microCT scans, figures of the more fragmentary fossils of MH1 and MH2, and comparative plots of *Au. sediba* with other fossil hominins and extant taxa (modern *H. sapiens* and *Pan troglodytes*).

SEGMENTATION PROTOCOL

To remove remaining matrix and further analyze the individual vertebrae, high-resolution microCT scans of the MH2 lower thoracic (U.W. 88-114, U.W. 88-43, and U.W. 88-44) and lumbar vertebrae (U.W. 88-127/153/234 and U.W. 88-126/138) were processed to yield virtual 3D surface models. Each vertebra was segmented with the three-dimensional visualization program, Amira 6.2® using the

following protocol. First, the microCT scan slices (TIFF images) were imported into Amira 6.2 and combined to produce a volume stack file (.am). Next, an *Edit New Label Field* module was connected to the stack file; and, through the combined use of the *magic wand* and *brush* tools, voxels were selected and assigned to each vertebral element separately. Voxel assignment to respective vertebrae was verified in all three orthogonal views. Once labeling for an element was complete, a *Generate Surface* module was performed to produce a *labels* file (.labels.am). A 3D surface model was then rendered from the labels file using an unconstrained smoothing setting of 5. Separate models for each element were then saved as polygon file (.ply) objects for further examination and potential refitting in GeoMag-ic® Studio software.

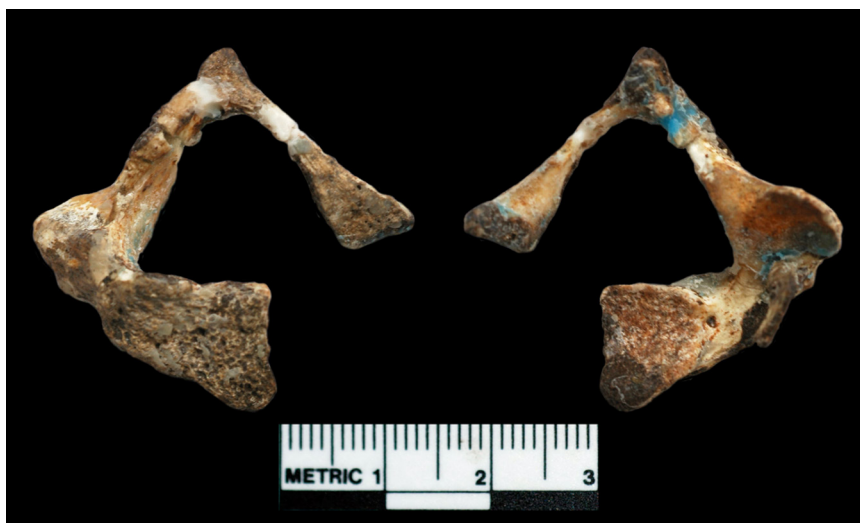


Figure A1. U.W. 88-72 (MH1) in superior (left) and inferior (right) views. The spinous process is pointing upward in this image, and the body is towards the bottom (scale is 30mm).

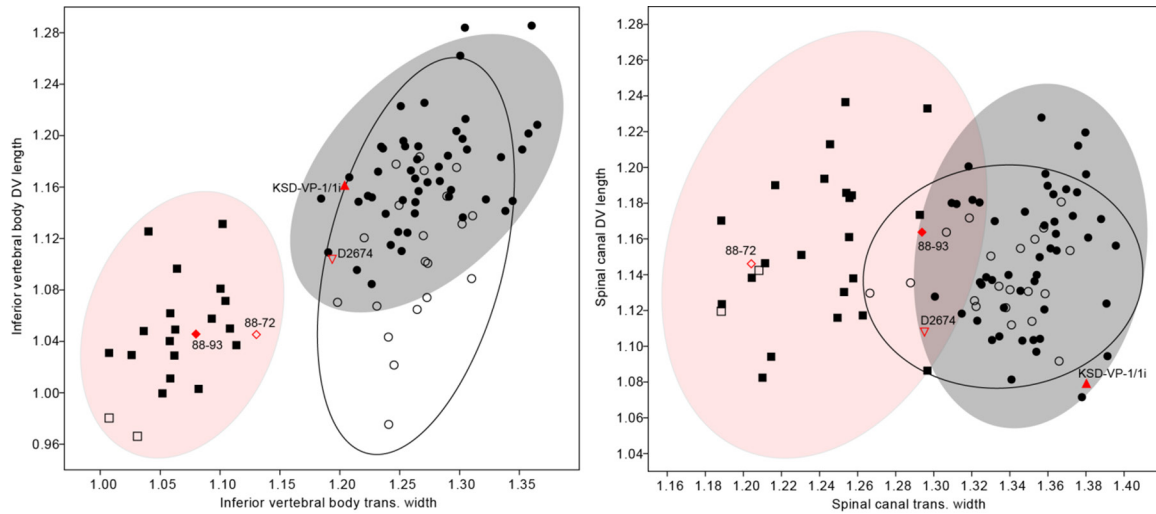


Figure A2. Inferior vertebral body and spinal canal dimensions in U.W. 88-72 (MH1), U.W. 88-93 (MH2), and other fossil hominin C3 vertebrae. All data are logged (base 10). Humans are shown as circles, chimpanzees as squares; adults are shown as filled symbols, subadults as open symbols. Fossils follow the same filled-open scheme, with *Au. sediba* shown as diamonds, *Au. afarensis* (KSD-VP-1/1 from Woranso-Mille) as triangles, and *H. erectus* (D2674 from Dmanisi) as inverted triangles. Shaded areas represent the 95% confidence ellipses of the data (red: chimpanzees; grey: adult humans; transparent with black outline: juvenile humans).

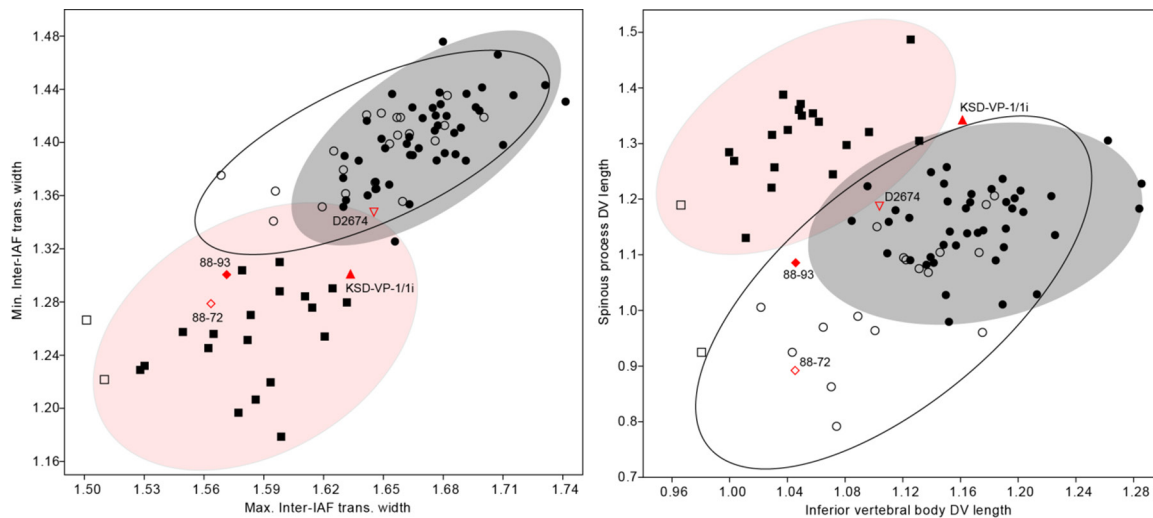


Figure A3. Maximum and minimum inter-IAF distances in U.W. 88-72 (MH1) and other fossil hominins. Data transformations, symbols, ellipses, and fossil specimens included follow Figure A2.

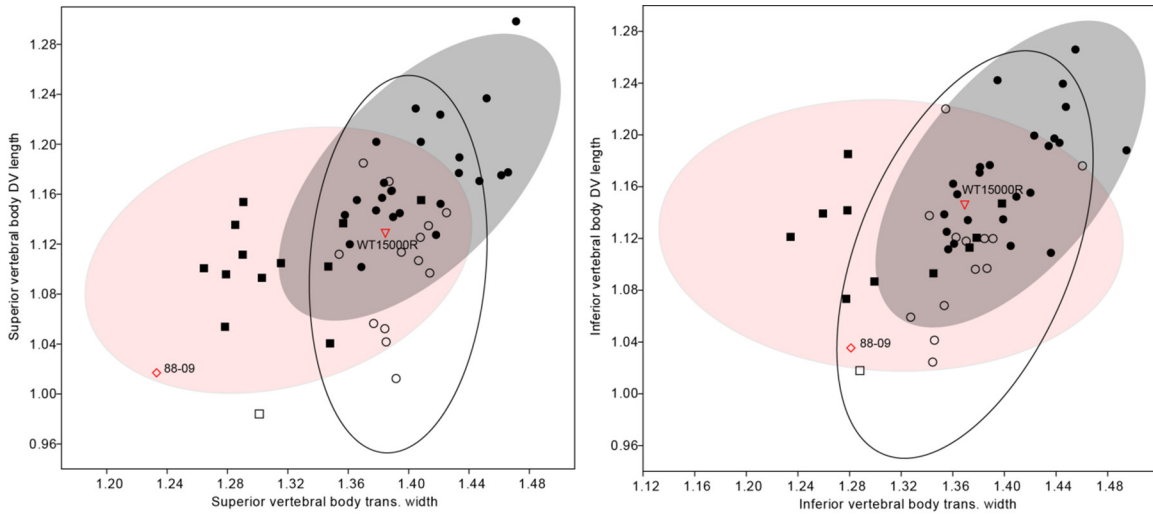


Figure A4. Vertebral body transverse and dorsoventral dimensions in U.W. 88-9 (MH1) and *Homo erectus* (KNM-WT 15000 from Nariokotome; here “WT15000”). Symbols and ellipses follow Figure A2.

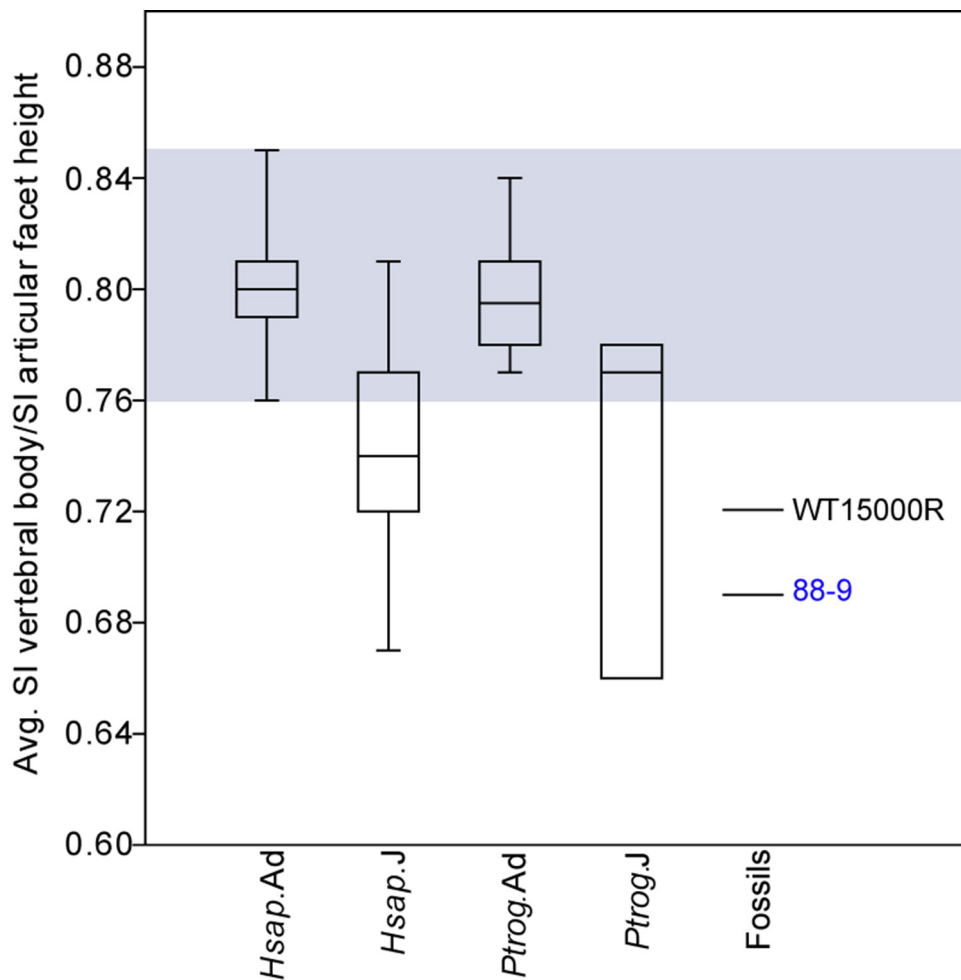


Figure A5. Ratio of average SI vertebral body height and SI inter-articular facet height in U.W. 88-9 (MH1) and *Homo erectus* (KNM-WT 15000 from Nariokotome). Note that subadult humans and chimpanzees produce lower ratios than adults and that both juvenile fossil last cervical vertebrae have short vertebral bodies relative to the SI inter-articular facet height. A gray box highlights adult human variation in this ratio. Group/specimen abbreviations are as follows: Hsap.Ad=adult humans; Hsap.J=subadult humans; Pant.Ad=adult chimpanzees; Pant.J=subadult chimpanzees; WT15000R=Nariokotome *H. erectus* specimen KNM-WT 15000 R.

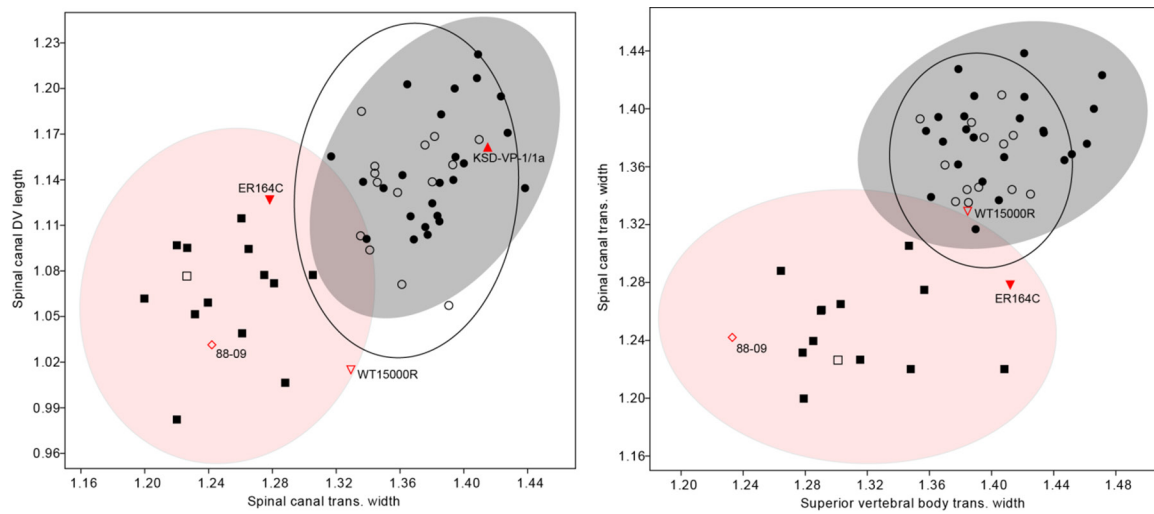


Figure A6. Spinal canal transverse and dorsoventral dimensions in U.W. 88-9 (MH1) and other fossil hominin last cervical vertebrae. Symbols, ellipses, and fossil specimens included follow Figures S2 and S4, with the addition of KNM-ER 164C (*Homo* sp.; Leakey et al. 1978).

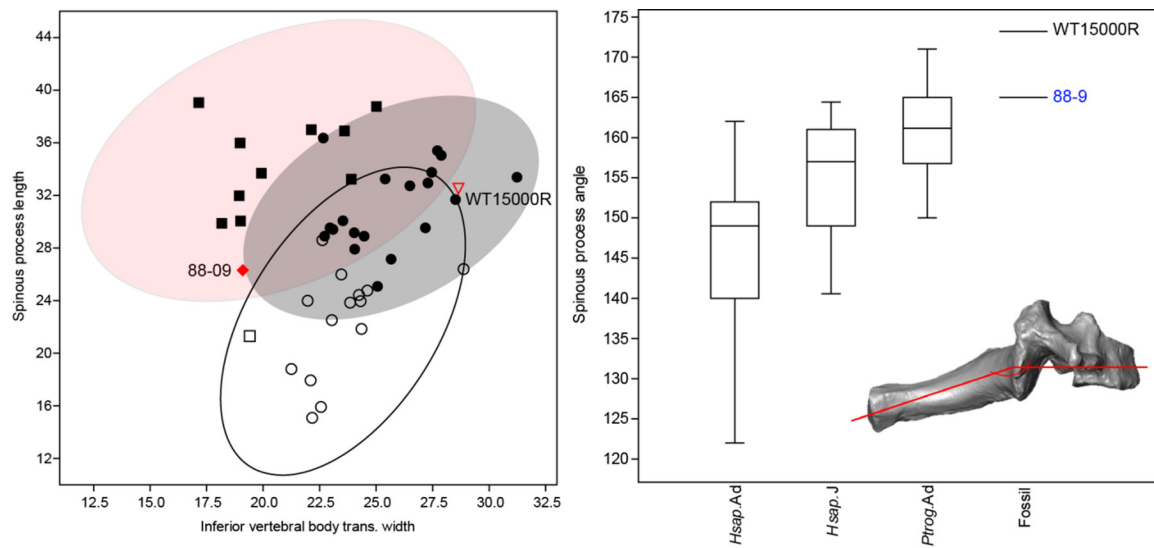


Figure A7. Spinous process DV length plotted against inferior vertebral body transverse width and spinous process angle in U.W. 88-9 (MH1) and other fossil hominin last cervical vertebrae. Spinous process angle is measured relative to coronal plane of the vertebra: higher values approach horizontal orientation; lower values are more inferiorly angled. Human adults are significantly different from human subadults ($p=0.005$) and from chimpanzees ($p<0.001$). Chimpanzee subadults are not different from adults, but this results could be due to small sample size of chimpanzee subadults ($n=2$) for this measurement. Symbols, ellipses, and fossil specimens included follow Figures A2 and A4.

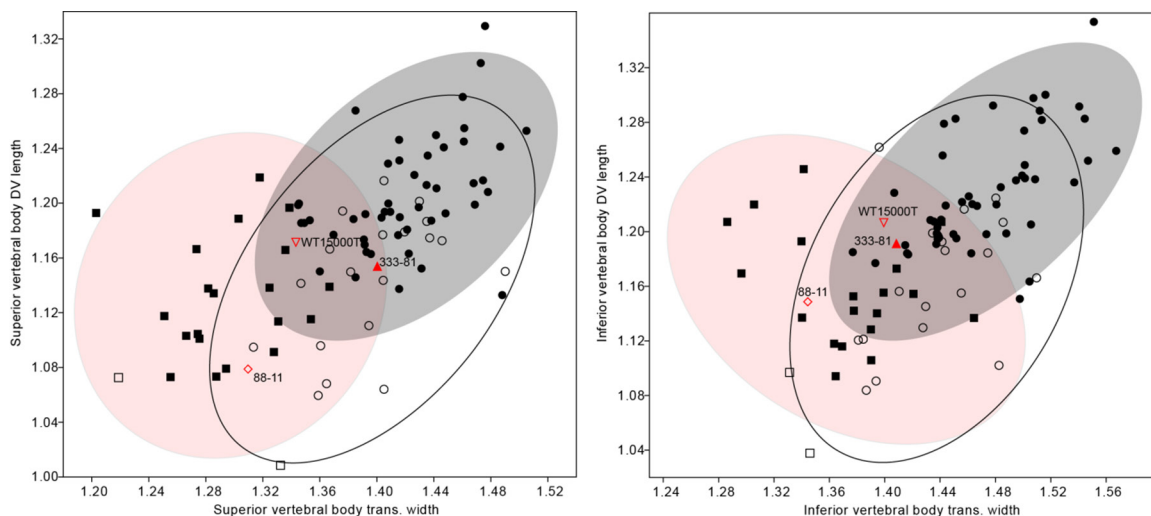


Figure A8. Vertebral body transverse and dorsoventral dimensions of U.W. 88-11 (MH1) and other fossil hominin T2 vertebrae. Symbols, ellipses, and fossil specimens included follow Figures A2 and A4, with the addition of A.L. 333-81 (Au. afarensis).

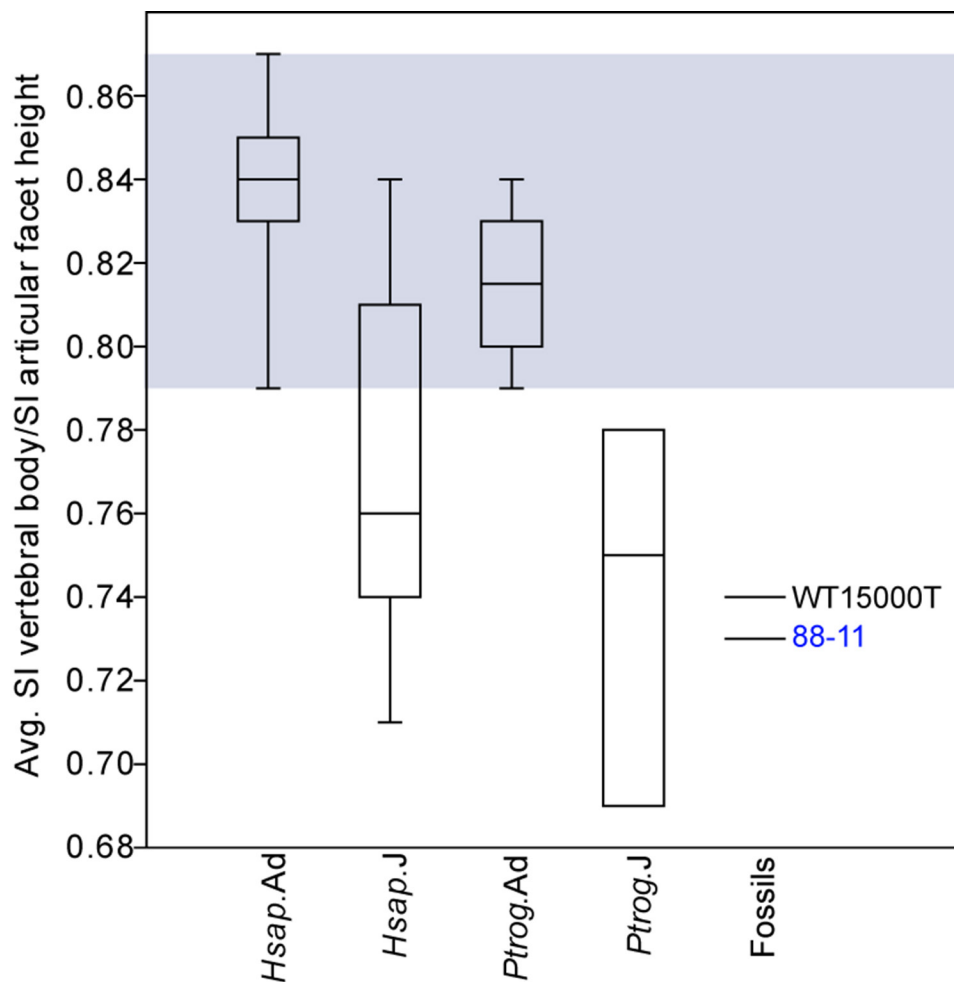


Figure A9. Ratio of average SI vertebral body height and SI inter-articular facet height in U.W. 88-11 (MH1). Note that both juvenile Au. sediba and H. erectus vertebrae have short vertebral bodies relative to the SI inter-articular facet height. Species/specimen abbreviations follow Figure A5. WT15000T=Nariokotome H. erectus specimen KNM-WT 15000 T.

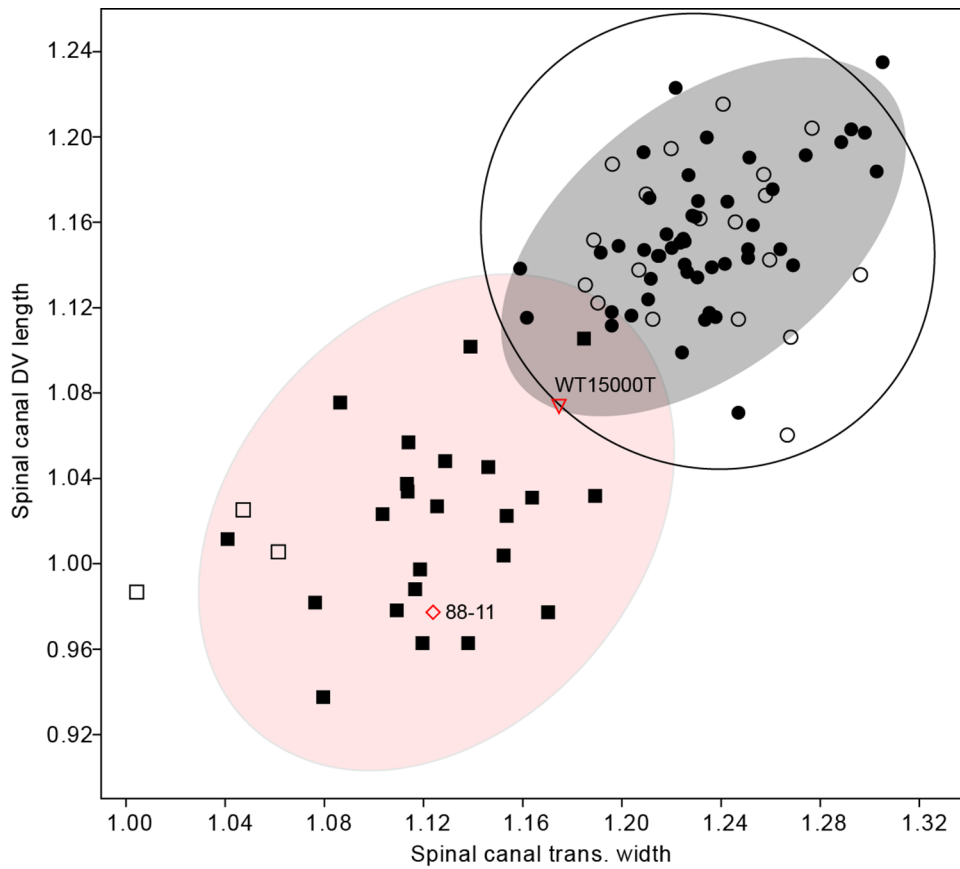


Figure A10. Spinal canal dimensions in U.W. 88-11 (MH1) and juvenile *H. erectus*. Symbols and ellipses follow Figure A2.

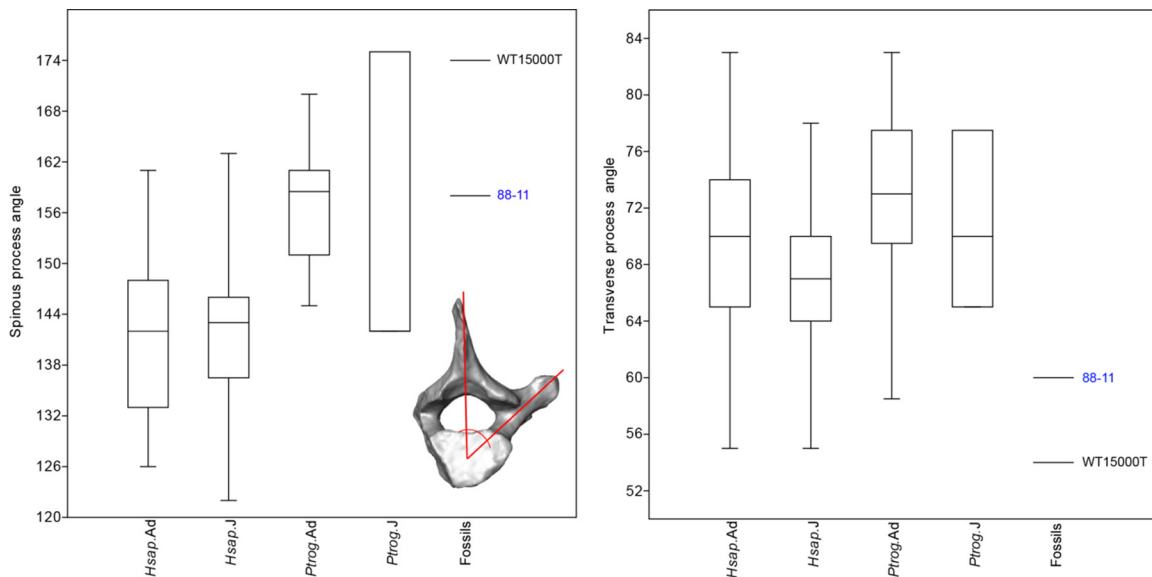


Figure A11. Spinous process and transverse angles of U.W. 88-11 (MH1) and juvenile *H. erectus*. Transverse process angle is measured relative to the sagittal midplane. Higher values approach a right angle (90°), where the long axis of the transverse process runs perpendicular to the sagittal midplane; lower values reflect more dorsally oriented transverse processes. See Figure 7 for details on spinous processes orientation is quantified. Species abbreviations follow Figure A9.

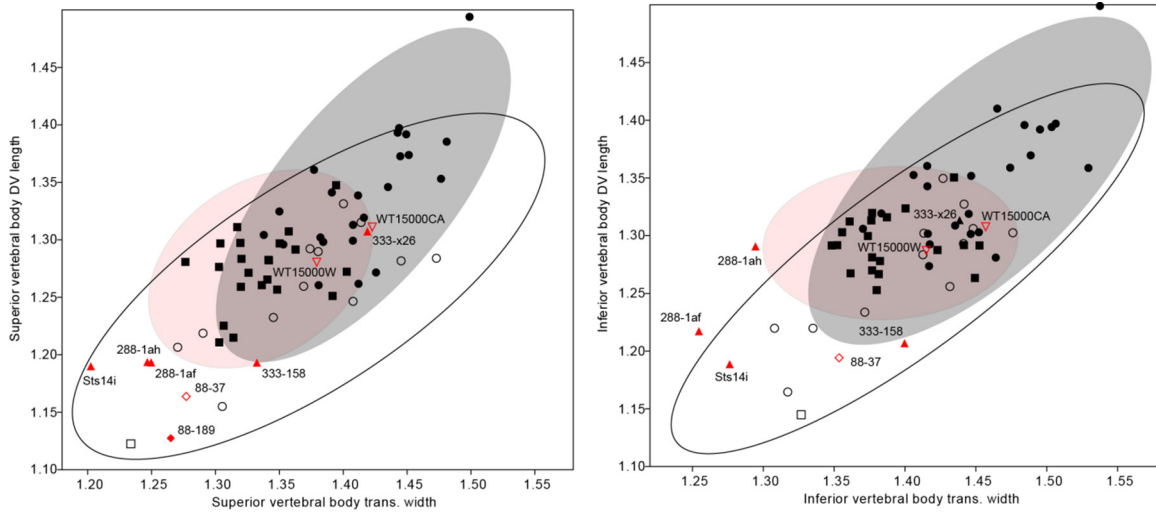


Figure A12. Vertebral body transverse and dorsoventral dimensions in U.W. 88-37 (MH1), U.W. 88-189 (MH2), and other fossil hominin middle thoracic vertebrae. *Au. afarensis* is represented by adult A.L. 288-1af and -1ah (T6 and T7 or T7 and T8; Johanson et al., 1982; Meyer et al., 2015) and A.L. 333-156 and 333-x26 (T6 and T7, the former from Ward et al., 2012); *Au. africanus* by Sts 14i (T6), and juvenile *H. erectus* by KNM-WT 15000 CA and W (T5 and T7; Walker and Leakey, 1993). Adult (filled circles) and subadult human (open circles) 95% confidence ellipses are shown, as is the adult chimpanzee (filled squares) ellipse; subadult chimpanzees are shown in open squares.

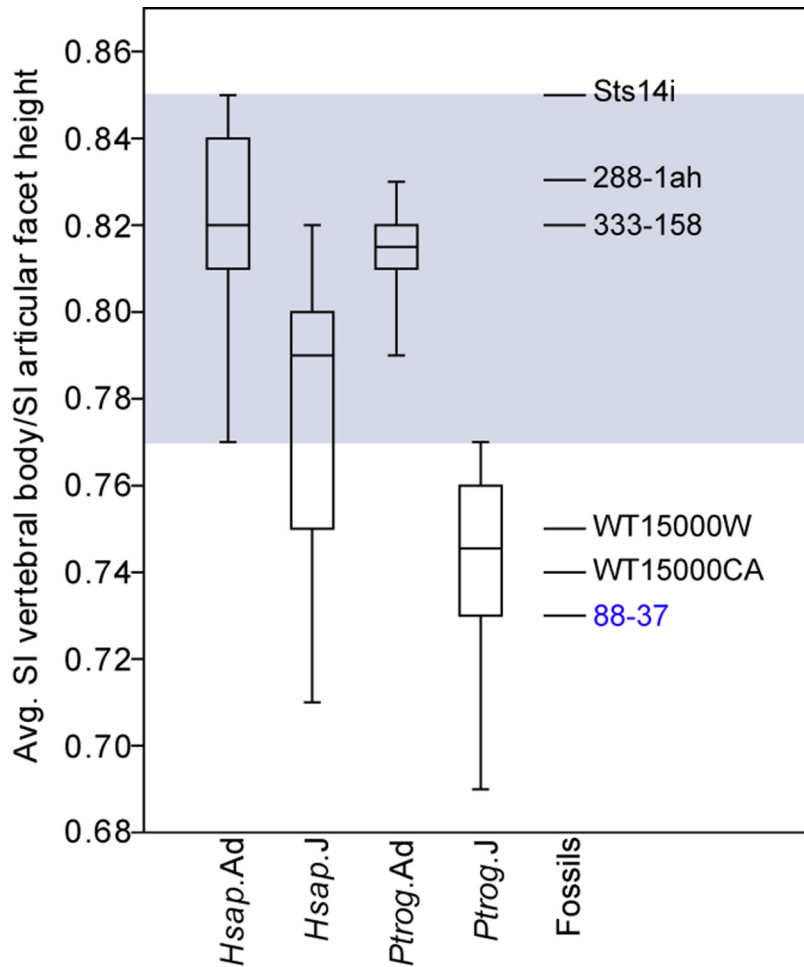


Figure A13. Ratio of average SI vertebral body height and SI inter-articular facet height in U.W. 88-37 (MH1) and other fossil hominin middle thoracic vertebrae. Subadult humans and chimpanzees demonstrate relatively shorter superior-inferior vertebral body heights than adults. Juvenile *Au. sediba* and *H. erectus* (KNM-WT 15000) fall out with the subadults, whereas adult australopiths (*Au. afarensis* and *Au. africanus*) fall out with the adults. Fossil specimens follow those listed in the Figure A12 caption.

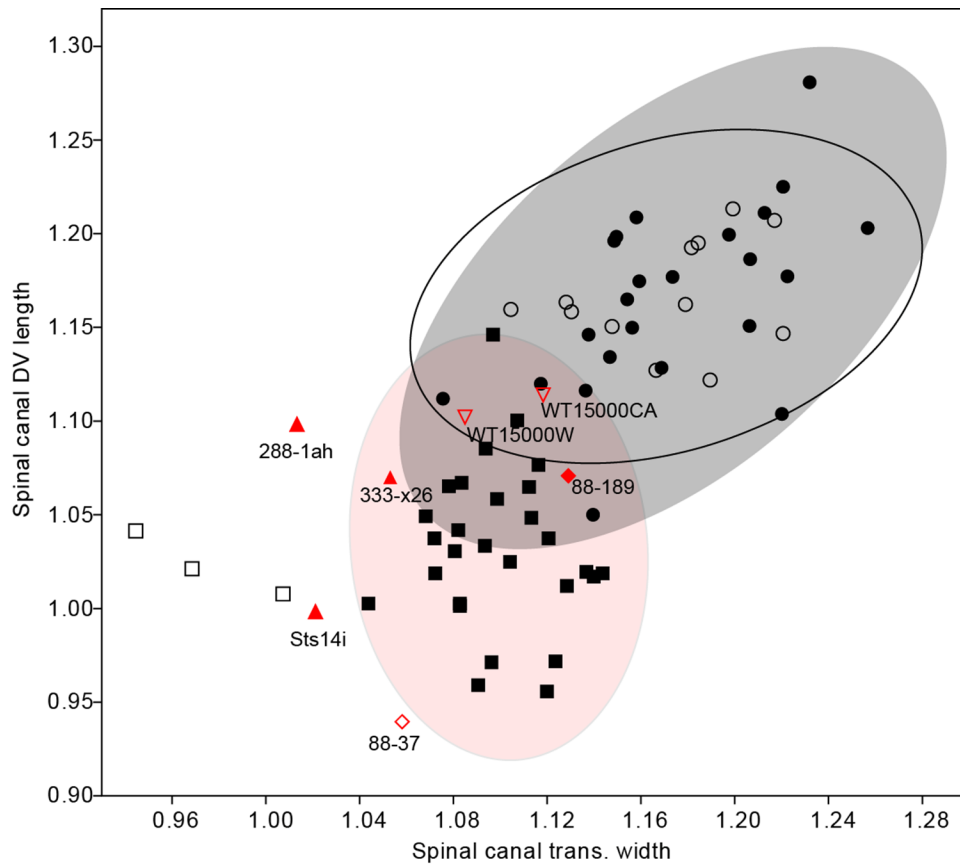


Figure A14. Spinal canal dimensions of U.W. 88-37 (MH1), U.W. 88-189 (MH2), and other fossil hominin middle thoracic vertebrae. Symbols and specimens follow Figure A12.

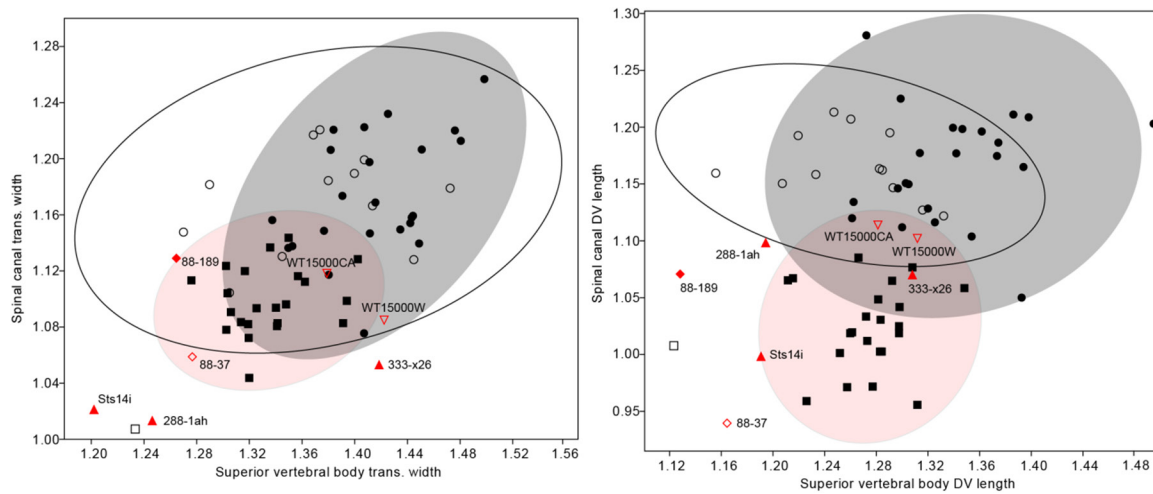


Figure A15. Vertebral body and spinal canal dimensions in U.W. 88-37 (MH1), U.W. 88-189 (MH2), and other fossil hominin middle thoracic vertebrae. Transverse width dimensions are plotted against each other (left), as are dorsoventral dimensions (right). Symbols and specimens follow Figure A12.

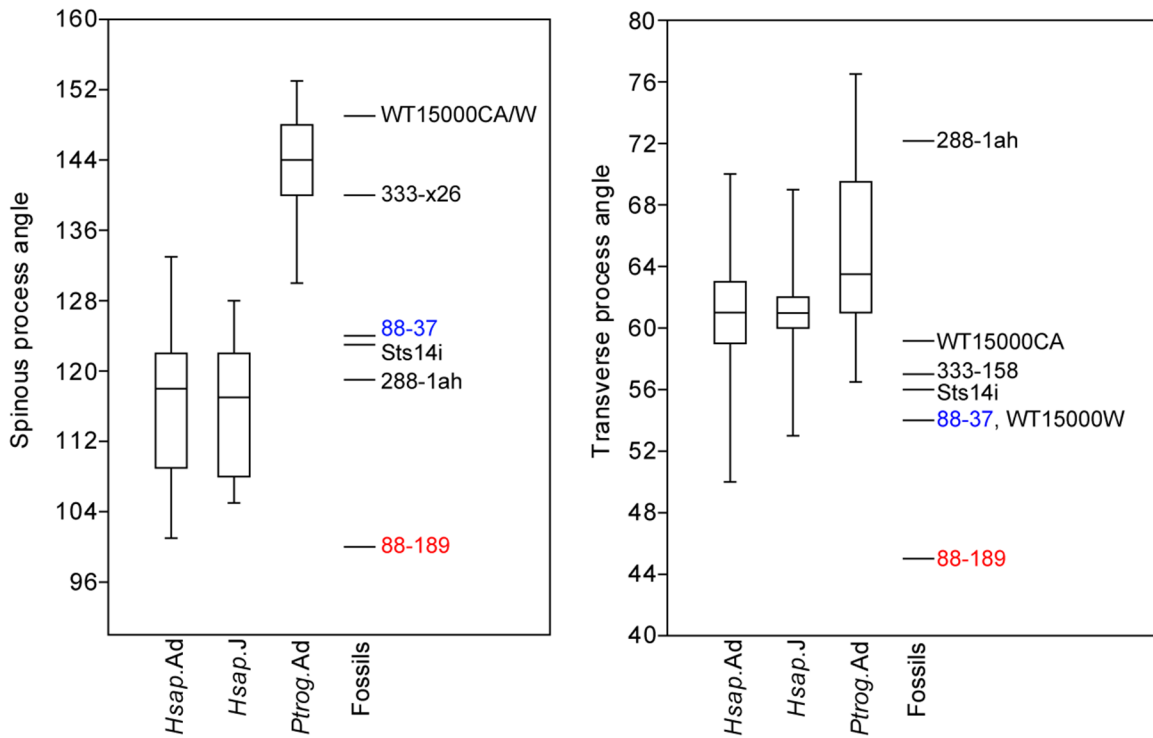


Figure A16. Spinous process angle and transverse process angle in U.W. 88-37 (MH1), U.W. 88-189 (MH2), and other fossil hominin middle thoracic vertebrae. *Au. afarensis* (A.L. 288-1ah, A.L. 333-x26, 333-158), *Au. africanus* (Sts14i), and juvenile *H. erectus* (KNM-WT 15000) are included.

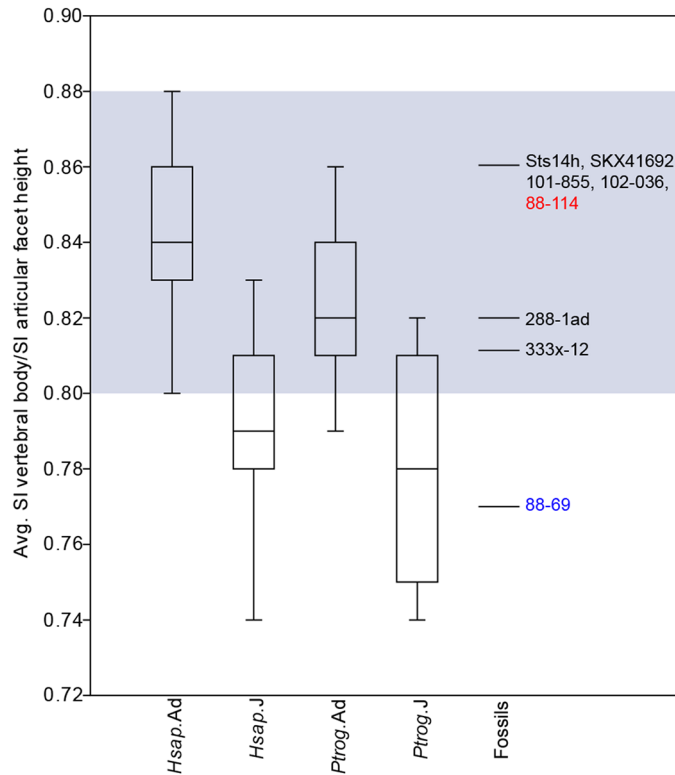


Figure A17. Ratio of average SI vertebral body height and SI inter-articular facet height in U.W. 88-69 (MH1), U.W. 88-114 (MH2), and other fossil hominin T10 vertebrae. Subadult humans and chimpanzees demonstrate relatively shorter superior-inferior vertebral body heights than adults. *Au. afarensis* is represented by A.L. 288-1ad and A.L. 333x-12, *Au. africanus* by Sts 14h, *Au. robustus* by SKX41692, and *H. naledi* by U.W. 101-855 and U.W. 102-036.

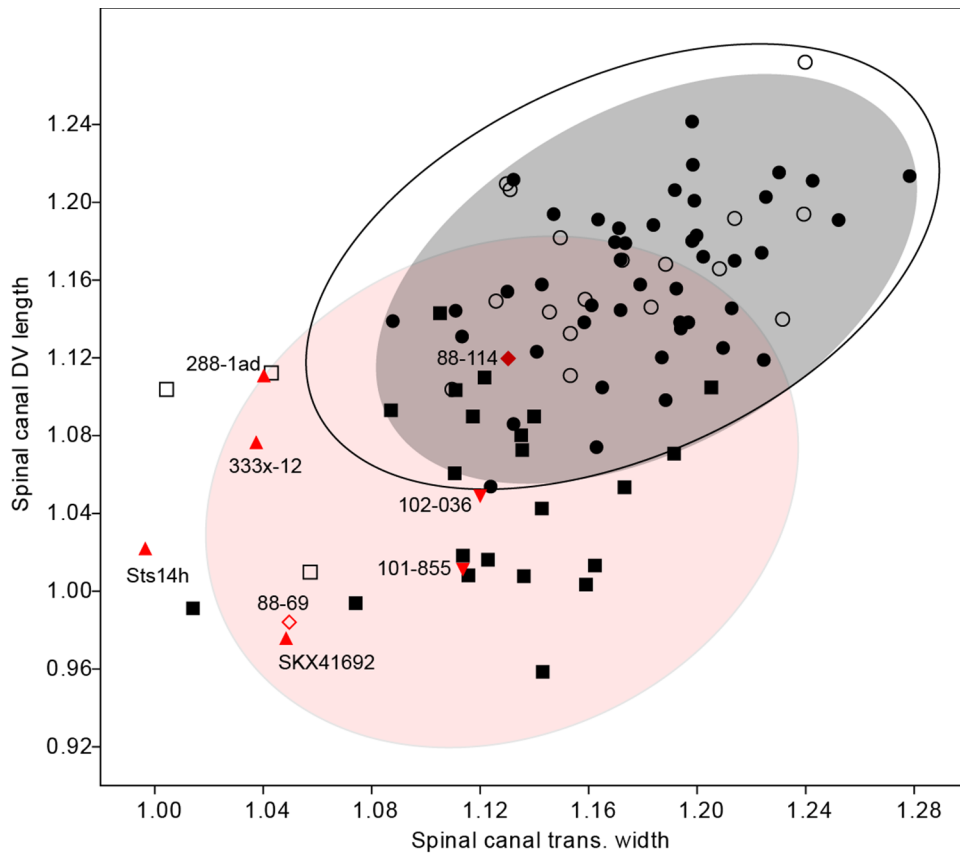


Figure A18. Spinal canal dimensions of U.W. 88-69 (MH1), U.W. 88-114 (MH2), and other fossil hominin T10 vertebrae. Fossil specimens follow those listed in the Figure 17 caption. Symbols and ellipses follow Figure A12.

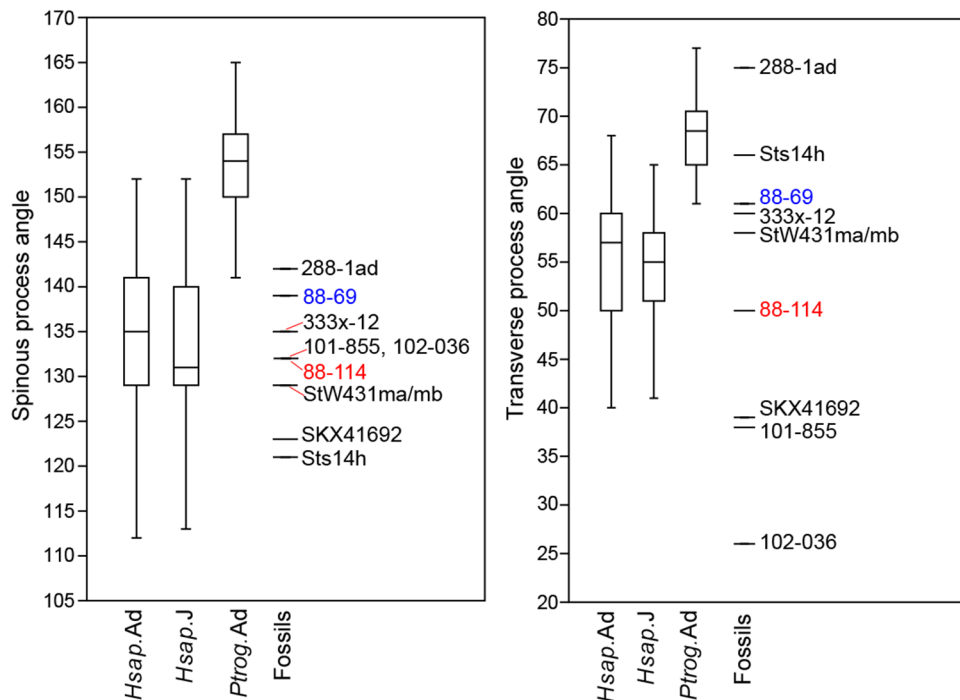


Figure A19. Spinous process angle and transverse process angle in U.W. 88-69 (MH1), U.W. 88-114 (MH2) and other fossil hominin T10 vertebrae. Specimens follow Figure A17, with the addition of StW431ma/mb (*Au. africanus* T10).



Figure A20. U.W. 88-70 (MH1) in right lateral (top left), dorsal (top middle), left lateral (top right), inferior (bottom left), ventral (bottom middle), and superior (bottom right) views (scale is 20mm).



Figure A21. U.W. 88-90 (MH1) in ventral (top left), dorsal (top right), superior (middle left), inferior (middle right), right lateral (bottom left), and left lateral (bottom right) views (scale is 30mm).

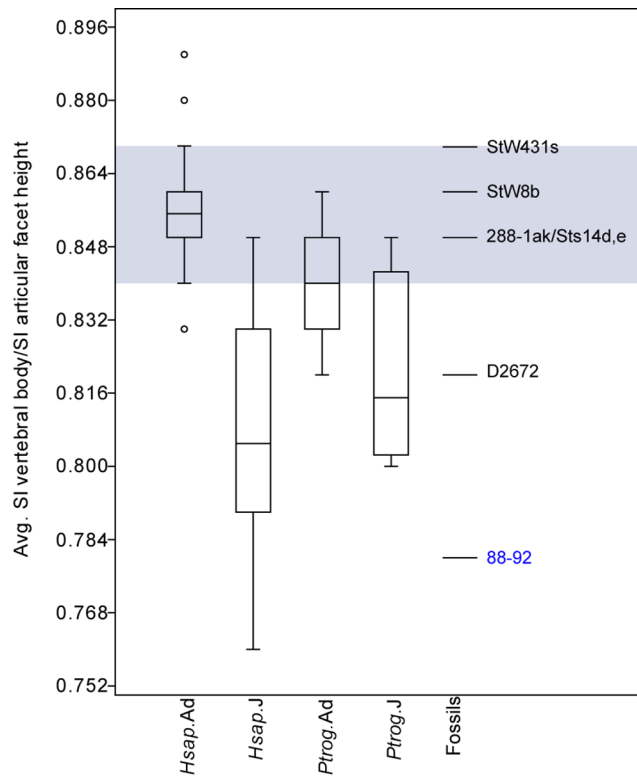


Figure A22. Ratio of average SI vertebral body height and SI inter-articular facet height in U.W. 88-92 (MH1) and other fossil hominin L1 and L2 vertebrae. Subadult humans and chimpanzees demonstrate relatively shorter superior-inferior vertebral body heights than adults. Juvenile *Au. sediba* and *H. erectus* (D2672) fall out with the subadults, whereas adult australopiths—*Au. afarensis* (A.L. 288-1ak) and *Au. africanus* (Sts 14d and e, StW431s, and StW8b)—fall within the adult distribution (gray box).

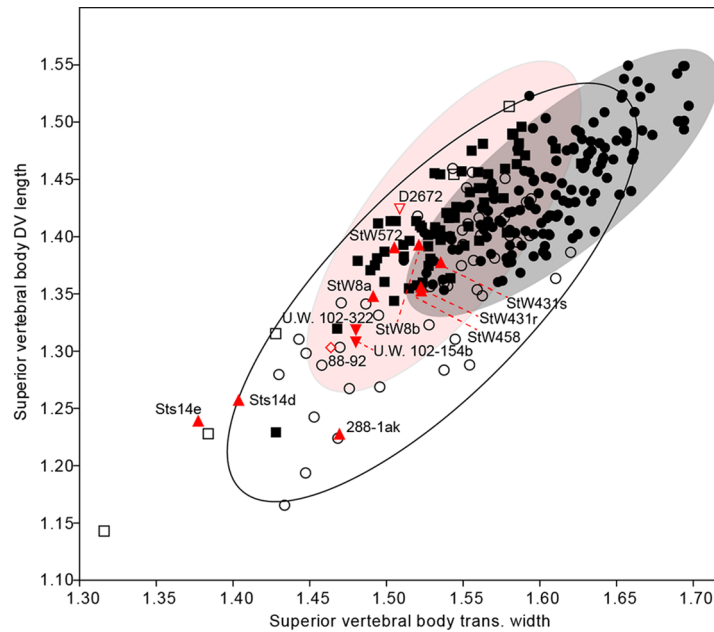


Figure A23. Superior vertebral body dimensions in U.W. 88-92 (MH1) and other fossil hominin L1 and L2 vertebrae. Human adults (filled circles) and subadults (open circles) are shown, as are adult and subadult chimpanzees (filled and open squares, respectively). 95% confidence ellipses are shown for adult and subadult humans and for adult chimpanzees. In addition to U.W. 88-92, the following fossils are included: A.L. 288-1ak (adult *Au. afarensis* L2 or L3), Sts 14e, StW 8a, StW 458 (adult *Au. africanus* L1 vertebrae), Sts 14d, StW 431s, StW 8b, StW 572 (adult *Au. africanus* L2 vertebrae), U.W. 102-154b and U.W. 102-322 (adult *H. naledi* L1 and L2), and D2672 (juvenile *H. erectus* L2). U.W. 88-92 is shown as an open diamond, adult australopiths as filled triangles, and juvenile *H. erectus* as an open inverted triangle.

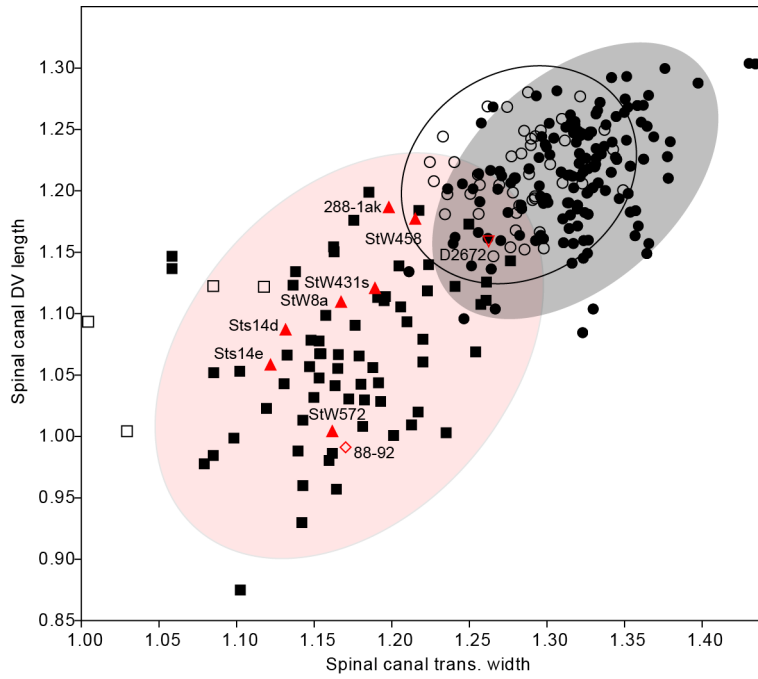


Figure A24. Spinal canal dimensions in U.W. 88-92 (MH1) and other fossil hominin L1 and L2 vertebrae. Symbols and specimens follow Figure A22.

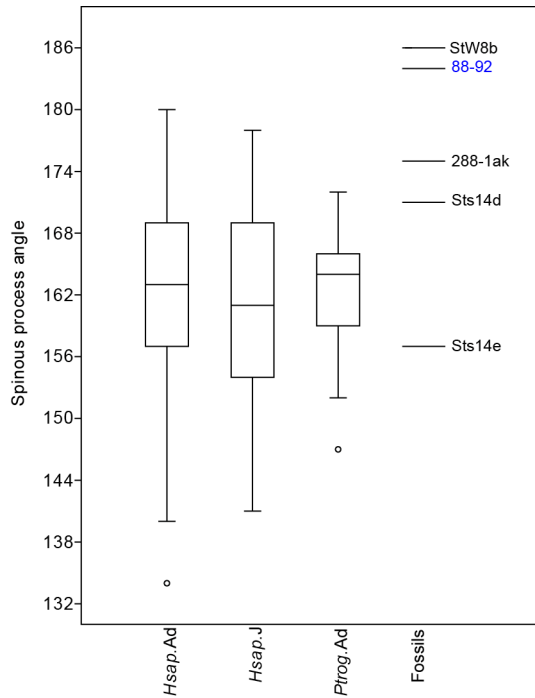


Figure A25. Spinous process orientation in U.W. 88-92 (MH1) and other fossil hominin L1 and L2 vertebrae. Humans adults, sub-adults, and chimpanzees do not differ significantly from one another, and all fossil hominins that preserve the spinous process angle fall within their ranges except U.W. 88-92 and StW8b (Au. africanus), which produce very high (slightly superiorly-directed) angles.

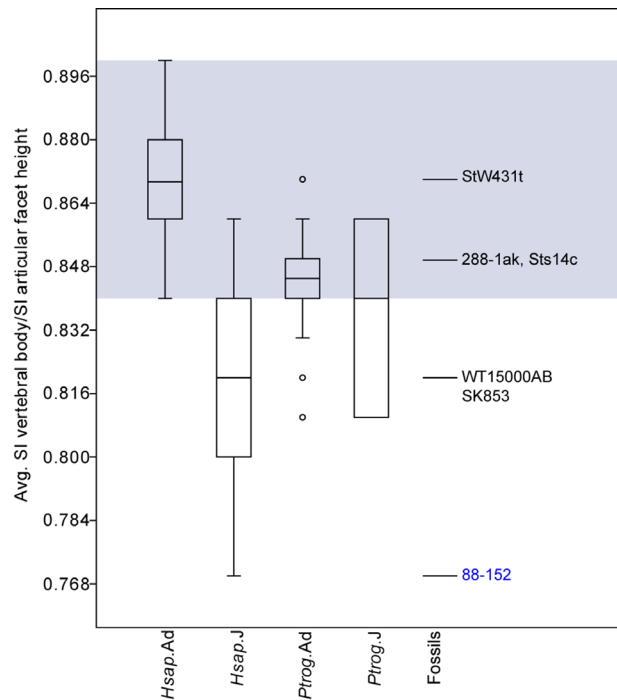


Figure A26. Ratio of average SI vertebral body height and SI inter-articular facet height in U.W. 88-152 (MH1) and other fossil hominin middle lumbar vertebrae. Subadult humans demonstrate relatively shorter SI vertebral body heights than adults. Juvenile *Au. sediba* falls out with subadult humans, whereas adult australopiths (*Au. afarensis* and *Au. africanus*) fall within the adult human distribution (gray box).

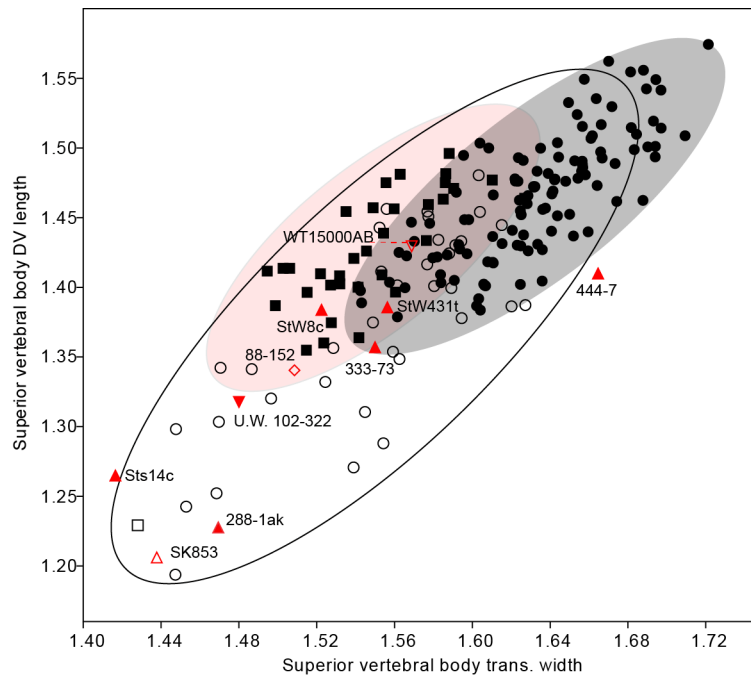


Figure A27. Superior vertebral body dimensions in U.W. 88-152 (MH1) and other fossil hominin middle lumbar vertebrae. Human L3 vertebrae are included, along with middle lumbar vertebrae (L2 or L3) of chimpanzees and the following fossil vertebrae (in addition to U.W. 88-152: A.L. 288-1ak, A.L. 333-73, A.L. 444-7 (adult *Au. afarensis* middle lumbar vertebrae), Sts 14c, StW 431t, StW 8c (adult *Au. africanus* L3 vertebrae), SK 853 (*Au. robustus* middle lumbar vertebra), U.W. 102-322 (adult *H. naledi* L3), and KNM-WT 15000 AB (juvenile *H. erectus* L3). Symbols and ellipses follow Figure A23.

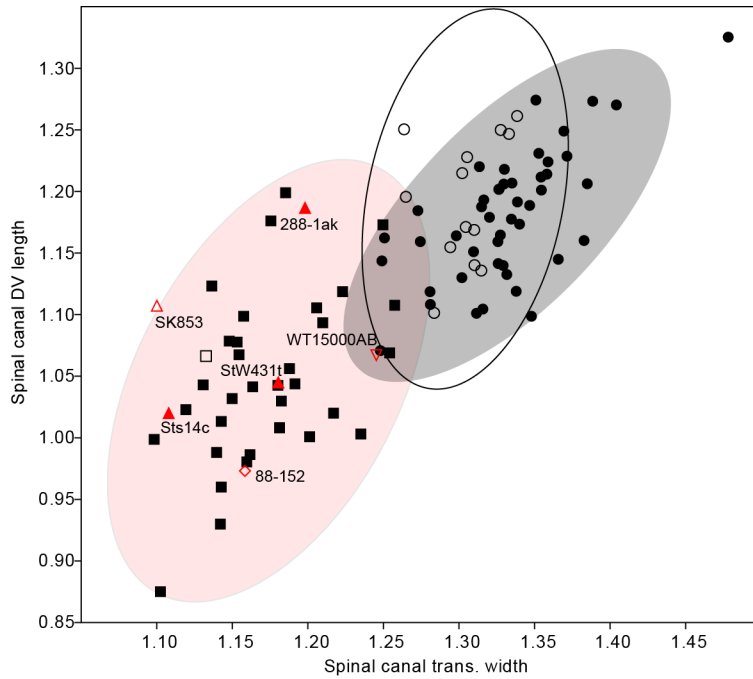


Figure A28. Spinal canal dimensions in U.W. 88-152 (MH1) and other fossil hominin middle lumbar vertebrae. Symbols and specimens follow Figure A27.

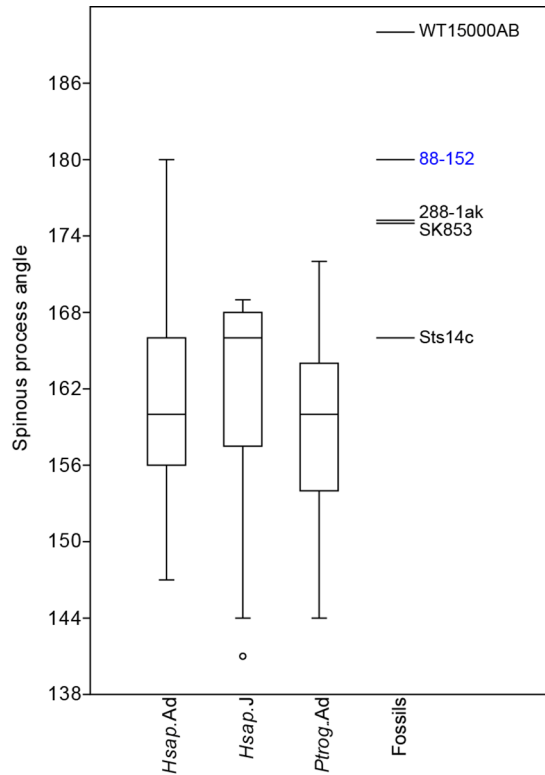


Figure A29. Spinous process orientation in U.W. 88-152 (MH1) and other fossil hominin middle lumbar vertebra. Adult humans, subadults, and adult chimpanzees are not significantly different from each other in spinous process angle. Adult female A.L. 288-1ak (*Au. afarensis*) and *Sts* 14c (*Au. africanus*) and juvenile SK 853 (*Au. robustus*) fall within extant groups, and U.W. 88-152 lies at the high end of adult human variation. In contrast, KNM-WT 15000 AB (juvenile *H. erectus*) produces a very high spinous process angle outside the range of extant taxa.

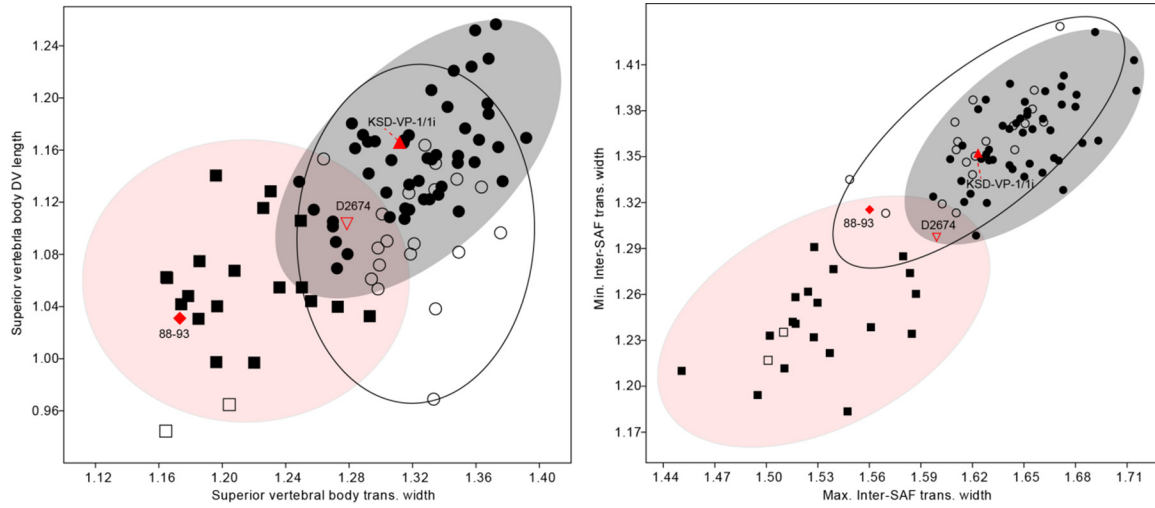


Figure A30. Superior vertebral body dimensions and inter-superior articular facet transverse widths in U.W. 88-93 (MH2) and other fossil hominin C3 vertebrae. Both adult and subadult *Au. sediba* specimens fall out with chimpanzees in having small body dimensions. In contrast, large male *Au. afarensis* (KSD-VP-1/1i) and juvenile *H. erectus* from Dmanisi (D2674) fall within the 95% confidence intervals of human adults and subadults. Note some overlap in the superior vertebral body between humans and chimpanzees but complete separation of the inferior vertebral body.

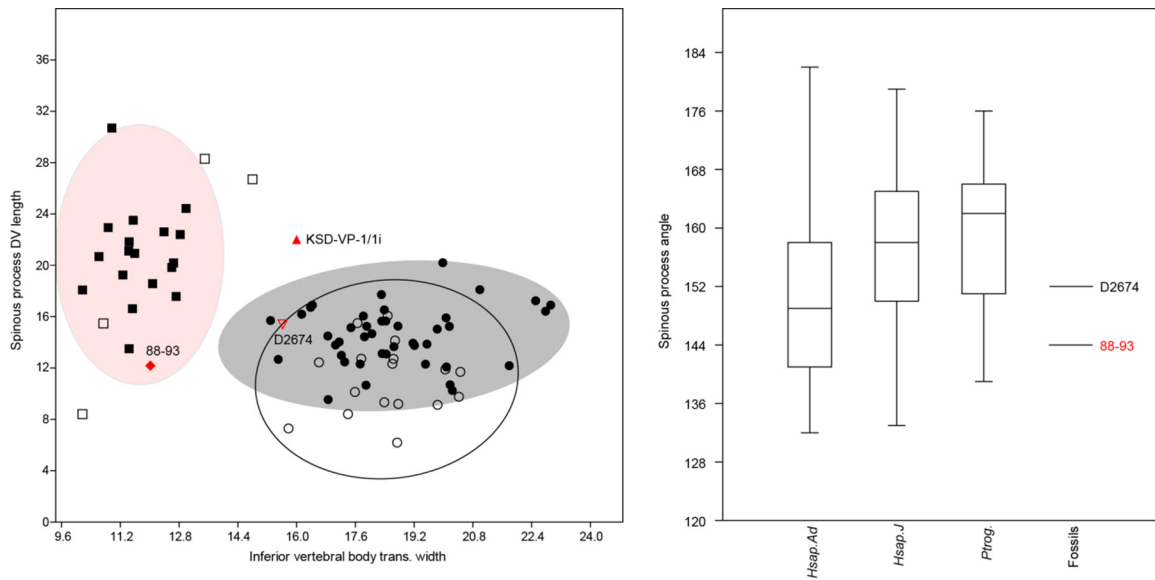


Figure A31. Spinous process DV length plotted against inferior vertebral body width, and spinous process angle in U.W. 88-93 (MH2) and other fossil hominins. Human adult and subadult spinous process angles are significantly different from each other ($p=0.015$), whereas those of chimpanzee adults and subadults are not, perhaps due to small sample size of chimpanzee subadults ($n=4$) for this measurement. Chimpanzee and adult human samples are significantly different from each other ($p=0.003$). Symbols and specimens follow Figure A30.

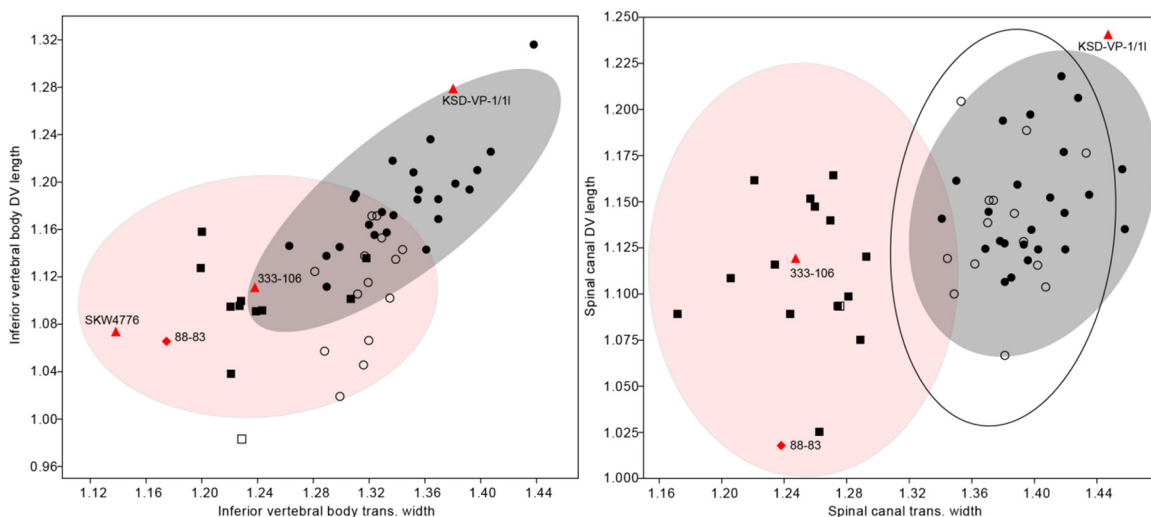


Figure A32. Inferior vertebral body and spinal canal dimensions in U.W. 88-83 (MH2) and other fossil hominin C6 vertebrae. In addition to U.W. 88-83, other fossils hominins include purported *Au. robustus* (SKX 4776) and *Au. afarensis* (A.L. 333-106 and KSD-VP-1/11).

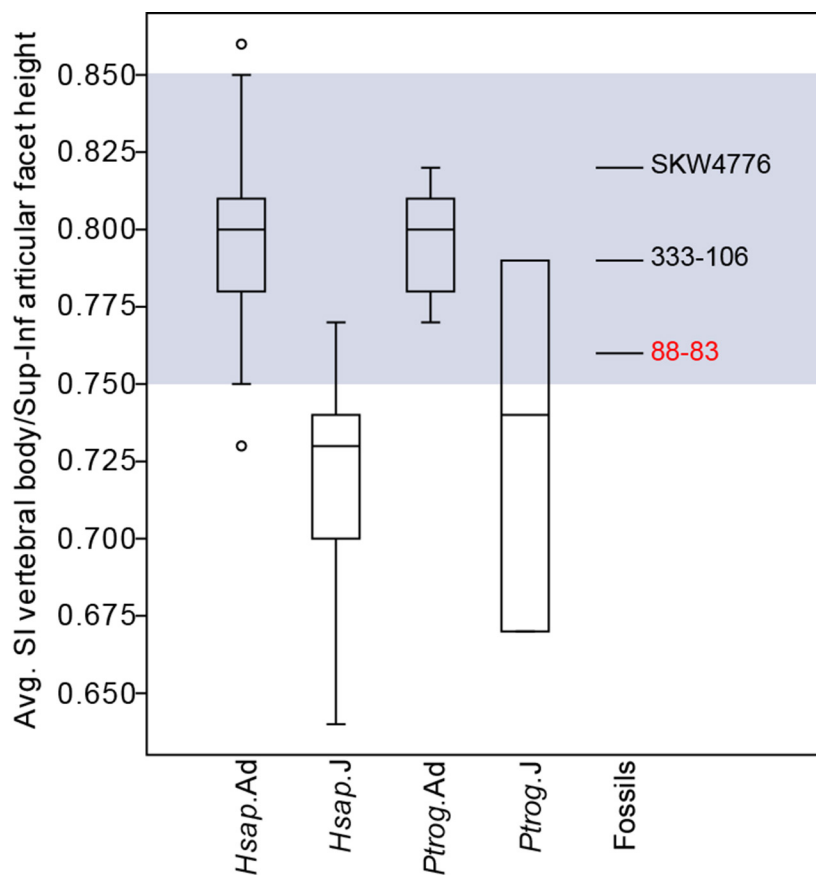


Figure A33. Ratio of average SI vertebral body height and SI inter-articular facet height in U.W. 88-83 (MH2) and other fossil hominin C6 vertebrae. U.W. 88-83 and the other adult fossils included here all fall within the adult human distribution (gray box).

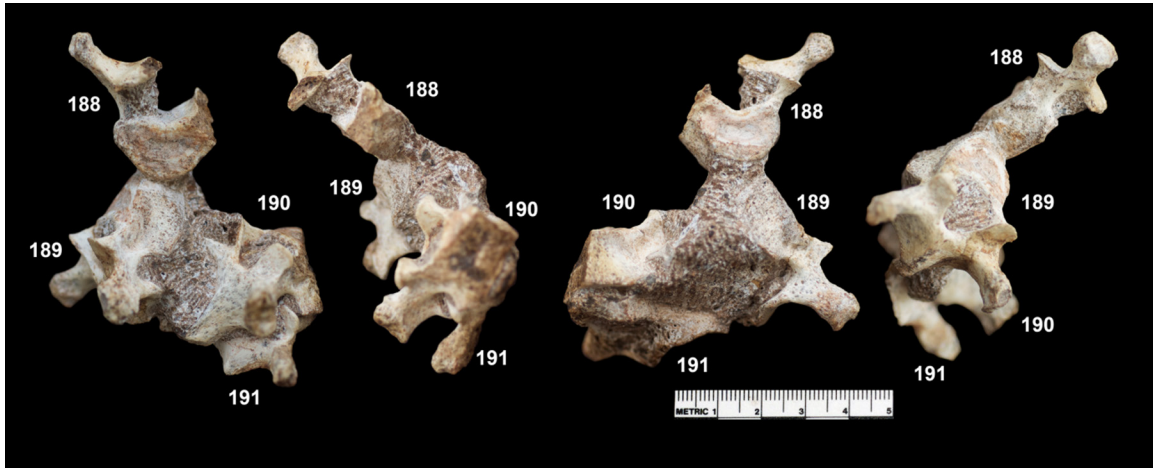


Figure A34. Upper thoracic block of MH2: U.W. 88-188, U.W. 88-189, U.W. 88-190, and U.W. 88-191 in various views. Far left: U.W. 88-188 in inferior view, U.W. 88-189 in left lateral view, U.W. 88-190 in dorso-lateral (right), U.W. 88-191 in dorso-lateral (right) view. Middle left: U.W. 88-188 in dorso-lateral (right) view, U.W. 88-189 in ventral view (partly obscured by matrix), U.W. 88-190 and U.W. 88-191 in anterior views. Middle right: U.W. 88-188 in superior view, U.W. 88-189 in ventro-lateral (left) view, U.W. 88-190 and U.W. 88-191 in ventro-lateral (left) views. Far right: U.W. 88-188 in left lateral view, U.W. 88-189 in dorso-superior view, U.W. 88-190 and U.W. 88-191 in dorsal views (scale is 50mm).

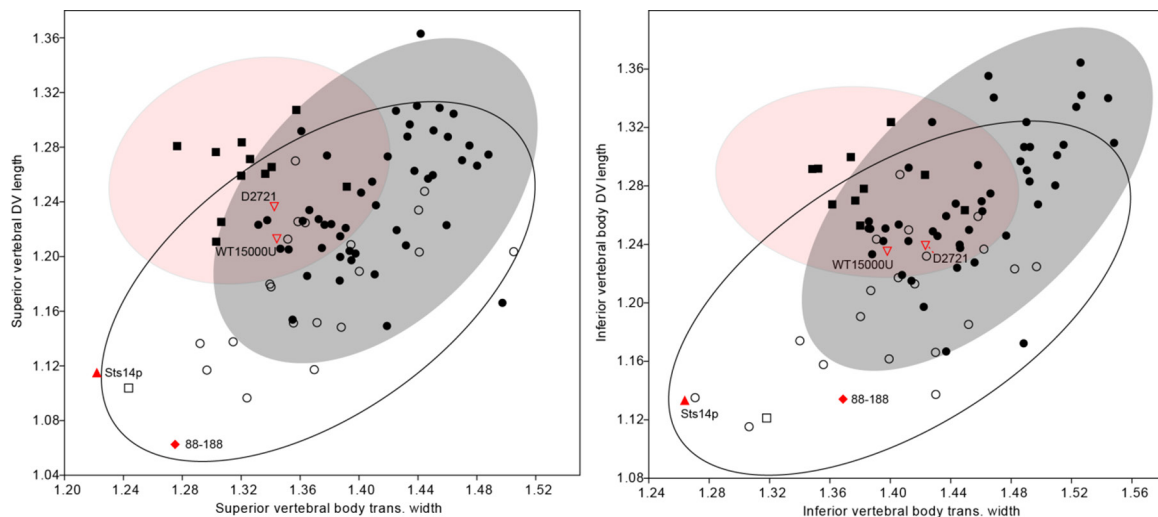


Figure A35. Superior and inferior vertebral body dimensions in U.W. 88-188 (MH2) and other fossil hominin T3 vertebrae. One adult *Au. africanus* (Sts 14p; filled triangle) and two juvenile *H. erectus* (KNM-WT 15000U and D2721; open inverted triangles) fossil vertebrae are available for comparison.

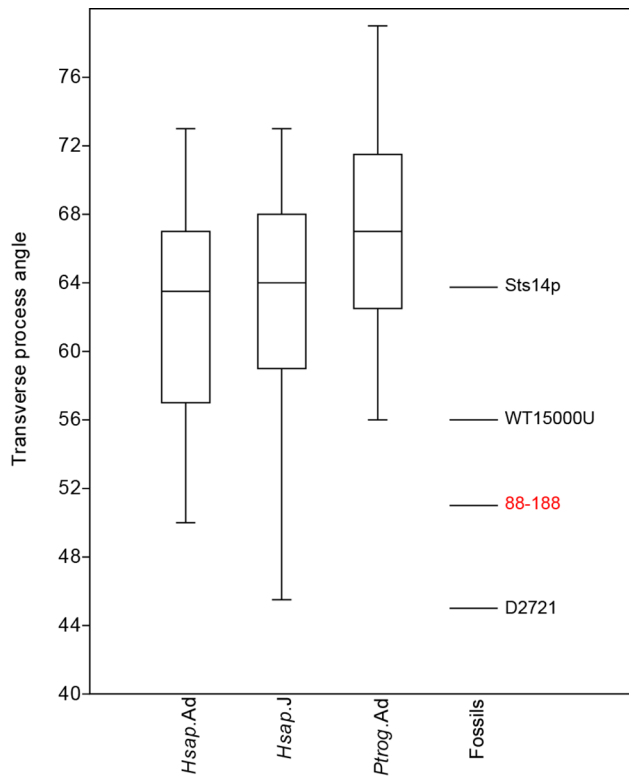


Figure A36. Dorsoventral transverse process angle in U.W. 88-188 (MH2) and other fossil hominin T3 vertebrae. An angle of 90° represents a horizontal transverse process relative to the sagittal midline. All specimens included here have dorsally-oriented transverse processes to some degree. Species and specimens are the same as in Figure A36. Chimpanzees have more ventrally-oriented transverse processes than human adults, although borderline significance is found ($p=0.055$; human subadults are not statistically distinct from chimpanzees, $p=0.08$).

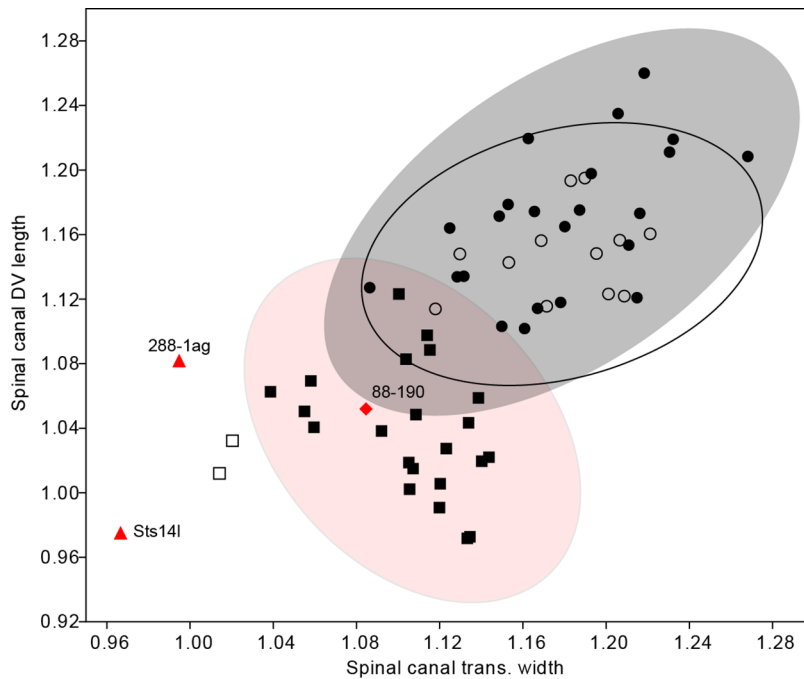


Figure A37. Spinal canal dimensions in U.W. 88-190 (MH2) and other fossil hominin T8 vertebrae. One T8 vertebra each for *Au. afarensis* (A.L. 288-1ag) and *Au. africanus* (Sts 14l) are preserved and included.

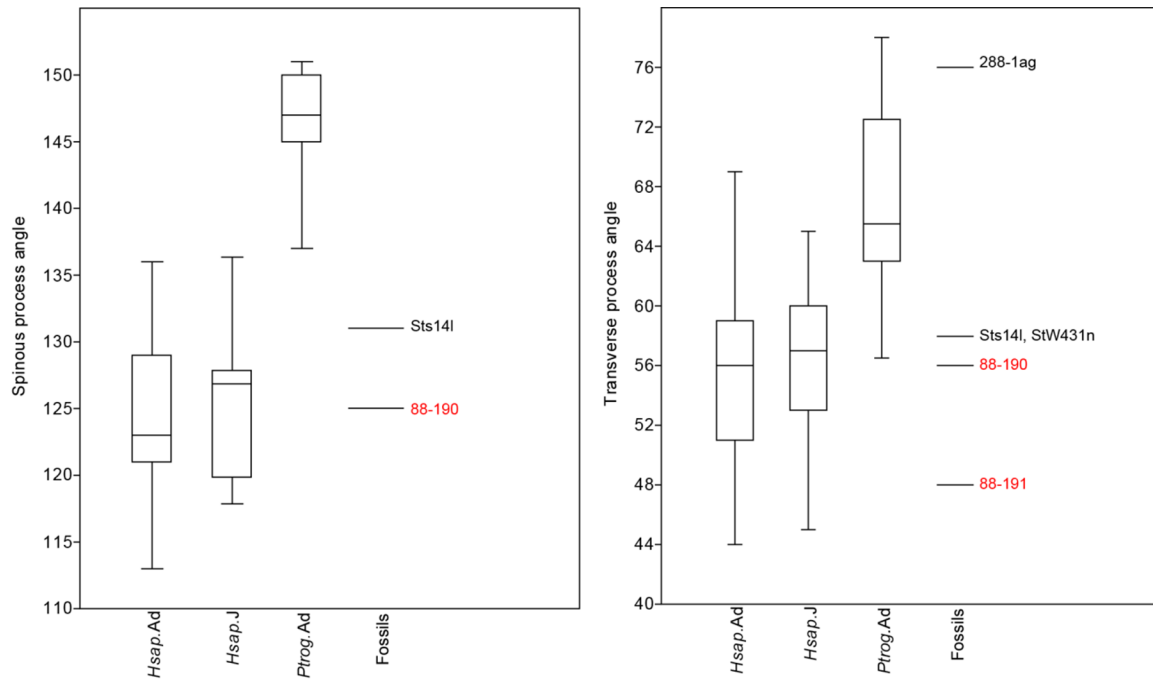


Figure A38. Spinous process angle in U.W. 88-190 (MH2) and transverse process angle in U.W. 88-190 and U.W. 88-191 and in other fossil hominin T8 and T9 vertebrae. Fossil T8 vertebrae included are U.W. 88-190 (MH2), A.L. 288-1ag (Au. afarensis), and Sts 141 (Au. africanus). Fossil T9 vertebrae are U.W. 88-191 (MH2) and StW 431n (Au. africanus).

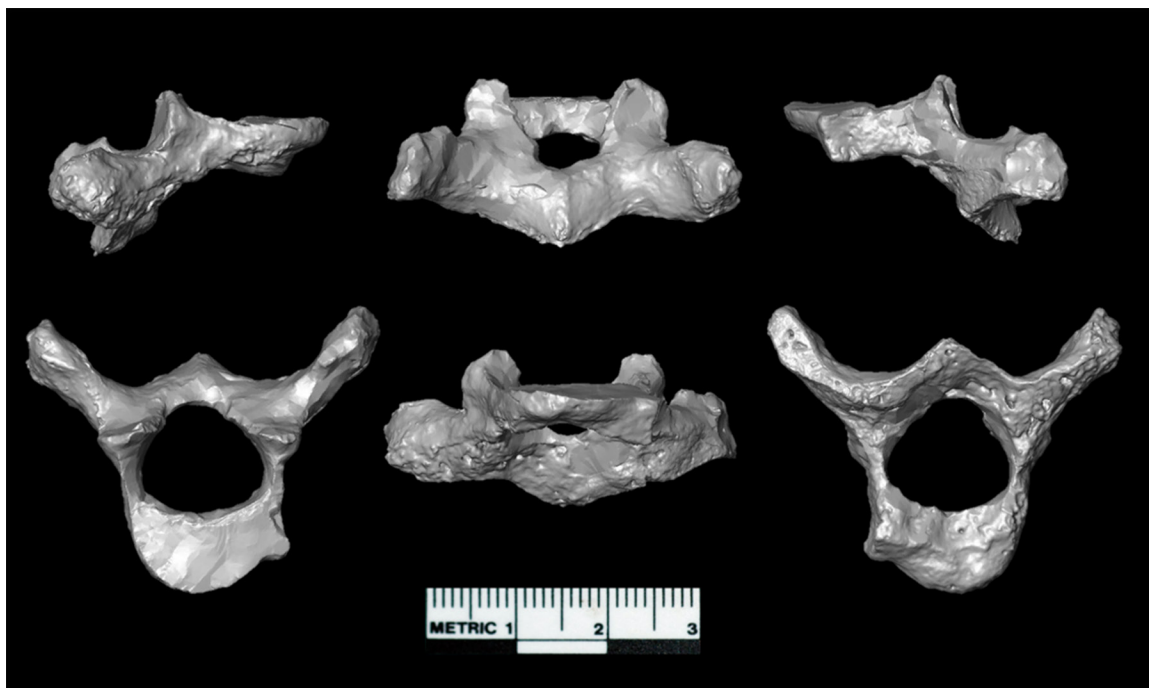


Figure A39. U.W. 88-191 (MH2) isolated virtually from the upper thoracic block. Views are right lateral (top left), dorsal (top middle), left lateral (top right), superior (bottom left), ventral (bottom middle), and inferior (bottom right) (scale is 30mm).



Figure A40. U.W. 88-96 (MH2) in right lateral (top row, left), superior (top, middle), left lateral (top, right), and inferior (bottom) views (scale is 30mm).



Figure A41. U.W. 88-114 (MH2) vertebral body (left set) and in articulation with the lower thoracic block (right). The isolated partial vertebral body is shown in superior (left), left lateral (middle), inferior (right), and ventral (bottom) views. The U.W. 88-114 right aspect of the vertebral body can be seen in superior view in articulation with the rest of the vertebra on the right (scale is 50mm).



Figure A42. Lower thoracic block of MH2: U.W. 88-43 (in block, top) and U.W. 88-44 (bottom) in right lateral (left), ventral (middle), and left lateral (right) views (scale is 50mm).

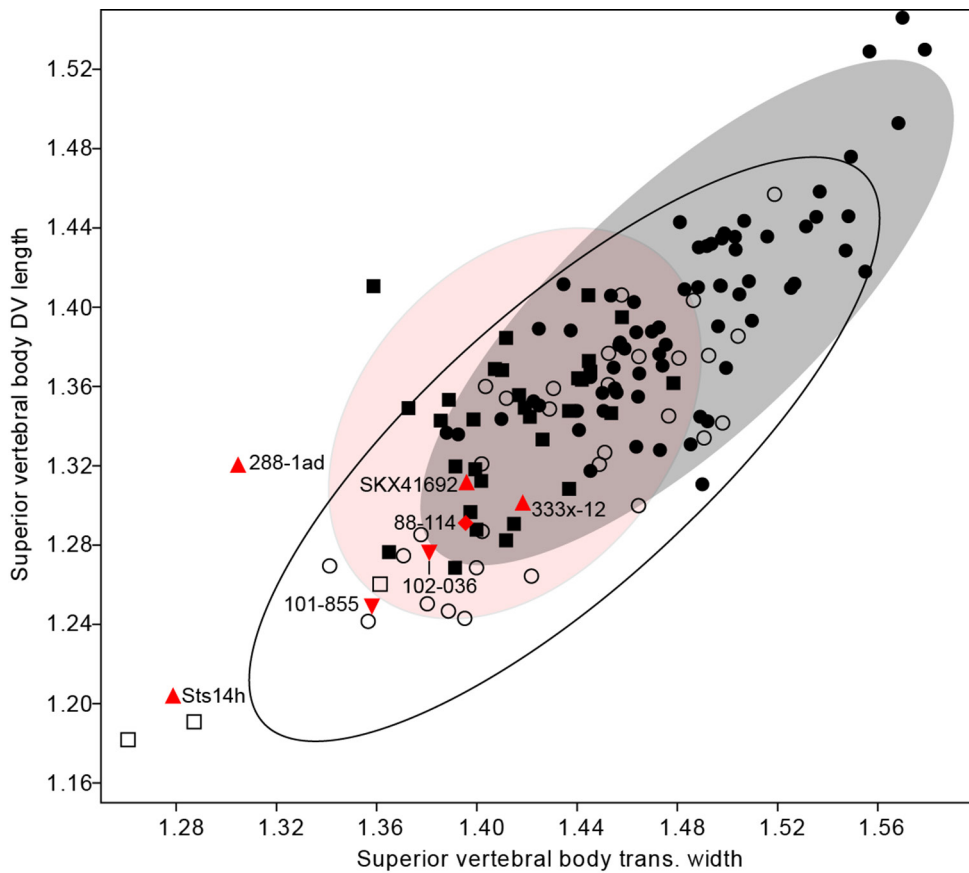


Figure A43. Superior vertebral body dimensions in U.W. 88-114 (MH2) and other fossil hominin T10 vertebrae. Fossil specimens are as follows: A.L. 288-1ad and A.L. 333x-12 (*Au. afarensis*), *Sts 14h* (*Au. africanus*), SKX 41692 (*Au. robustus*), and U.W. 101-855 and U.W. 102-036 (*H. naledi*).

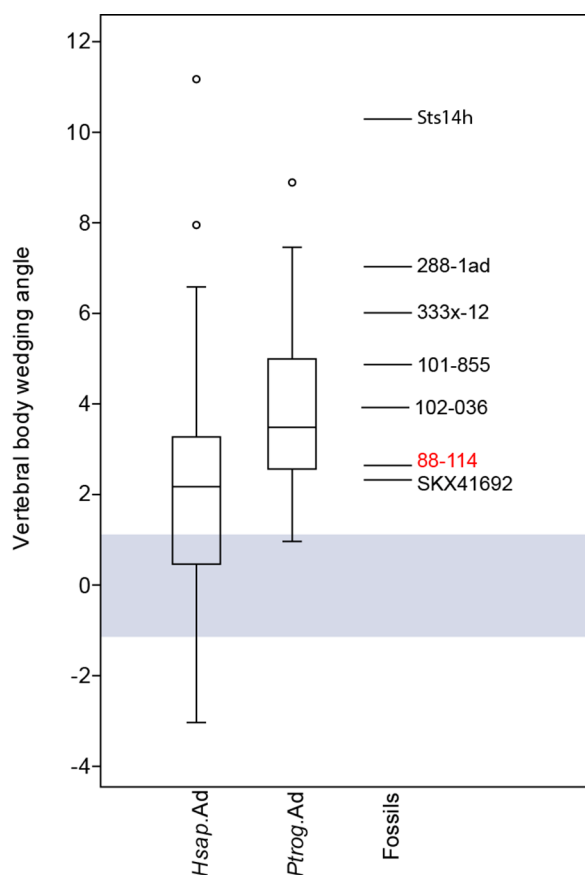


Figure A44. Vertebral body wedging angle in U.W. 88-114 (MH2) and other fossil hominin T10 vertebrae. Specimens included follow Figure A43. Humans and chimpanzees are significantly different from each other ($p < 0.001$). An approximately neutral area (wedging angle between 1 and -1) is outlined in a gray box. All fossil hominins have ventrally wedged T10 vertebrae.

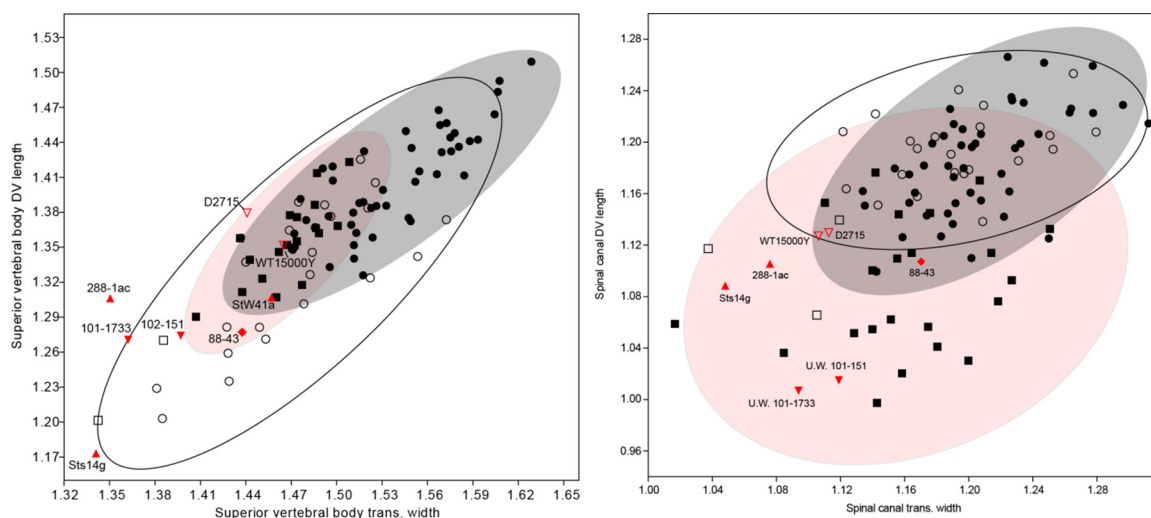


Figure A45. Superior vertebral body and spinal canal dimensions in U.W. 88-43 (MH2) and other fossil hominin T11 vertebrae. Fossil specimens are as follows: A.L. 288-1ac (Au. afarensis), Sts 14g and StW41a (Au. africanus), U.W. 101-1733 and U.W. 102-151 (H. naledi), and D2715 and KNM-WT 15000Y (H. erectus). Au. afarensis and Au. africanus are shown in red triangles, fossil Homo in inverted triangles, Au. sediba in diamonds, modern humans in circles, and chimpanzees in squares (closed symbols=adults, open symbols=subadult specimens).

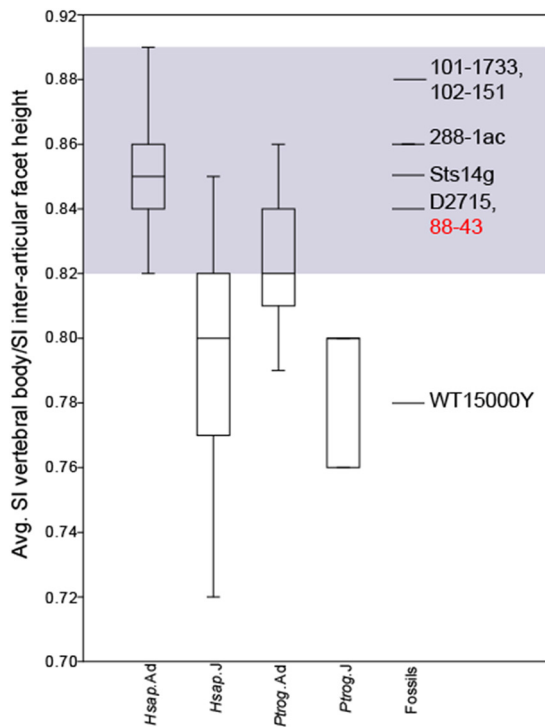


Figure A46. Ratio of average SI vertebral body height and SI inter-articular facet height in U.W. 88-43 (MH2) and other fossil hominin T11 vertebrae. The adult human distribution is highlighted in a gray box that U.W. 88-43 and other adult fossil hominins fall within. Fossil specimens included are the same as in Figure A45.

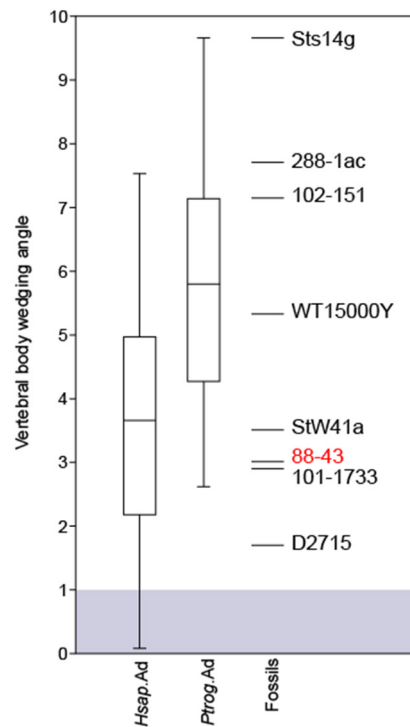


Figure A47. Vertebral wedging angle in U.W. 88-43 (MH2) and other fossil hominin T11 vertebrae. Humans and chimpanzees are significantly different from each other ($p < 0.001$). A gray box outlines relatively neutral wedging (wedging angle between 1 and -1). All fossil hominins have ventrally wedged T11 vertebrae. Fossil specimens included are the same as in Figure A45.

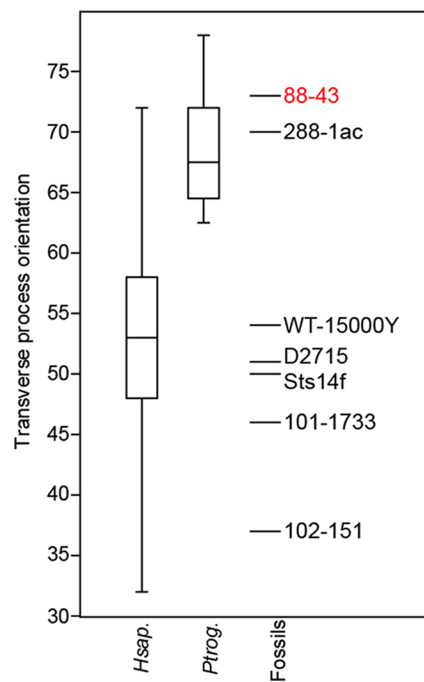
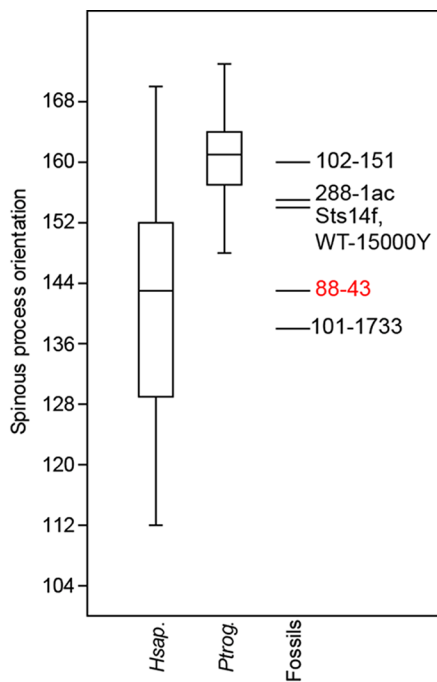


Figure A48. Spinous and transverse process orientation in U.W. 88-43 (MH2) and other fossil hominin T11 vertebrae. Humans and chimpanzees are significantly different from each other in both measures ($p < 0.001$). Fossil specimens included are the same as in Figure A45.

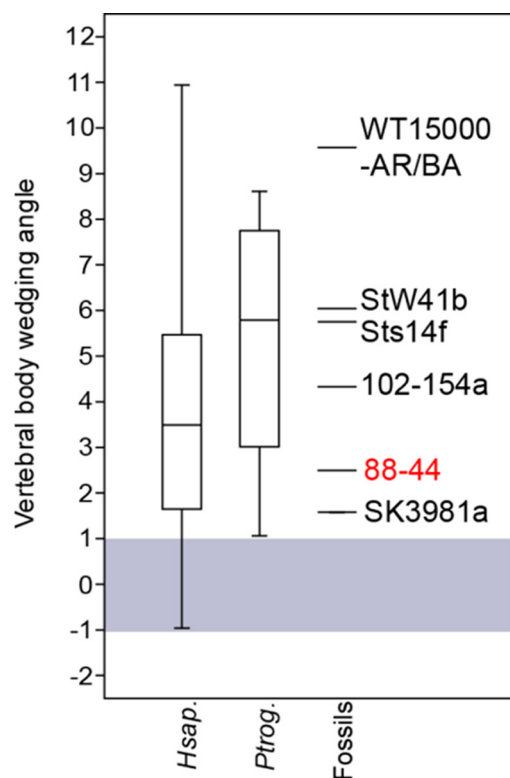


Figure A49. Vertebral wedging angle in U.W. 88-44 (MH2) and other fossil hominin T12 vertebrae. Humans and chimpanzees are significantly different from each other ($p < 0.001$). A gray box outlines relatively neutral wedging (wedging angle between 1 and -1). Fossil specimens are as follows: *Sts 14f* and *StW 41b* (*Au. africanus*), *SK 3981a* (*Au. robustus*), U.W. *102-154a* (*H. naledi*), and KNM-WT 15000AR/BA (*H. erectus*).

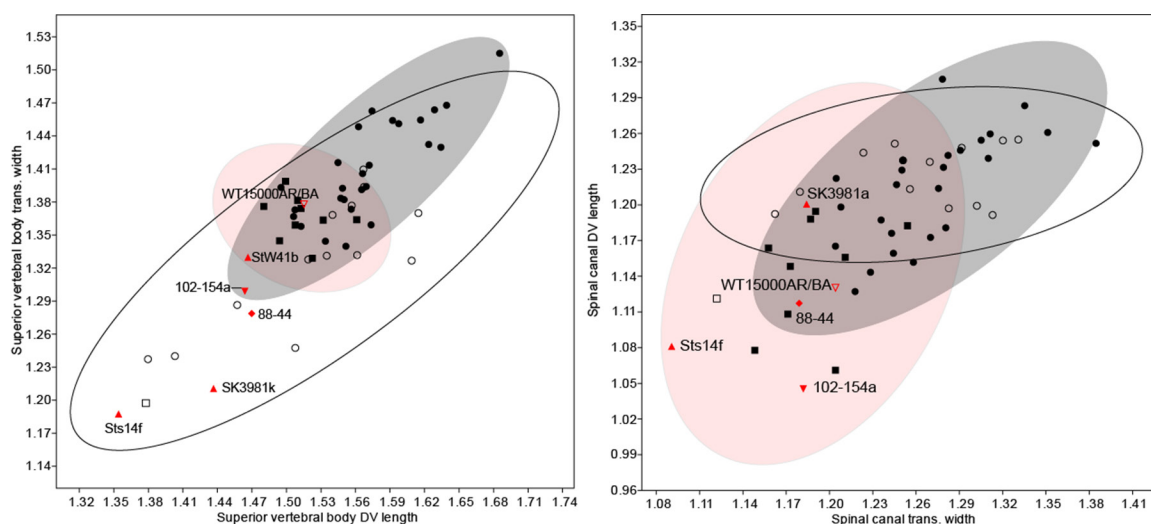


Figure A50. Superior vertebral body and spinal canal dimensions in U.W. 88-44 (MH2) and other fossil hominin T12 vertebrae. Specimens are the same as those in the Figure A49 caption; symbols follow Figure A45.

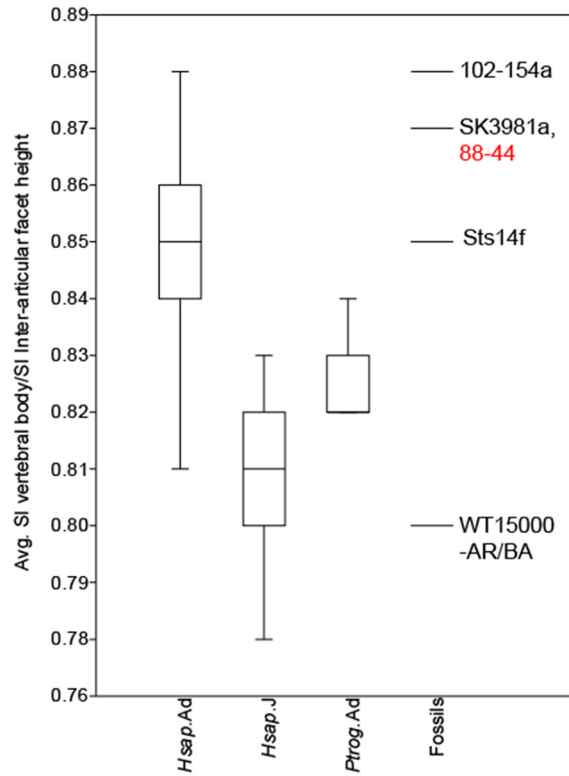


Figure A51. Ratio of average height of the SI vertebral body and the SI inter-articular facet height in U.W. 88-44 (MH2) and other fossil hominin T12 vertebrae. Human adults and subadults are significantly different from one another ($p < 0.001$). Specimens are the same as those in Figure A49.



Figure A52. Lower lumbar vertebrae and sacrum of MH2: U.W. 88-127/153 (top element), U.W. 88-126/138 (middle element), and U.W. 88-137/125 (sacrum) in dorsal (far left), left lateral (middle left), ventral (middle right), and right lateral (far right) views. Notice that the superior portion of the neural arch of the penultimate lumbar vertebra (U.W. 88-234) is not present in this image.

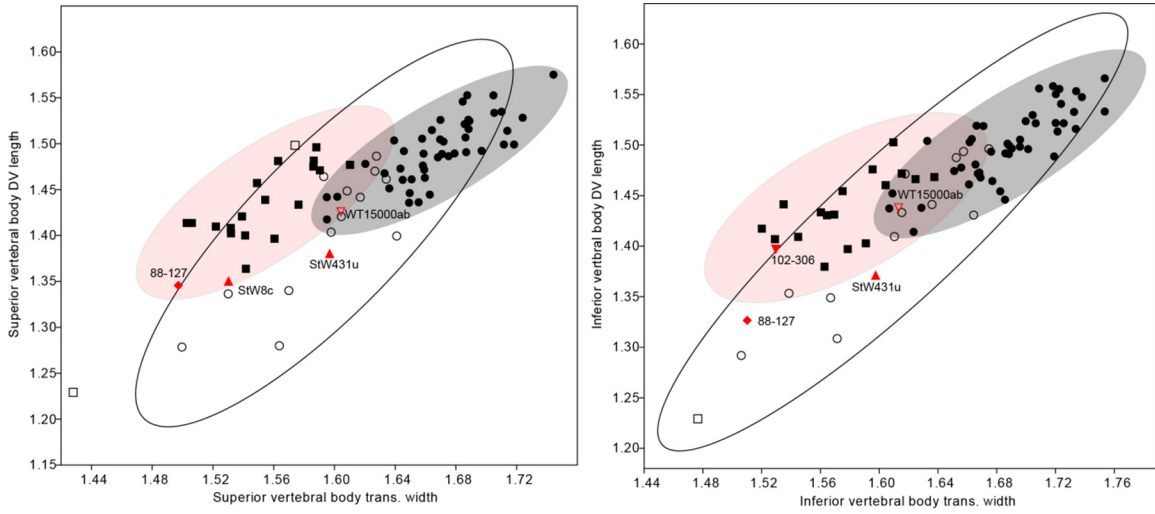


Figure A53. Superior and inferior body dimensions in U.W. 88-127 (MH2) and other fossil hominin penultimate lumbar vertebrae. In addition to adult female *Au. sediba*, adult male *Au. africanus* specimens StW8c and StW431u and *H. naledi* U.W. 102-306 are included. The superior and inferior vertebral bodies of Sts 14b (adult female *Au. africanus*) are damaged and cannot be measured.

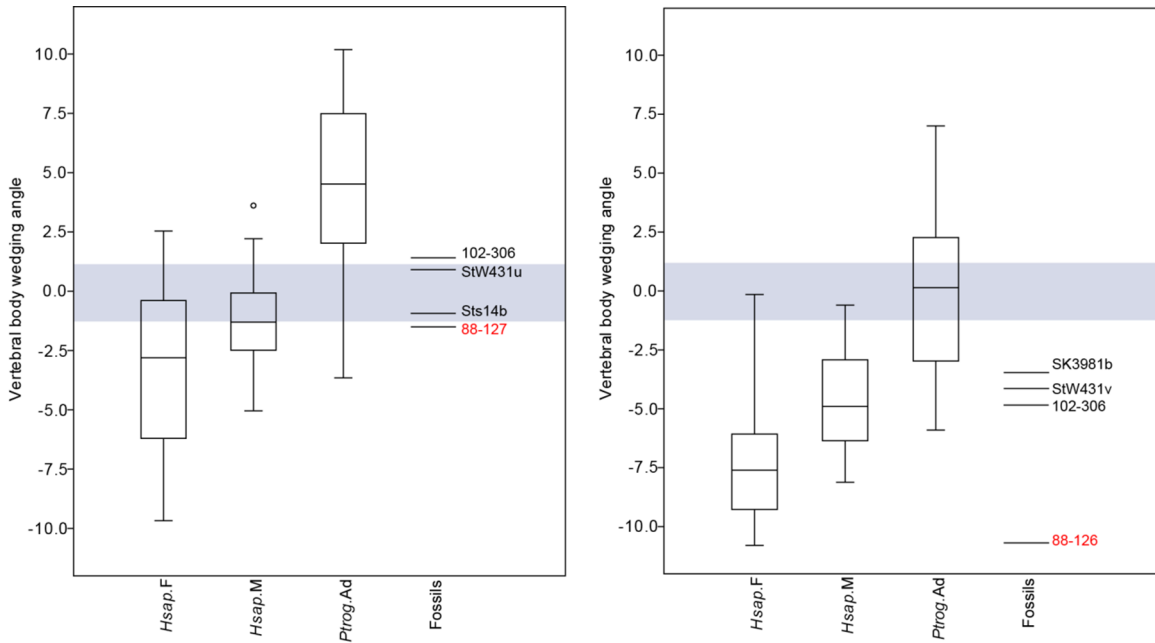


Figure A54. Vertebral body wedging angle in U.W. 88-127 and U.W. 88-126 (MH2) and other fossil hominin L4 and L5 vertebrae. In addition to the lower lumbar vertebrae of *Au. sediba*, the following specimens are included: Sts 14b and StW 431u (L4 vertebrae of *Au. africanus*), StW 431v (L5 of *Au. africanus*), and SK 3981b (L5 of *Au. robustus*). In both analyses, penultimate lumbar vertebrae (left) and ultimate lumbar vertebrae (right), human females possess significantly more dorsally wedged vertebrae than males ($p=0.04$ and $p=0.003$, respectively), and both in turn possess significantly more dorsally wedged vertebrae than chimpanzees ($p<0.0001$ for all comparisons). Gray boxes show approximate neutral wedging ($-1<wedging\ angle<1$).

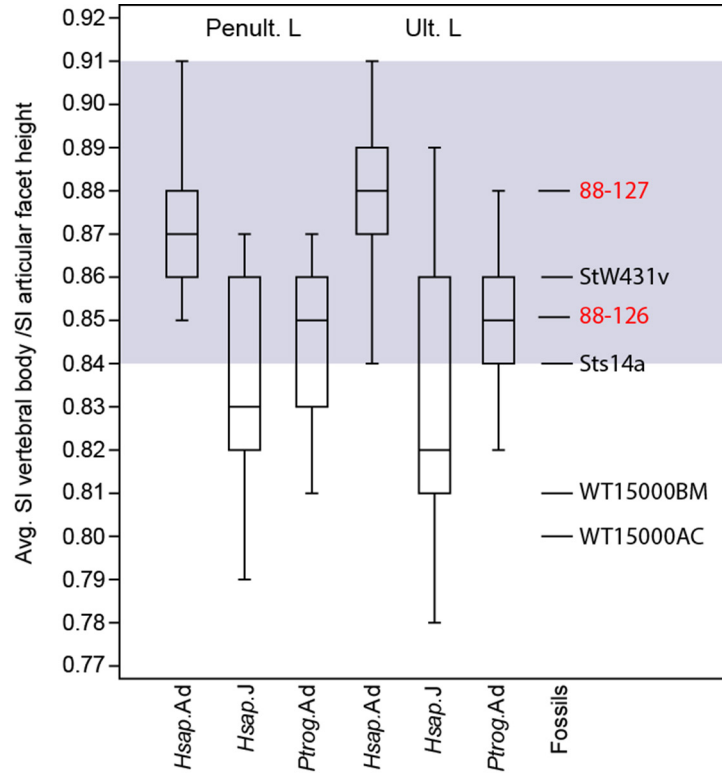


Figure A55. Ratio of average SI vertebral body height and SI inter-articular facet height in U.W. 88-126 and U.W. 88-127 (MH2) and other fossil hominin ultimate and penultimate lumbar vertebrae. Subadult humans demonstrate relatively shorter SI vertebral body heights than adults. Among fossil hominins, only subadult *H. erectus* (KNM-WT 15000) vertebrae fall out with subadults, whereas adult hominins fall within the adult human distribution (gray box).

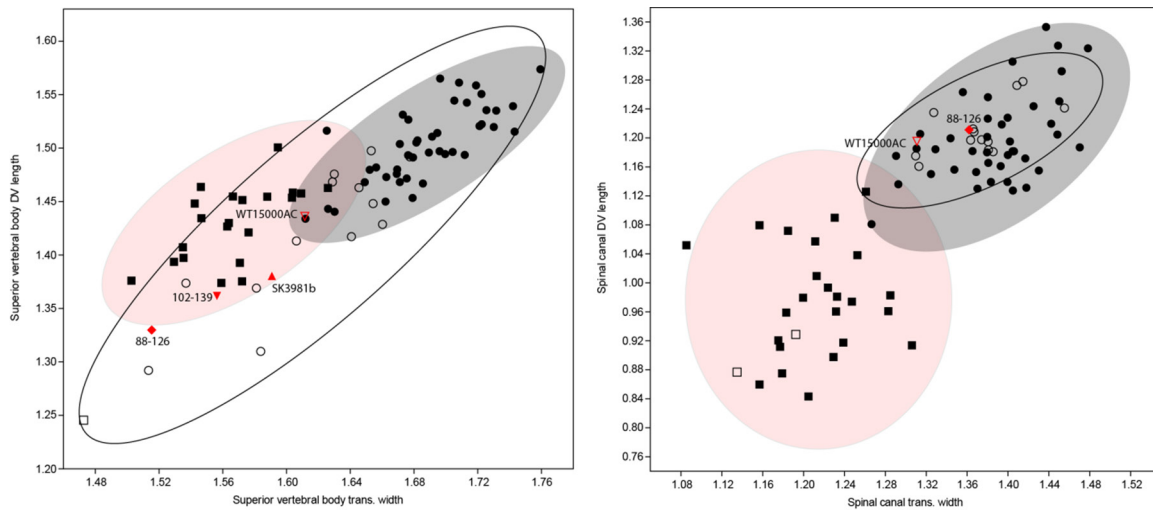


Figure A56. Superior vertebral body and spinal canal dimensions in U.W. 88-126 (MH2) and other fossil hominin last lumbar vertebrae. Specimens are SK 3981b (*Au. robustus*; closed triangle), U.W. 102-139 (*H. naledi*; closed inverted triangle), and KNM-WT 15000 AC (*Nariokotome H. erectus*; open inverted triangle).

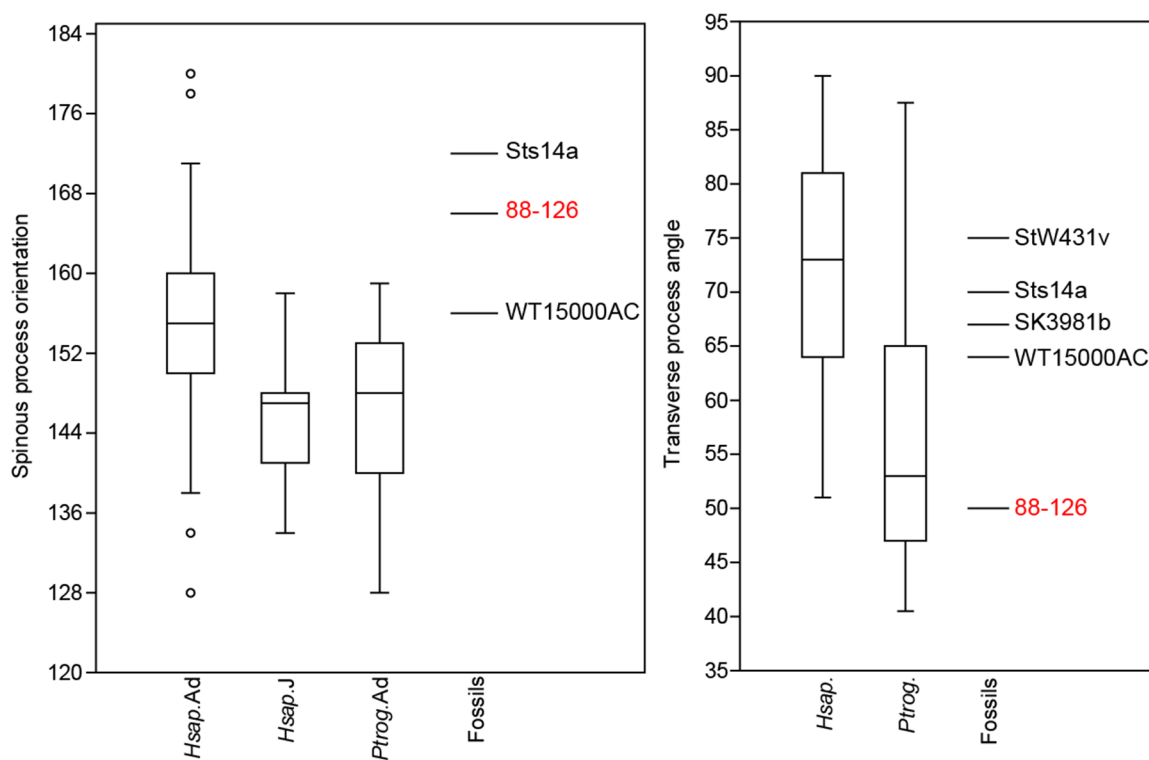


Figure A57. Spinous process and transverse process angle in U.W. 88-126 (MH2) and other fossil hominin last lumbar vertebrae. Human adults and subadults are significantly different from each other in spinous process orientation ($p=0.023$), whereas they are not in transverse process angle. Human adults are different from chimpanzees in both measures ($p=0.001$ for spinous process; $p<0.001$ for transverse process), but human subadults are not different than chimpanzees in spinous process orientation.

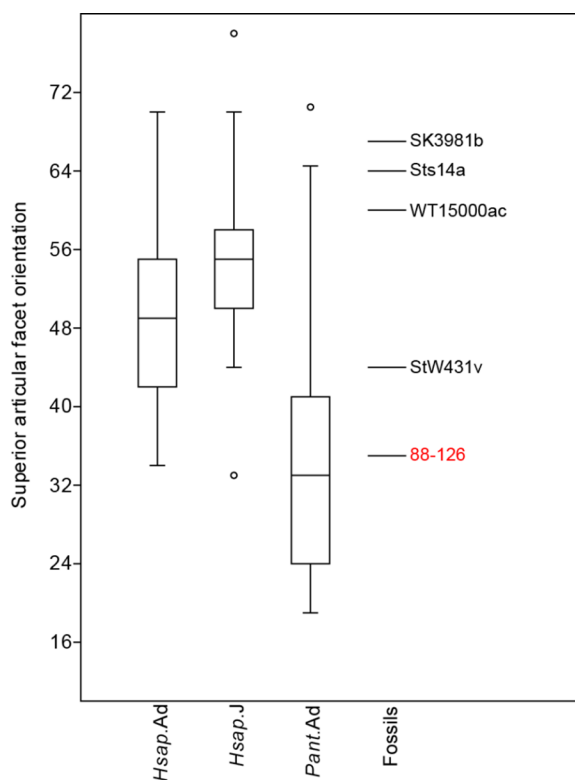


Figure A58. Superior articular facet angle in U.W. 88-126 (MH2) and other fossil hominin last lumbar vertebrae. Humans adults and subadults are not statistically distinct ($p=0.08$), whereas humans and chimpanzees are significantly different from each other ($p<0.001$). U.W. 88-126 falls at the low end of variation in the human sample and near the chimpanzee median.



Figure A59. U.W. 88-15 (MH1) in internal, inferior, superior, and external views (top to bottom) (scale is 50mm).



Figure A60. U.W. 88-131 (MH1) in superior, internal, inferior, and external views (top to bottom) (scale is 50mm).



Figure A61. U.W. 88-155 (MH1) in superior, external, inferior, and internal views (top to bottom) (scale is 50mm).



Figure A62. U.W. 88-165 (MH2) in external, inferior, internal, and superior views (top to bottom) (scale is 50mm).



Figure A63. U.W. 88-74 (MH1) in external, internal, superior, and inferior views (scale is 50mm).



Figure A64. U.W. 88-17 (MH1) in external, superior, internal, and inferior views (scale is 50mm).



Figure A65. U.W. 88-13 (MH1) in external, superior, internal, and inferior views (scale is 50mm).

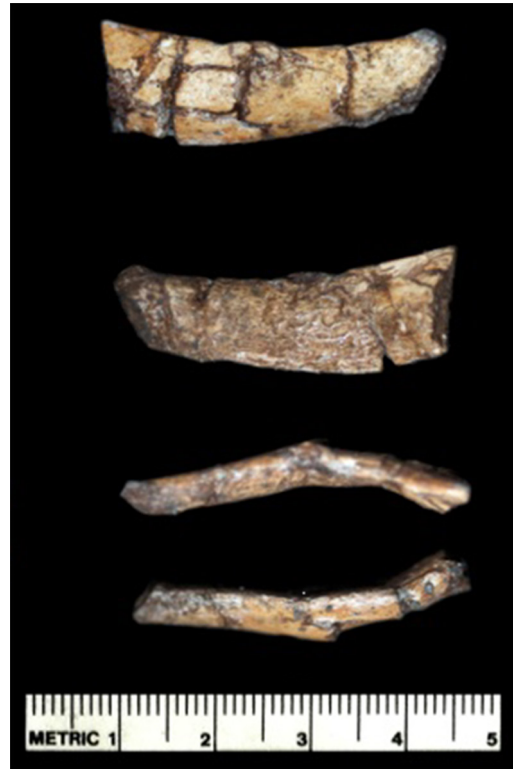


Figure A66. U.W. 88-141 (MH1) in external, internal, superior, and inferior views (scale is 50mm).



Figure A67. Upper rib fragments of MH2: (a) U.W. 88-187, (b) U.W. 88-178. Top: superior view; second row: inferior view; third row: dorsal view; bottom: ventral view (scale=50mm).



Figure A68. U.W.88-167 (MH2) in superior (left) and inferior (right) views (scale is 50mm).



Figure A69. U.W.88-154 (MH2) in superior (left) and inferior view (right) (scale is 50mm).



Figure A70. Views of U.W. 88-60 (MH2) in inferior, external, superior, and internal views (top to bottom) (scale is 50mm).



Figure A71. U.W. 88-145 (MH2) in external, inferior, internal, and superior views (top to bottom) (scale is 50mm).



Figure A72. U.W. 88-59 (MH2) in external, superior, internal, and inferior views (top to bottom) (scale is 50mm).



Figure A73. U.W. 88-143 (MH2) in external, superior, internal, and inferior views (top to bottom) (scale is 50mm).



Figure A74. U.W. 88-144 (MH2) in external, inferior, internal, and superior views (scale is 50mm).



Figure A75. U.W. 88-147 (MH2) in external, inferior, internal, and superior views (from top to bottom) (scale is 50mm).

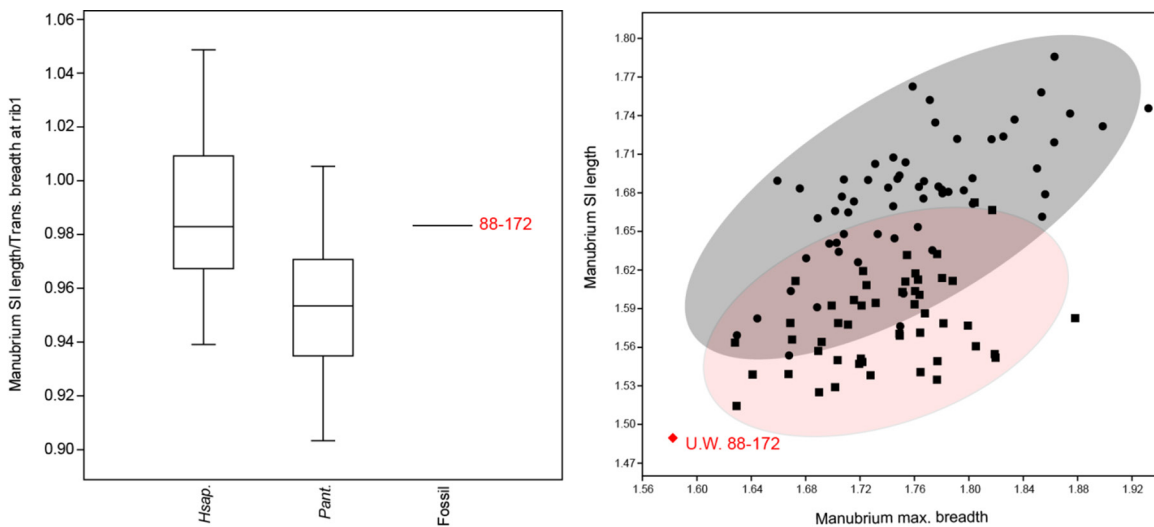


Figure A76. Manubrium SI length and breadth in U.W. 88-172 (MH2) and the comparative sample. Humans have longer (relative to both breadth measurements) manubrium sterni than chimpanzees ($p < 0.001$), although there is substantial overlap. U.W. 88-172 is small, but the SI length/transverse breadth index it produces is nearly identical with the human median value.

APPENDIX II
Standard measurement of the *Au. sediba* vertebrae and ribs.

TABLE A1. STANDARD MEASUREMENTS ON MH1 VERTEBRAE
(in mm for linear measurements and degrees for angles).

Measurements ¹	U.W.	U.W.	U.W.	U.W.	U.W.	U.W.	U.W.	U.W.	U.W.
	88-72 C3	88-9 C7	88-11 upper T	88-37 middle T	88-69 lower T	88-70 lower T	88-90 lower T	88-92 middle L	88-152 middle L
1. Body sup. transv. width (M α W7)	-	17.1	20.4	18.9	-	-	-	29.1	32.3
2. Body sup. dorsoven. dia. (M α 4)	-	10.4	12	14.6	-	-	-	20.1	21.9
3. Body inf. transv. width (M α 8)	(13.5) ²	19.1	22.1	22.6	-	-	-	29.3	32
4. Body inf. dorsoven. dia. (M α W5)	11.1	10.9	14.1	15.6	-	-	-	21.8	22.4
5. Body ventral height (M α W1)	-	7.1	8.7	9.1	-	-	-	15.7	16.3
6. Body dorsal height (M α W2)	-	7.7	9.1	10.3	13	-	-	17.1	15.7
7. Body wedging angle (in degrees)	-	2.9°	1.9°	5°	-	-	-	4°	-1.6°
8. Canal dorsoven. dia. (M α W10)	14	10.8	13.3	11.5	11.2	-	-	14.8	14.4
9. Canal transv. dia. (M α W11)	16	17.5	9.5	8.7	9.6	-	-	9.8	9.4
10. Sup.-inf. inter-AF height	-	17.9	21.3	22.7	25.9	-	-	35.8	36.5
11. Max. inter-SAF dist.	-	37.6	29.6	21.3	21.6	-	-	28.3	28.3
12. Min. inter-SAF dist.	-	17.2	11.4	8.3	8.5	-	-	11.9	12
13. Max. inter-IAF dist.	36.6	37.3	26	23.2	24.2	-	-	(22)	24.4
14. Min. inter-IAF dist.	19	15.9	9.8	7.2	9.4	-	-	11.6	11
15. SAF sup.-inf. dia.	-	8.6	9	7.2	9.1	-	-	11.5	14.1
16. SAF transv. dia.	-	10.7	9.5	7	6.7	-	-	11.8	11.3
17. IAF sup.-inf. dia.	9.2	8.9	9.2	9.9	10	-	-	13.3	14.1
18. IAF transv. dia.	8.9	12.4	8.7	8.2	8.4	-	-	9.6	8.6
19. Spinous process angle (M α W12)	-	165°	158°	124°	139°	145°	-	184°	180°
20. Spinous process length (M α W13)	(7.8) ²	26.3	25.9	30	-	-	-	21.3	23.1
21. Transverse process angle	NA	NA	60°	54°	61°	-	-	74°	82°
22. Transverse process length	-	17	18.4	17.5	16.6	-	-	17.6	21.5
23. SAF orientation (in degrees)	-	69°	97°	104°	106°	-	-	28°	30°
24. Pedicle sup.-inf. height	-	5.4	8.2	9	7.9	-	-	12.3	9
25. Pedicle transv. width	-	4.9	6.5	4.7	4.1	-	-	6.5	8.6
26. Pedicle dorsoven. length	-	3.9	3.6	6.5	4.7	-	-	6.1	5.4
27. Lamina sup.-inf. height	-	9.4	11.1	13.8	14.6	-	-	17.5	15.4
28. Lamina transv. width	-	36.3	27.6	24	24.8	-	-	19	20.2

¹Measurements are defined in Materials and Methods.

²Parentheses indicate that the structure is incomplete and its measurement is estimated.

TABLE A2. MEASUREMENTS ON MH 2 VERTEBRAE
(in mm for linear measurements and degrees for angles).

	U.W. 88-93	U.W. 88-83	U.W. 88-188 upper T	U.W. 88-189 mid/low T	U.W. 88-190 mid/low T	U.W. 88-191 lower T	U.W. 88-96 mid/low T	U.W. 88-114 antepenult. T	U.W. 88-43 penult. T	U.W. 88-44 last T	U.W. 88-127/153 penult. L	U.W. 88-126/138 last L
1. Body sup. transv. width (MαW7)	14.9	13.2	18.8	18.4	-	-	-	24.9	27.4	29	31.4	32.8
2. Body sup. dorsoven. dia. (Mα4)	10.7	10.9	11.6	13.6	-	-	-	19.6	18.9	18	22.2	21.4
3. Body inf. transv. width (Mα8)	12	15	23.4	26.4	25.7	-	-	27.8	28.5	28	32.4	29
4. Body inf. dorsoven. dia. (MαW5)	11.1	11.6	13.6	15.2	-	-	-	19.2	19.1	18.5	21.2	19.6
5. Body ventral height (MαW1)	8.5	8.2	11.6	11.6	-	-	-	16.5	16.6	19.7	22.1	21
6. Body dorsal height (MαW2)	8	9.4	11.9	12.2	12.9	-	-	17.6	17.6	20.5	21.5	17
7. Body wedging angle (in degrees)	-2.6°	6.3°	1.5°	2.5°	-	-	-	3.2°	3°	2.6°	-1.6°	-10.7°
8. Canal dorsoven. dia. (MαW10)	19.7	17.3	14.5	13.4	10.9	12.7	-	13.6	14.8	15.1	-	23
9. Canal transv. dia. (MαW11)	14.6	10.8	10.6	10.4	13.9	13.4	-	13.3	12.8	13.1	-	16.3
10. Sup.-inf. inter-AF height	12.2	17.8	22.6	22.5	22.2	-	-	27	28.8	31	32.6	31.5
11. Max. inter-SAF dist.	36.3	37.5	25.6	25.6	26.9	22.2	-	21.9	25.2	18.1	-	28.5
12. Min. inter-SAF dist.	20.7	20.5	13.4	9.2	6.9	9.7	-	8.1	8.4	11.3	-	-
13. Max. inter-IAF dist.	37.3	36	24.5	24.2	26.2	-	-	25.5	18.9	21	(28) ¹	32.2
14. Min. inter-IAF dist.	20	16.5	-	7.9	8.2	-	-	9.7	12.7	8.7	11.6	15.6
15. SAF sup.-inf. dia.	7.8	9	9.1	9	9.1	(8.3)	-	9.8	8.6	10	-	13.4
16. SAF transv. dia.	8.2	9.7	6.8	8.1	7.4	(6.8)	-	7.5	8.3	7.8	-	10.8
17. IAF sup.-inf. dia.	9.8	7.9	-	7.8	6.9	-	-	7.9	7.5	10.3	15.1	14.4
18. IAF transv. dia.	8.5	10.3	-	9.4	8	-	-	8	7.4	8.2	11.5	11.7
19. Spinous process angle (MαW12)	144°	131°	-	100°	125°	-	151°	132°	143°	-	-	166°
20. Spinous process length (MαW13)	12.2	-	-	-	-	-	-	-	24.4	-	28	23.6
21. Transverse process angle	-	-	51°	45°	54°	43°	66°	50°	73°	-	-	50°
22. Transverse process length	9.8	14.5	18.1	18.7	20.1	17.9	19.1	16.8	14	-	-	-
23. SAF orientation (in degrees)	77°	67°	110°	103°	104°	-	-	104°	107°	24°	33°	26°
24. Pedicle sup.-inf. height	6.7	4.5	8.2	8.6	9	-	-	10.8	11	11.8	-	11.2
25. Pedicle transv. width	4.5	4.4	4.2	3.7	3.4	-	-	3.6	4.6	5.4	-	10.9
26. Pedicle dorsoven. length	5.7	4.8	5.9	8	6.4	-	-	5.9	4.6	5	-	7
27. Lamina sup.-inf. height	7.3	10.2	13.2	13.2	13.4	-	-	15.1	14.5	14.9	-	14
28. Lamina transv. width	34.5	33	25.3	24.7	27	-	(25.4) ¹	24	17	17.9	-	30.5

¹Parentheses indicate that the structure is incomplete and its measurement is estimated.

TABLE A3. STANDARD MEASUREMENTS OF MH1 RIBS (in mm).

	U.W. 88-148 Rib1(r)	U.W. 88-86/41 Rib6/7(r)	U.W. 88-15/131 Rib6/7(l)	U.W. 88-155 Rib7/8(l)	U.W. 88-165 Rib7-9(r)	U.W. 88-74 Rib7-9(l)	U.W. 88-17 Rib11-12(l)	U.W. 88-13 Indet. ¹
29. Rib shaft Sup.-Inf. height (MβR1)	4.3	9.2	9.6	5.2	10.2	16.4	4.5	10.7
30. Rib shaft Int.-Ext. thick. (MβR2)	12.5	11.5	11.5	10.1	4.8	6.1	3.5	4.9
31. Rib artic. tubercle Sup.-Inf. height	4.1	9	8.1	-	-	-	-	-
32. Rib artic. tubercle Med.-Lat. width	6.1	6.7	12.8	-	-	-	-	-
33. Rib neck Sup.-Inf. (minimum) dia.	5.4	9.9	10.1	-	-	-	-	-
34. Rib neck Int.-Ext. (minimum) width	7.5	6.6	6.8	-	-	-	-	-

